MAGNETIC RESONANCE IMAGING STUDIES OF CARDIAC CHANGES IN DIABETIC AND HYPERTENSIVE RATS

By

A. I. M. Al-Shafei

Darwin College, Cambridge

Submitted for the degree of Doctor of Philosophy

Department of Physiology and

The Herchel Smith Laboratory for Medicinal Chemistry

University of Cambridge

January, 2001

Acknowledgements

I wish to acknowledge the assistance and encouragement of all those who, in varying ways, varying degrees, and indeed at many different stages of my life, have contributed to this thesis.

Let me first thank my supervisor Dr Christopher L-H Huang for giving me the opportunity to study at Cambridge University. His careful guidance, enthusiasm, generous support provided a wonderful atmosphere full of scientific spirit. I was most fortunate to work in his research group. I am also very grateful to Professor Laurie D. Hall, my co-supervisor, for the privilege of working in the Herchel Smith laboratory and for his encouragement, understanding and positive attitude.

Very many thanks must go to Professor Roger C. Thomas, the Head of the Department of Physiology, Cambridge University for giving me the opportunity to study at Cambridge University.

I am deeply indebted to Dr Richard G. Wise, Dr Gao Amin and Dr Adam Wilkinson for their instruction and assistance in imaging techniques.

I would like to thank sincerely Mr Simon Smith and Mr Cyril Harbrid for their patient and diligent help in resolving numerous technical problems and Mrs Agnes Hunt and Ms Lynda Smith for solving the administrative problems.

My special thanks are due to Mr Wafic Rida Said and Karim Rida Said Foundation for supporting me for the period of my study at the University of Cambridge.

I would also like to thank Dr Herchel Smith for his generous endowment.

I wish to express my sincere gratitude to the entire staff in the Herchel Smith Laboratory for Medicinal Chemistry, the University of Cambridge for their kind help and companionship.

Last in chronology, but foremost in my mind, are the people closest to me. I wish to thank my parents who have been the "wind beneath my wings" for such a long time. So I dedicate this thesis to them for helping me over the years, for the unconditional love and their unwavering faith in me has never ceased to provide a great source of strength. A big thank you goes out to the crew and last

but not least my sister "Ghada" who was there when I needed her through thick and thin, your help will never be forgotten "Thanks".

MAGNETIC RESONANCE IMAGING STUDIES OF CARDIAC CHANGES IN DIABETIC AND HYPERTENSIVE RATS

A. I. M. Al-Shafei

Darwin College

January, 2001

Magnetic resonance imaging (MRI) was applied as a non-invasive technique to characterize, for the first time, the structural and functional changes in the left and right ventricles following induction of diabetes in streptozotocin-treated rats. The effects of the angiotensin-converting enzyme inhibitor captopril upon such changes were also investigated. Finally, the MRI methods were also used to characterize the corresponding right ventricular changes in the spontaneously hypertensive rats (SHR), also for the first time.

The MRI studies of the diabetic heart were performed on male Wistar rats subdivided into four groups, each containing four animals. Diabetes was induced in three groups by single intraperitoneal streptozotocin injections at the age of 7, 10 and 13 weeks respectively, leaving an untreated control group. A further group was maintained on captopril-containing drinking water immediately after the induction of diabetes at the age of 7 weeks. All animals were scanned at the age of 16 weeks, thus providing groups that had been diabetic for 9, 6, and 3 weeks respectively that were all age-matched to the single control group. The cine magnetic resonance imaging protocol imaged both ventricles at twelve time-points through the cardiac cycle covering systole and most of diastole. The subsequent quantitative analysis derived the anatomical and functional indices of left and right ventricular myocardial volume, end-diastolic volume (EDV), end-systolic volume (ESV), stroke volume (SV), and ejection fraction (EF). They also characterized the kinetics of left and right ventricular contraction and relaxation through the initial rates of left and right ventricular ejection and filling and by plotting such rates, dV/dt, through the studied twelve time-points through the cardiac cycle.

The MRI measurements yielded consistent myocardial volumes in both ventricles through all twelve time-points and in all the five experimental groups. Furthermore, the myocardial densities of both ventricles deduced from the post-mortem weights and myocardial volumes as measured by

MRI closely agreed between groups and with previous reports. The subsequent analysis demonstrated significant relative left and right ventricular hypertrophy as reflected in the myocardial volume normalized to body weight, associated with diastolic and systolic functional abnormalities that developed between 3 and 6 weeks of diabetes. There was a further deterioration at 9 weeks. Such deteriorations were greatest between 3 and 6 weeks of diabetes in the left ventricle and between 6 and 9 weeks of diabetes in the right ventricle. Finally, captopril treatment commenced immediately after the induction of diabetes prevented the development of the relative hypertrophy in both ventricles and markedly relieved the diastolic and systolic abnormalities.

MRI has been recently used to characterize the anatomical and physiological parameters describing the left ventricle in the SHR rats but has not been applied to the right ventricle. This, together with recent histological evidence of pulmonary hypertension in SHR rats prompted an MRI study of the right ventricle of the SHR rats. The experiments compared eight SHR and eight normotensive Wistar-Kyoto control rats (WKY). Each group of eight rats was subdivided into equal two-age matched categories of 8 and 12 weeks. As before, the right ventricle of all the experimental rats was imaged at twelve time-points through the cardiac cycle covering the whole of systole and most of diastole and the analysis derived the right ventricular myocardial volume, EDV, ESV, SV, and EF as well as right ventricular volume changes with time and dV/dt values. The analysis demonstrated for the first time hypertrophy of the right ventricles associated with diastolic and systolic dysfunction in the SHR rats.

These studies thus use MRI for the first time successfully to demonstrate directly the development of cardiac changes in the left and right ventricles in an animal model of diabetes and right ventricular changes in an animal model of hypertension.

Key words: Magnetic resonance imaging
Spontaneously hypertensive rats
Myocardial volume
End-systolic volume
Ejection fraction
Systolic dysfunction.
Streptozotocin-diabetic rat
Cardiac cycle
End-diastolic volume
Stroke volume
Diastolic dysfunction

Declarations

I, A. I. M. Al-Shafei, hereby certify that this thesis has been written by me, that is the record of my work carried out by me and that has not been submitted in any previous application for a higher degree.

Date: 19/1/2021 Signature: A. I. M. Al-Shafei

In submitting this thesis to the University of Cambridge, I understand that I am giving permission for it to be made available for use in accordance with the regulations of the University Library for the time being in force, subject to any copyright vested in the work not affected thereby. I also understand that the title and abstract will be published, and a copy of the work may be made and supplied to any bona fide library or research worker.

Date: 19/1/2021 Signature: A. I. M. Al-Shafei

CONTENTS

CHAPTER 1
INTRODUCTION

1.1 Importance of diabetic cardiac disease

Diabetes mellitus and systemic arterial hypertension are considered to be the commonest two chronic diseases seriously affecting the cardiovascular system worldwide and particularly in developed countries. Prolonged diabetes mellitus is associated with the development of premature and accelerated large vessel disease or diabetic macroangiopathy. Diabetics also show a higher incidence of microangiopathy or small vessel disease. Diabetics thus suffer an increased morbidity and mortality largely attributable to cardiovascular complications (Crall and Roberts, 1978; Kannel, 1985; Stehouwer et al., 1997). The latter may reflect a substantially increased incidence of coronary artery disease (Kannel and McGee, 1979). There is also a higher mortality following acute myocardial infarction that may result from a higher incidence of post-infarction congestive cardiac failure and cardiogenic shock (Kereiakes, 1985). This increased mortality may be exacerbated by poor glycaemic control (Oswald et al., 1984), diabetic ketoacidosis (Husband et al., 1985) and the increased incidence of the more extensive anterior myocardial infarction, which more seriously impairs ventricular function than infarctions elsewhere (Weitzman et al., 1982). Finally, the high fatty acid levels seen in diabetics with acute myocardial infarction might predispose to the development of post-infarction arrhythmias (Oliver et al., 1968).

However, there is significant evidence that diabetes also affects the myocardium directly to result in a specific diabetic cardiomyopathy (Goodwin and Oakley, 1972; Rubler et al., 1972; Hamby et al., 1974). Thus, the Framingham study reported a higher incidence of congestive heart failure that could not be entirely accounted for by the high incidence of coronary atherosclerosis, hypertension, or cardiac autonomic neuropathy in diabetics (Kannel et al., 1974). This has been variously attributed to intramural vessel abnormalities (Blumenthal, 1960; Ledet, 1968, 1976; Rubler et al., 1972; Hamby et al., 1974; Seneviratne, 1977; Sanderson et al., 1978; Zoneraich et al., 1980), uncontrolled hyperglycaemia (Shapiro et al., 1980; Uusitupa et

CHAPTER 1
INTRODUCTION

1.1 Importance of diabetic cardiac disease

Diabetes mellitus and systemic arterial hypertension are considered to be the commonest two chronic diseases seriously affecting the cardiovascular system worldwide and particularly in developed countries. Prolonged diabetes mellitus is associated with the development of premature and accelerated large vessel disease or diabetic macroangiopathy. Diabetics also show a higher incidence of microangiopathy or small vessel disease. Diabetics thus suffer an increased morbidity and mortality largely attributable to cardiovascular complications (Crall and Roberts, 1978; Kannel, 1985; Stehouwer et al., 1997). The latter may reflect a substantially increased incidence of coronary artery disease (Kannel and McGee, 1979). There is also a higher mortality following acute myocardial infarction that may result from a higher incidence of post-infarction congestive cardiac failure and cardiogenic shock (Kereiakes, 1985). This increased mortality may be exacerbated by poor glycaemic control (Oswald et al., 1984), diabetic ketoacidosis (Husband et al., 1985) and the increased incidence of the more extensive anterior myocardial infarction, which more seriously impairs ventricular function than infarctions elsewhere (Weitzman et al., 1982). Finally, the high fatty acid levels seen in diabetics with acute myocardial infarction might predispose to the development of post-infarction arrhythmias (Oliver et al., 1968).

However, there is significant evidence that diabetes also affects the myocardium directly to result in a specific diabetic cardiomyopathy (Goodwin and Oakley, 1972; Rubler et al., 1972; Hamby et al., 1974). Thus, the Framingham study reported a higher incidence of congestive heart failure that could not be entirely accounted for by the high incidence of coronary atherosclerosis, hypertension, or cardiac autonomic neuropathy in diabetics (Kannel et al., 1974). This has been variously attributed to intramural vessel abnormalities (Blumenthal, 1960; Ledet, 1968, 1976; Rubler et al., 1972; Hamby et al., 1974; Seneviratne, 1977; Sanderson et al., 1978; Zoneraich et al., 1980), uncontrolled hyperglycaemia (Shapiro et al., 1980; Uusitupa et

al., 1983), changes in myocardial lipid metabolism (Paulson and Crass, 1980), changes in calcium handling (Ganguly et al., 1983; Dhalla et al., 1998) or a primary hypertrophy of the myocytes themselves (Rubler et al., 1972; Fischer et al., 1979). In addition, extensive fibrosis might explain some of the functional abnormalities seen in diabetes (Rubler et al., 1972; Regan et al., 1981). Finally, growing evidence implicates angiotensin II in the pathogenesis of diabetic cardiomyopathy by its inducing myocardial interstitial fibrosis owing to fibroblast proliferation in the cardiac wall (Schorb et al., 1993). The latter may act through activation of an intracardiac renin-angiotensin system (Dostal et al., 1992a, b) in diabetes leading to enhanced angiotensin II production (Rösen et al., 1995).

It is necessary first to establish, characterize and understand the pathophysiology of diabetic cardiomyopathy before considering therapeutic regimes. Earlier animal studies included haemodynamic studies of alloxan-diabetic dogs (Regan et al., 1974), studies of isolated perfused diabetic rat hearts (Miller, 1979) and of isolated papillary muscles from diabetic rats (Fein et al., 1980, Warley et al., 1995). However, data from intact organisms are primarily available from human studies. Thus, non-invasive human studies investigated systolic time intervals, echocardiographic measurements of left ventricular wall thickness and indicators of left ventricular diastolic and systolic function. There have also been radionuclide ventriculography examinations for left ventricular ejection function in diabetic patients. However, both these techniques reported conflicting results.

1.2 Hypertensive cardiac disease

Systemic hypertension is a major risk factor for coronary artery disease and heart failure (Kannel et al., 1972; Dustan et al., 1974; Frohlich, 1991). However, most published studies of its cardiac complications have concerned anatomical, electrophysiological and kinetic changes in the left ventricular myocardium (Grossman, 1980; Frohlich et al., 1991). They have described a left ventricular hypertrophy that may reflect an adaptation to an elevated systemic vascular resistance (Grossman, 1980; Frohlich et al., 1991). However, such hypertrophy is associated with an increased risk of ischaemic myocardial pathology and ventricular arrhythmias (Messerli et al., 1984; Frohlich, 1991). Aharinejad et al. (1996) reported that the spontaneously hypertensive rats (SHR) show histological features suggestive of a pulmonary hypertension. However, there has been no detailed investigation on the structural and functional properties of the right ventricle in SHR rats.

1.3 MRI as a cardiovascular investigative tool

Magnetic resonance imaging offers a powerful non-invasive imaging technique offering a sub-millimeter resolution that has been widely accepted in clinical practice for both anatomical and physiological studies on living organs. These features make it an ideal technique for long-term chronic studies of diabetes and hypertension in intact living animals; it makes possible serial studies of the pathological changes in a single animal or a group of animals through extended periods. Magnetic resonance techniques specifically useful for cardiac imaging have rapidly developed over the past several years (Higgins, 1986; Stratemeier et al., 1986; Markiewicz et al., 1987; Sechtem et al., 1987; Semelka et al., 1990). MRI additionally offers excellent soft tissue contrast much superior to that obtained with conventional x-ray computed tomography. This enhanced contrast permits the acquisition of high quality cardiac images without the need for administering the contrast media demanded by conventional or cine x-ray computed tomography. In addition, dynamic or cine magnetic resonance images using electrocardiographic gating enables data acquisition at equivalent time-points in the cardiac cycle over successive cardiac cycles. Thus changes in the dynamics of the cardiac cycle in both human and rat hearts can be characterized with good time resolution. All these features make MRI an attractive experimental and clinical tool for chronic cardiovascular physiology.

1.4 Aims of the present study

The present study adopted MRI methods to visualize structure and function in the entire heart in intact animal models of diabetes mellitus. The streptozotocin-induced diabetic (STZ-diabetic) rat modeled the long-term cardiac complications of diabetes (Warley et al., 1995; Rodrigues et al., 1997). The experiments that followed studied changes in the structure and function of the right ventricle in the spontaneously hypertensive rat (SHR) (Trippodo and Frohlich, 1981). Such animal models made it possible to follow the evaluation of chronic pathology over a manageable time scale.

The present experiments thus introduced MRI to characterize the structural and functional changes in the left and right ventricles associated with experimental diabetic cardiomyopathy for the first time. It characterized left and right ventricular contraction and relaxation through the cardiac cycle in the normal as well as the diabetic heart and evaluated the therapeutic effects of the angiotensin-converting enzyme inhibitor captopril in ameliorating the structural and physiological abnormalities associated with diabetic cardiomyopathy. The present study

similarly examined right ventricular structural and physiological properties in the SHR, also for the first time.

1.5 Organization of the present dissertation

The chapters that follow in this thesis are organized as follows:

Since MRI was the main research tool used in this work, Chapter 2 provides a brief description of the physical principles of MRI.

Chapter 3 outlines past epidemiological studies of the cardiovascular complications of diabetes mellitus and emphasizes the importance of diabetes as a major source of cardiovascular risk. It points out that prolonged diabetes predisposes to development of premature and accelerated disease of large blood vessels or diabetic macroangiopathy, which presents as coronary artery disease, cerebrovascular disease or peripheral vascular disease. Such coronary artery disease contributes significantly to mortality in diabetes. It describes evidence that suggests that diabetes also directly leads to structural and functional abnormalities in the myocardium that may produce a pathological condition commonly termed diabetic cardiomyopathy or diabetes specific cardiac muscle disorder. The assessment of such cardiac changes in experimental diabetes is the primary interest of the present work.

Chapter 4 accordingly outlines what is known about the pathology of cardiomyopathic changes in diabetes. It reviews the literature covering the associated pathological findings including vascular, metabolic, myocyte, and interstitial changes. This Chapter also outlines evidence for an involvement of angiotensin II in the pathogenesis of this condition. The latter prompted the inclusion of an MRI study of the therapeutic effect of captopril in the present study.

Thereafter, Chapter 5 summarizes some of the experimental animal and human studies of cardiac function in diabetes. It also discusses the various techniques used so far to evaluate the structural and functional abnormalities of diabetic myocardium. However, no single technique could characterize all the indices describing myocardial structure and function in diabetes, and the studies performed so far have concentrated on the left ventricle and have almost completely omitted right ventricular changes in diabetes. Furthermore, independent investigators report conflicting results about the cardiac consequences of diabetic disease.

Chapter 6 then presents the materials and methods used in the MRI study of the diabetic heart and describes in detail use of the experimental animals, the induction of diabetes and the physiological monitoring of the animal before and during the imaging session. It goes on to describe the imaging hardware and the MRI pulse sequence used and the imaging sessions and the analysis of the acquired image data.

The results of this MRI study of the diabetic heart are then presented and discussed in Chapters 7-10. The internal consistency of the diabetic MRI data was corroborated in that the measured myocardial volumes in both ventricles were conserved through the cardiac cycle at all twelve time-points that were studied in the five experimental groups. Furthermore, the myocardial densities of both ventricles, calculated from the ratio of the post-mortem weight of each ventricle to the MRI-measured myocardial volume were consistent through all experimental groups and in agreement with previous reports. These Chapters further report: (a) significant relative left and right ventricular hypertrophy associated with diastolic and systolic functional abnormalities at 6 weeks, (b) a further deterioration in the hypertrophy and the diastolic and systolic dysfunctions of both ventricles between 6 and 9 weeks, (c) a greater rate of progression of the hypertrophy and associated functional abnormalities between 3 and 6 weeks in the left ventricle and between 6 and 9 weeks in the right ventricle, and (d) that treatment with captopril immediately after the induction of diabetes prevents the development of the relative hypertrophy in both ventricles and markedly reduces the diastolic and systolic abnormalities.

Chapter 11 of this thesis describes an MRI study of the right ventricle of the SHR rats. It starts with an introduction emphasizing the clinical importance of the cardiovascular complications of hypertension; in particular left ventricular hypertrophy. Yet, structural and functional changes in the right ventricle have not been studied in SHR rats using MRI and are therefore the object of the present study. It then presents the materials and methods used in this study, which were similar to those of the MRI study of the diabetic heart with specific modifications. Finally, it presents and discusses the results obtained. Interestingly, the SHR rats showed hypertrophy of their right ventricles and these were associated with diastolic and systolic dysfunction in the cardiac cycle.

Chapter 12 sums up the experimental findings with concluding remarks.

For the convenience of the reader, the tables of the results chapters were placed at the end of each respective chapter.

CHAPTER 2
MRI THEORY

2.1 Definition

MRI stands for Magnetic Resonance Imaging. It is a non-invasive imaging technique using magnetic fields and non-ionizing radiofrequency of low energy to obtain high quality anatomical and functional images of different body organs with high soft tissue contrast. Unlike regular radiographic and computerized axial tomography (CAT) scans, MRI does not use x-rays or any other form of ionizing radiation and usually does not require administration of contrast media. MRI has been primarily used as a diagnostic clinical tool but it has now found application in fundamental anatomical and physiological studies. MRI is based on the phenomenon of nuclear magnetic resonance (NMR). The latter results from the enhanced absorption of radiofrequency energy by the nuclei of atoms when placed in an external static magnetic field and when such energy is close to a specific frequency, called the Larmor or resonance frequency (Newhouse and Wiener, 1991; Brown and Semelka, 1995; English and Moore, 1995; Edelman et al., 1996; Farr and Allisy-Roberts, 1996; Higgins et al., 1997). Initially, the technique was referred to as Nuclear Magnetic Resonance Imaging (NMRI). The "nuclear" part of the title was omitted about 15 years ago to avoid any suggestion that the measurement involves radioactive processes (Newhouse and Wiener, 1991; Brown and Semelka, 1995; English and Moore, 1995; Edelman et al., 1996; Farr and Allisy-Roberts, 1996; Higgins et al., 1997).

2.2 Physical principles of magnetic resonance imaging

2.2.1 Nuclear magnetism

Matter is composed of atoms. Atoms, principally, consist of three fundamental particles: protons, which bear a positive charge, neutrons, which have no charge, and electrons, which have a negative charge. The only exception is the hydrogen atom, which has a single proton in the nucleus and one orbiting electron (Newhouse and Wiener, 1991; Brown and Semelka, 1995;

English and Moore, 1995; Edelman et al., 1996; Farr and Allisy-Roberts, 1996; Higgins et al., 1997). The nucleus of an atom consists of protons and neutrons while the electrons travel around the nucleus in orbitals. All the individual particles rotate around their axes; a property called spin (Newhouse and Wiener, 1991; Brown and Semelka, 1995; English and Moore, 1995; Edelman et al., 1996; Farr and Allisy-Roberts, 1996; Higgins et al., 1997). Classically, spin is the tendency to act like a spinning ball of charge. A nucleus may contain more than one proton or neutron, and so the spins of protons and neutrons add together. In some nuclei, they add to zero. In others, they add to a number other than zero. Nuclei in which the spins of protons and neutrons add to a number other than zero are said to have a net spin. Any nucleus with either an odd atomic number (number of protons) or an odd atomic weight (the sum of the number of protons and the number of neutrons) has a net spin. A nucleus that has a net spin also acts like a ball of spinning charge. Only nuclei that have a net spin are NMR sensitive when placed in a static magnetic field. The simplest nucleus that contains an odd number of protons is the hydrogen atom, which contains just one proton and no neutrons (Newhouse and Wiener, 1991; Brown and Semelka, 1995; English and Moore, 1995; Edelman et al., 1996; Farr and Allisy-Roberts, 1996; Higgins et al., 1997). It is well known that the total body water accounts for 72% of the lean human body mass and hydrogen is a major constituent of water. Furthermore, hydrogen is also found in lipids and other organic compounds (English and Moore, 1995). Hydrogen is, therefore, considered to be the most abundant tissue element. Additionally, hydrogen has a relatively large gyromagnetic ratio (γ) of 42.576 MHz T^{-1} (Edelman et al., 1996) giving a relatively large MRI signal (Edelman et al., 1996). It is, therefore, particularly effective at producing the tissue magnetization that eventually results in the emission of a marked radio frequency signal contribution (Newhouse and Wiener, 1991; Brown and Semelka, 1995; English and Moore, 1995; Edelman et al., 1996; Farr and Allisy-Roberts, 1996; Higgins et al., 1997). At present, all clinical applications of MRI involve detection of contribution from the hydrogen nucleus. Other nuclei that exhibit a net spin and are of biological importance include: ^{13}C, ^{19}F, ^{23}Na, ^{31}P, and ^{39}K (Newhouse and Wiener, 1991; Brown and Semelka, 1995; English and Moore, 1995; Edelman et al., 1996; Farr and Allisy-Roberts, 1996; Higgins et al., 1997). Theoretically, it is possible to perform NMR imaging with any of these nuclei, but this would be more difficult than imaging using hydrogen nuclei because of their more limited abundance and lower sensitivity for the MRI signal (Newhouse and Wiener, 1991; Brown and Semelka, 1995; English and Moore, 1995; Edelman et al., 1996; Farr and Allisy-Roberts, 1996; Higgins et al., 1997).

The spinning motion of nuclei with a net spin generates a tiny magnetic field around them. This tiny magnetic field is called the magnetic moment (m). The spinning hydrogen proton can be

viewed as if it is a tiny bar magnet itself with a north and south poles (Figure 2.1) (Newhouse and Wiener, 1991; Brown and Semelka, 1995; English and Moore, 1995; Edelman et al., 1996; Farr and Allisy-Roberts, 1996; Higgins et al., 1997). As the magnetic field is a vector quantity with both magnitude and direction, it is similarly possible to define a magnitude and orientation for the nuclear magnetic moment (Newhouse and Wiener, 1991; Brown and Semelka, 1995; English and Moore, 1995; Edelman et al., 1996; Farr and Allisy-Roberts, 1996; Higgins et al., 1997).

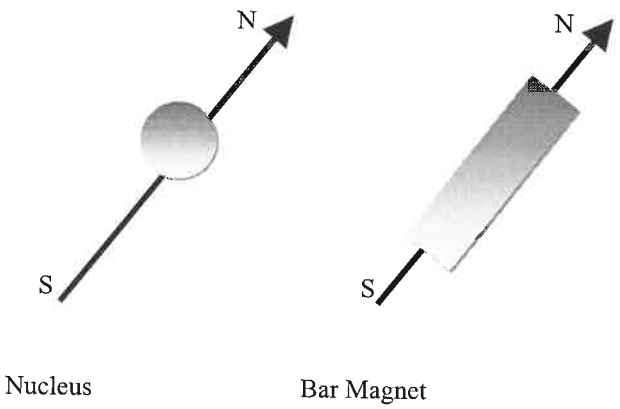

Figure 2.1: The hydrogen proton, spinning around its axis, generates a magnetic moment and can be thought as a bar magnet with a north and south poles.

It is the orientation of the nuclear spin vector and how it changes during the application of precisely timed pulses of radiofrequency (RF) energy in conjunction with magnetic field gradients that ultimately determine the features of the emitted MRI signal (Newhouse and Wiener, 1991; Brown and Semelka, 1995; English and Moore, 1995; Edelman et al., 1996; Farr and Allisy-Roberts, 1996; Higgins et al., 1997). When the tissue is not subjected to an external magnetic field, the orientation or direction of the magnetic moments of the nuclei is random and varies randomly with time (Newhouse and Wiener, 1991; Brown and Semelka, 1995; English and Moore, 1995; Edelman et al., 1996; Farr and Allisy-Roberts, 1996; Higgins et al., 1997). Accordingly, a zero sum is the result of performing a vector addition of these magnetic moments; and hence, no net magnetization is observed in the tissue.

However, if the tissue is placed in a strong static magnetic field B_0, such as a magnetic resonance scanner, the field exerts a force on these randomly oriented nuclear magnetizations and forces some of them to align with it (Newhouse and Wiener, 1991; Brown and Semelka, 1995; English and Moore, 1995; Edelman et al., 1996; Farr and Allisy-Roberts, 1996; Higgins et al., 1997). The protons align themselves in either of two directions; "parallel (spin-up)", of

low energy or "anti-parallel (spin-down)", of high energy, to the applied magnetic field, with the majority being in the parallel direction. Thus, most of the protons cancel each other out in pairs (spin-up and spin-down), and it is the unpaired protons that produce the net magnetic vector (M_0) in the direction of the external main magnetic field (B_0). The result is that the tissue has now itself become a net magnet. This net magnetic vector is known as the longitudinal magnetization (Newhouse and Wiener, 1991; Brown and Semelka, 1995; English and Moore, 1995; Edelman et al., 1996; Farr and Allisy-Roberts, 1996; Higgins et al., 1997).

The stronger the externally applied magnetic field, the greater the moment it will exert on the nuclear magnetizations and thus, the more protons would be aligned parallel to it and, accordingly the more the ultimate strength of the tissue's net longitudinal magnetization (Newhouse and Wiener, 1991; Brown and Semelka, 1995; English and Moore, 1995; Edelman et al., 1996; Farr and Allisy-Roberts, 1996; Higgins et al., 1997). In MR imaging, we use powerful magnets with strong magnetic fields in order to maximize MR signal available from the tissue. However, it is not the longitudinal magnetization but the transverse magnetization that we are measuring.

The ultimate strength of the tissue's net longitudinal magnetization is thus related to the externally applied magnetic field strength to which the tissue is exposed. In addition, it is also related to the tissue's chemical and physical properties: these features reflect the tissue's magnetic susceptibility (Newhouse and Wiener, 1991; Brown and Semelka, 1995; English and Moore, 1995; Edelman et al., 1996; Farr and Allisy-Roberts, 1996; Higgins et al., 1997). The tissue's magnetic susceptibility is defined as the degree to which the tissue is magnetized in response to magnetic fields to which it is being exposed (Newhouse and Wiener, 1991; Brown and Semelka, 1995; English and Moore, 1995; Edelman et al., 1996; Farr and Allisy-Roberts, 1996; Higgins et al., 1997). Different tissues in the same magnetic field exhibit different magnetic susceptibilities and accordingly, the ultimate strength of their net longitudinal magnetizations are different.

2.2.2 Precession

In addition to causing the protons to align with it, the static magnetic field causes them to "wobble" in a regular manner called precession (Newhouse and Wiener, 1991; Brown and Semelka, 1995; English and Moore, 1995; Edelman et al., 1996; Farr and Allisy-Roberts, 1996; Higgins et al., 1997). As a result of precession, the direction of the magnetic moment of the spinning proton tilts and rotates around the direction of the magnetic field B_0 with a fixed frequency, called the Larmor frequency (Figure 2.2). The precession movement of a spinning

proton is directly comparable to the movement of a spinning top, which spins around its axis until its speed slows, allowing gravity to cause it to precess about the direction of the earth's gravitational pull until it falls over (Newhouse and Wiener, 1991; Brown and Semelka, 1995; English and Moore, 1995; Edelman et al., 1996; Farr and Allisy-Roberts, 1996; Higgins et al., 1997).

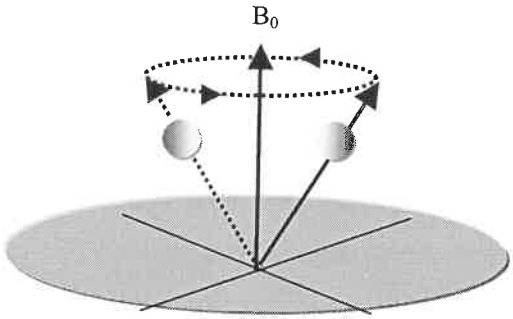

Figure 2.2: Diagrammatic representation of the precession of a hydrogen nucleus (a proton) around an externally applied main magnetic field (B_0). The spinning proton precess about the direction of the static magnetic field, much like a spinning top that sweeps out a cone-shaped path around the direction of the gravitational field of the earth.

The rate of precession of protons in a magnetic field is dependent on that particular element and is directly related to the strength of the externally applied magnetic field to which they are being exposed. The stronger the magnetic field the higher the precession frequency. The relationship can be expressed by equation (2.1), the Larmor equation:

$$\omega_0 = \gamma B_0 \qquad (2.1)$$

The term ω_0 is the angular frequency (precessional or Larmor frequency) in megahertz (MHz), B_0 is the magnetic field strength that the protons experience in tesla (T), and γ is a constant for each nucleus called the gyromagnetic or magnetogyric ratio in MHz T^{-1} (Newhouse and Wiener, 1991; Brown and Semelka, 1995; English and Moore, 1995; Edelman et al., 1996; Farr and Allisy-Roberts, 1996; Higgins et al., 1997). The larger the value of the gyromagnetic ratio, the larger is the energy difference between the low (parallel) and the high (anti-parallel) energy states for a given B_0, and thus greater the net tissue magnetization is produced by a given magnetic field strength. ^1H was found to have relatively higher gyromagnetic ratio (42.576 MHz T^{-1}) than other nuclei with net spin and this actually explains the high sensitivity for the MR signal from hydrogen nuclei.

As a result of precession and its tilting effect on the magnetic moment (*m*), the magnetic moment of a spinning proton splits into a longitudinal component (*the m_z vector*) that points in the direction of the externally applied magnetic field i.e. in the Z-direction, and a transverse component (*the m_{xy} vector*), which rotates in the XY plane (Figure 2.3) (Newhouse and Wiener, 1991; Brown and Semelka, 1995; English and Moore, 1995; Edelman et al., 1996; Farr and Allisy-Roberts, 1996; Higgins et al., 1997).

The *m_z vectors* add up to a combined or net longitudinal magnetization vector (M_0) that points in the direction of the externally applied field (B_0) (Figure 2.4) (Newhouse and Wiener, 1991; Brown and Semelka, 1995; English and Moore, 1995; Edelman et al., 1996; Farr and Allisy-Roberts, 1996; Higgins et al., 1997). Being in the same direction as B_0, this net longitudinal magnetization (M_0) cannot be measured directly as B_0 is much stronger than it.

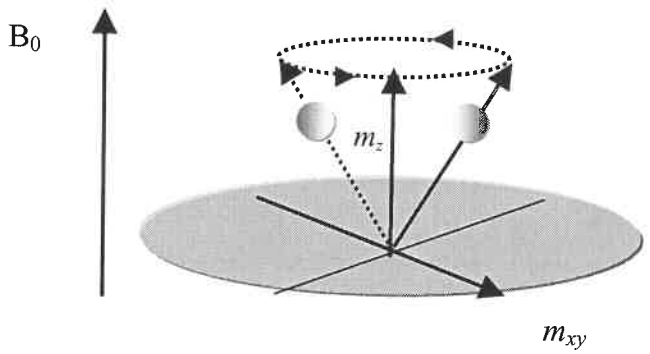

Figure 2.3: Diagrammatic represe ıtion of the transverse and longitudinal components of the magnetic moment. When exposed to a strong magnetic field, the spinning protons precess around the axis of the applied magnetic field at its Larmor frequency and as a result of this precessional movement, their magnetic moments splits into longitudinal (m_z) and transverse (m_{xy}) components.

Because of the inevitable inhomogeneities of the externally applied magnetic field and the destructive interference between the local tiny fields of each spinning proton and those of its neighbours, protons effectively precess independently and as a result only their m_z vectors point in one direction giving rise to a net longitudinal magnetization (M_0), whereas their m_{xy} vectors would point in all directions and cancel each other out in pairs. Consequently, the net transverse magnetization M_{xy} would be zero (Newhouse and Wiener, 1991; Brown and Semelka, 1995; English and Moore, 1995; Edelman et al., 1996; Farr and Allisy-Roberts, 1996; Higgins et al., 1997).

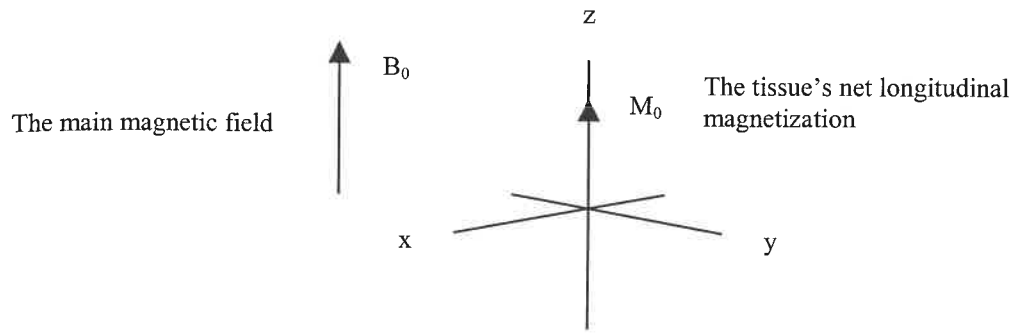

Figure 2.4: Diagrammatic representation of the longitudinal magnetization.

2.2.3 Resonance and radiofrequency

In order to acquire an MR signal, a pulse of radiofrequency (RF) current is passed through the radiofrequency coils that surround the patient. This RF pulse exchanges energy with the precessing protons and, as a result, some protons precessing in the low energy parallel direction are excited and acquire sufficient energy for them to change their precession direction to the high energy anti-parallel one (English and Moore, 1995; Farr and Allisy-Roberts, 1996). The more energy that is added to the system, the greater the number of protons that are excited to the high-energy direction. As a consequence, a greater number of the protons will cancel each other out in pairs and M_0 will reduce, disappear, or even reverse, depending on the energy given to the protons which in turn depends on the length and strength of the RF pulse (Farr and Allisy-Roberts, 1996). Thus, the RF pulse will tilt the net longitudinal magnetization away from the main magnetic field by an angle known as the flip angle, which is proportional to the strength and the duration of the applied RF pulse (English and Moore, 1995).

An important point relevant in this context is that the RF pulse not only excites protons to their high-energy direction but it also causes their precession to become synchronized and fall in phase (English and Moore, 1995; Farr and Allisy-Roberts, 1996). As a result, their m_{xy} vectors will now point in one direction and add up together to produce a net transverse magnetic vector (M_{xy}), which rotates in the XY plane at the Larmor frequency (Figure 2.5) (Farr and Allisy-Roberts, 1996). It is this transverse magnetic vector that eventually gives rise to the measurable MR signal.

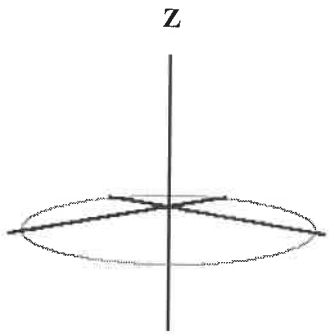

Figure 2.5: An RF pulse can be applied to produce any flip angle, depending on the duration and strength of the pulse. Following a 90° RF pulse net tissue magnetization is tilted 90° and is now in the transverse plane (M_{xy}). This net magnetization begins to precess around the longitudinal axis.

2.2.3.1 Resonance

The RF generator should be accurately tuned in such away that its frequency must very accurately match the Larmor (precessional/resonant) frequency of the precessing protons. In other words, the RF pulse should be in resonance with the precessing protons. Otherwise the RF pulse will not exchange energy effectively with the precessing protons and this would adversely affect the emitted MR signal (Newhouse and Wiener, 1991; Brown and Semelka, 1995; English and Moore, 1995; Edelman et al., 1996; Farr and Allisy-Roberts, 1996; Higgins et al., 1997).

2.2.4 The magnetic resonance signal

The rotation movement of the transverse magnetic vector (M_{xy}) in the XY plane induces an alternating (RF) voltage of a few microvolts in the antenna (RF coils) (Farr and Allisy-Roberts, 1996). It is this alternating voltage that eventually gives rise to the MR signal. Thus, An RF amplifier (receiver) is then used to amplify the emitted MR signal. The amplified signal is then sampled and processed by a computer. It is then used to control the pixel grey level in the MR image. The stronger the signal being emitted from a voxel is, the brighter the pixel will be in the MR image.

The vector M_0 cannot produce an MRI signal as it falls in the direction of the main magnetic field. It is the net transverse magnetic vector (M_{xy}) that actually produces the signal. However as M_{xy} is produced by tipping M_0, it is the strength of the M_0 immediately before the application of the RF pulse that determines the strength of the emitted RF signal (Newhouse and Wiener, 1991; Farr and Allisy-Roberts, 1996).

The ultimate strength of the emitted MR signal depends on the following factors:

(1) The strength of the externally applied magnetic field (B_0). The stronger the magnetic field to which the tissue is exposed, the greater the force it exerts on its contained protons and the greater the number of protons that would align parallel rather than anti-parallel to it;
(2) The proton or spin density (PD, number of protons per cubic millimeter) of the voxel;
(3) The gyromagnetic ratio of the nucleus;
(4) The T_1 (longitudinal or spin-lattice relaxation time); and
(5) The T_2 (transverse or spin-spin relaxation time).

Finally, the MRI device uses methods of spatial-encoding in order to determine the exact location in the tissue from which each portion of the emitted radio frequency signal comes from. This is crucial in generating an MR image (Newhouse and Wiener, 1991; Brown and Semelka, 1995; English and Moore, 1995; Edelman et al., 1996; Farr and Allisy-Roberts, 1996; Higgins et al., 1997).

2.2.4.1 Free induction decay (FID)

Over the interval the RF pulse is applied the protons precess in phase and give a peak emitted MR signal. However, the RF pulse can only be applied for a brief time. Immediately after it is switched off, the precessing protons both return to their original low-energy direction and once again begin to precess independently and therefore lose phase coherence (Newhouse and Wiener 1991; Farr and Allisy-Roberts 1996, Edelman et al., 1996; Higgins et al., 1997). Consequently, M_0 recovers while M_{xy} decreases or decays and accordingly, the strength of the MR signal decays, although its frequency remains the same (Figure 2.6). This MR signal is called the free induction decay and the decrease in strength occurs as a result of energy loss or relaxation (Newhouse and Wiener, 1991; Brown and Semelka, 1995; English and Moore, 1995; Edelman et al., 1996; Farr and Allisy-Roberts, 1996; Higgins et al., 1997).

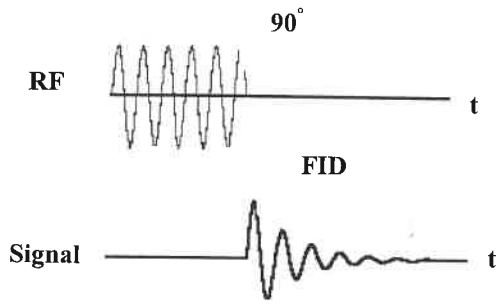

Figure 2.6: The free induction decay (FID) represents the signal amplitude induced into the receiver coil and the decay of that signal over time. A strong signal is acquired immediately after an RF pulse as a result of bringing all protons in phase. Over time, however, the protons dephase and signal is lost.

2.2.5 Relaxation

2.2.5.1 Transverse, T_2 or spin-spin relaxation

As previously mentioned, the application of a 90° RF pulse with frequency that exactly matches the precessional frequency of the protons excites these protons and so the net longitudinal magnetization tilts away from the main field by 90°. In addition, the RF pulse forces the protons to precess coherently (English and Moore, 1995; Farr and Allisy-Roberts, 1996). As a result, the transverse component of their magnetic moments (*the m_{xy} vectors*) will, on average, point in one direction and add up to a net transverse magnetic vector (M_{xy}), which rotates in the XY plane at the Larmor frequency. Consequently, the net magnetization becomes no longer longitudinal but transverse. Whilst the RF pulse is applied the protons precess in phase and their combined magnetic moments give the maximum signal. Once the RF pulse is turned off, the protons begin to precess independently with the rate of their precession depending on the strength of the effective magnetic field experienced by the individual protons. The reasons why the individual protons experience minute differences in the effective or local magnetic field are the inevitable small inhomogeneities in the external magnetic field even in modern magnets. Additionally, the magnetic moments of the individual protons interact with those of the nearby protons (English and Moore, 1995). As a result, the protons precess at different rates, some precessing faster and some slower, and the energy is exchanged among neighbouring spins, hence the name spin-spin relaxation (Newhouse and Wiener, 1991; Brown and Semelka, 1995; English and Moore, 1995; Edelman et al., 1996; Farr and Allisy-Roberts, 1996; Higgins et al., 1997). Thus, the protons tend to dephase and their m_{xy} vectors cancel each other out in pairs. The net transverse magnetization therefore decreases or decays, until there is eventually no longer any net transverse magnetization (Figure 2.7) (Newhouse and Wiener, 1991; Brown and Semelka, 1995; English and Moore, 1995; Edelman et al., 1996; Farr and Allisy-Roberts, 1996; Higgins et al., 1997).

The signal induced by the transverse magnetization decreases with a time constant T_2 (Newhouse and Wiener, 1991; Brown and Semelka, 1995; English and Moore, 1995; Edelman et al., 1996; Farr and Allisy-Roberts, 1996; Higgins et al., 1997), which is the time constant the MRI signal takes to fall to 37% of its maximum value (Farr and Allisy-Roberts, 1996). Thus, after two T_2 time constants, only 14% of the signal remain and after three T_2 time constants, only 5% of the signal remain (Farr and Allisy-Roberts, 1996).

It is noteworthy that T_2 is longer for liquids than for solids. Understandably, the MR signal decays more slowly in tissues with longer T_2 values.

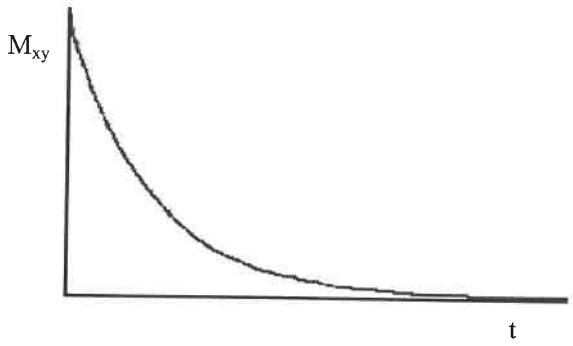

Figure 2.7: The diminution of the net tissue's transverse magnetization (M_{xy}) as a function of time (t). Immediately after the application of a 90° RF pulse, the spins have the same phase and produce the detectable MR signal. Once the RF pulse has been terminated, a phase angle (θ) develops over time between the precessing protons and partial dephasing of the spins occurs and the signal decays. Eventually, complete dephasing of the signal occurs and the signal disappears.

2.2.5.1.1 T_2* effect

Even with modern magnet design, it is impossible to achieve complete homogeneity of the magnetic field. As a result of this inevitable inhomogeneity, protons lose phase coherence more quickly than it would if the field were completely homogeneous (Figure 2.8) (Newhouse and Wiener, 1991; Brown and Semelka, 1995; English and Moore, 1995; Edelman et al., 1996; Farr and Allisy-Roberts, 1996; Higgins et al., 1997). The time taken for the loss of the transverse magnetization under these circumstances is known as the time constant T_2*. The effect of T_2* can be overcome by using a special pulse sequence when performing an MR scan.

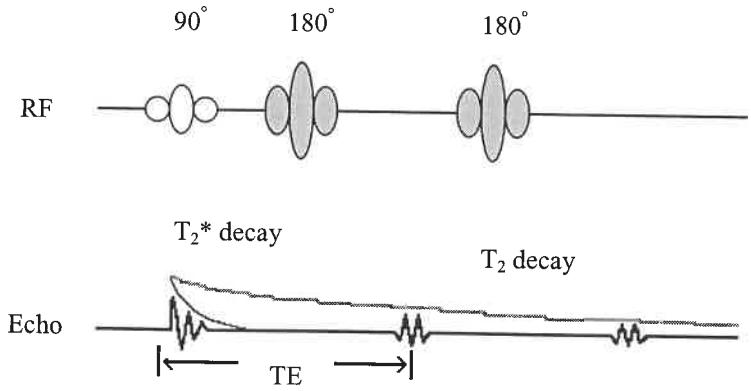

Figure 2.8: Because of the inhomogeneity of the magnetic environment caused by the spatial variation of the external and the magnetic interactions among neighbouring spins, the net transverse magnetization decays much faster at a rate characterized by T_2*. If a spin echo is used, signal is, then, lost at a rate characterized by T_2.

2.2.5.2 Longitudinal, T_1 or spin-lattice relaxation

Immediately after the RF pulse is switched off, the excited protons begin to return, some earlier than others, from the high-energy anti-parallel or anti-aligned orientation to their original low energy aligned or parallel direction (Newhouse and Wiener, 1991; Brown and Semelka, 1995; English and Moore, 1995; Edelman et al., 1996; Farr and Allisy-Roberts, 1996; Higgins et al., 1997). This occurs as a result of T_1 relaxation, which is also called spin-lattice relaxation as nuclear magnetic resonance was originally used to examine solids whose component particles took the form of a lattice and the spins lose energy to the lattice on their return to their original low energy position.

Thus, T_1 relaxation is associated with recovery of the longitudinal net magnetization and its returns to its original state of M_0 again in the direction of the main magnetic field. The net magnetization increases relatively slowly and does so exponentially with a time constant T_1 (Newhouse and Wiener, 1991; Brown and Semelka, 1995; English and Moore, 1995; Edelman et al., 1996; Farr and Allisy-Roberts, 1996; Higgins et al., 1997) (Figure 2.9), which the time constant needed for 63 % of the excited protons to return to their original initial resting state. Thus, longitudinal magnetization is recovered 63%, 87%, and 95% after 1 T_1, 2 T_1, 3 T_1 constants respectively.

T_1 is dependent on the main magnetic field strength as well as chemical and physical properties of the environment in which the protons reside. Higher magnetic fields are associated with longer T1 times (Newhouse and Wiener, 1991; English and Moore, 1995; Farr and Allisy-Roberts, 1996). An important point relevant in this context is that the longitudinal magnetizations of tissues with shorter T_1 relaxation times recovers more quickly than those of tissues with longer T_1 relaxation times.

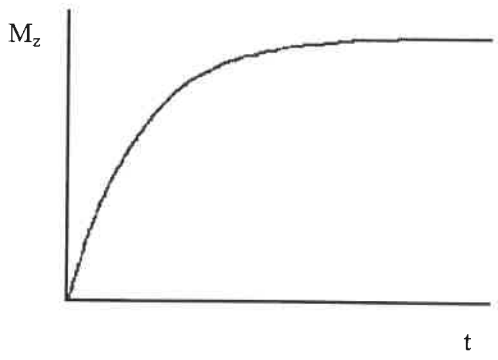

Figure 2.9: The recovery of the tissue's longitudinal magnetization (M_z) as a function of time (t). Immediately after excitation there is no longitudinal magnetization. When the stimulating RF pulse is turned off, the excited protons relax back to their resting state and the longitudinal magnetization recovers towards the maximal value (M_0) at a rate determined by the T_1 relaxation time.

2.2.5.2 Longitudinal, T_1 or spin-lattice relaxation

Immediately after the RF pulse is switched off, the excited protons begin to return, some earlier than others, from the high-energy anti-parallel or anti-aligned orientation to their original low energy aligned or parallel direction (Newhouse and Wiener, 1991; Brown and Semelka, 1995; English and Moore, 1995; Edelman et al., 1996; Farr and Allisy-Roberts, 1996; Higgins et al., 1997). This occurs as a result of T_1 relaxation, which is also called spin-lattice relaxation as nuclear magnetic resonance was originally used to examine solids whose component particles took the form of a lattice and the spins lose energy to the lattice on their return to their original low energy position.

Thus, T_1 relaxation is associated with recovery of the longitudinal net magnetization and its returns to its original state of M_0 again in the direction of the main magnetic field. The net magnetization increases relatively slowly and does so exponentially with a time constant T_1 (Newhouse and Wiener, 1991; Brown and Semelka, 1995; English and Moore, 1995; Edelman et al., 1996; Farr and Allisy-Roberts, 1996; Higgins et al., 1997) (Figure 2.9), which the time constant needed for 63 % of the excited protons to return to their original initial resting state. Thus, longitudinal magnetization is recovered 63%, 87%, and 95% after 1 T_1, 2 T_1, 3 T_1 constants respectively.

T_1 is dependent on the main magnetic field strength as well as chemical and physical properties of the environment in which the protons reside. Higher magnetic fields are associated with longer T1 times (Newhouse and Wiener, 1991; English and Moore, 1995; Farr and Allisy-Roberts, 1996). An important point relevant in this context is that the longitudinal magnetizations of tissues with shorter T_1 relaxation times recovers more quickly than those of tissues with longer T_1 relaxation times.

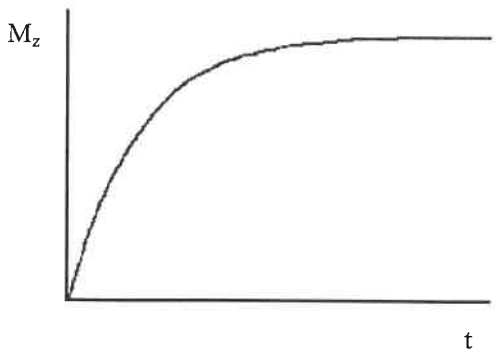

Figure 2.9: The recovery of the tissue's longitudinal magnetization (M_z) as a function of time (t). Immediately after excitation there is no longitudinal magnetization. When the stimulating RF pulse is turned off, the excited protons relax back to their resting state and the longitudinal magnetization recovers towards the maximal value (M_0) at a rate determined by the T_1 relaxation time.

2.2.6 MRI hardware

MRI experiments require the following basic components, each of which is considered in turn:

1. The Main Magnet
2. Shim Coils
3. Gradient Coils
4. RF (transmitter/receiver) Coils
5. Computer

2.2.6.1 The main magnet

The main magnet is the basic component of an MRI scanner (Newhouse and Wiener, 1991; Brown and Semelka, 1995; English and Moore, 1995; Edelman et al., 1996; Farr and Allisy-Roberts, 1996; Higgins et al., 1997). Magnets are of different designs and magnetic field strengths and are available in a variety of shapes and sizes (Brown and Semelka, 1995). Magnets used for clinical imaging have magnetic field strengths somewhere between 0.6 to 2.0 Tesla (T), where 1 T = 10,000 G (Gauss). Their magnetic field has to be very homogeneous so as to minimize the loss of phase coherence shown by proton precession following application of the RF pulse. This homogeneity of the magnetic field can be improved by shimming. There are three types of main magnet:

(a) Permanent magnets: As the name suggests, permanent magnets are always magnetic. They are made of special rare earth alloys that have the capacity for retaining strong magnetic fields. Their major advantage is that they do not use any energy to generate the magnetic field. However, these magnets have limited field strengths of 0.2 to 0.3 T, which is their main disadvantage. Other disadvantages are their thermal instability as they are susceptible to changes in the ambient temperature, and their heavy weight (English and Moore, 1995; Farr and Allisy-Roberts, 1996).

(b) Resistive magnets: These magnets use electrical energy to generate their magnetic fields and are therefore also called electromagnets. In a resistive magnet, an electrical current is passed through a loop of wire and generates a magnetic field that persists as long as there is a flowing current. The main disadvantage of resistive magnets is that their magnetic field strengths are limited to less than 0.4 T because of their high power consumption and resistive heating. With very high field strengths, resistive magnets generate large quantities of heat that must be

dissipated. The main advantages of the resistive magnets are that they are the cheapest and smallest, weighing some 2 tons (English and Moore, 1995; Farr and Allisy-Roberts, 1996).

(c) Super-conducting magnets: At present, super-conducting magnets are the ones most widely used in MR machines with fields strengths more than 0.5 T. As resistive magnets, they also make use of electricity to generate their magnetic fields, but resistive heating is no more a problem as these magnets contain a special current carrying conductor cooled down to super-conducting temperature of –269° C. Cooling markedly reduces the resistance to the flow of electric current and at this particularly very low temperature the current conducting material practically loses all its resistance to electric current flow. So once an electrical current is established, it continues to flow and generates a constant magnetic field with high field strength and excellent homogeneity while using virtually no power. This is the main advantage of super-conducting magnets. The main disadvantages of the super-conducting magnets are their high costs, and the need for helium and nitrogen for cooling (English and Moore, 1995; Farr and Allisy-Roberts, 1996).

2.2.6.2 Shim coils

It is extremely important to ensure that the externally applied magnetic field, i.e. the principal field of the magnet, is as homogeneous as possible. In practice, this can be achieved by shimming, which is of two types:

(a) Active Shimming, in which direct current is passed through ten to twelve current-carrying shim coils placed within the bore of the main magnet. As each of these receives its own current, it generates its own magnetic field that is added to the main magnetic field, making it more homogeneous (English and Moore, 1995; Farr and Allisy-Roberts, 1996).

(b) Passive Shimming, in which homogeneity of the static magnetic field is improved by the placement of iron plates inside and/or outside the magnet bore in a standard configuration (English and Moore, 1995; Farr and Allisy-Roberts, 1996).

2.2.6.3 Gradient coils

Specific gradient coils are used to produce deliberate linear variations in the main magnetic field, i.e. changes in magnetic field with distance. Usually three pairs of gradient coils, one for each orthogonal direction (X, Y and Z directions) are used. In order to acquire a magnetic resonance image, direct current is passed through these three sets of coils and gradients are

switched on and off in a precisely timed manner according to the pulse sequence used. This is of particular importance as not only will it enable slice selection but it will also enable spatial encoding in the image to determine the exact location in the body from which each portion of the emitted radio frequency signal originates (Newhouse and Wiener, 1991; Brown and Semelka, 1995; English and Moore, 1995; Edelman et al., 1996; Farr and Allisy-Roberts, 1996; Higgins et al., 1997).

As a result of the application of these magnetic field gradients, each different point along the X, Y and Z directions experiences a slightly different magnetic field from other points and since the rate of precession of the protons is directly related to the magnetic field strength in which they are placed, protons at different points along the gradient will therefore precess at different frequencies depending on their sites (Newhouse and Wiener, 1991; Brown and Semelka, 1995; English and Moore, 1995; Edelman et al., 1996; Farr and Allisy-Roberts, 1996; Higgins et al., 1997).

2.2.6.4 RF (transmitter/receiver) coils

RF coils are effectively the antenna of the MRI system; they are responsible for transmitting the RF signal to the patient and/or receiving the emitted MR signal. Thus, RF coils can either be receive only, in which case the body-coil is used as a transmitter; or both transmit and receive (transceiver). In order to exchange energy effectively with the precessing protons, the RF coils must be accurately tuned to the resonant frequency of the protons.

2.2.6.5 Computer

All components of the hardware with the exception of the main magnet are under the control of a highly sophisticated computer system made of a pulse control module, image processor and systems manager (Newhouse and Wiener, 1991; Brown and Semelka, 1995; English and Moore, 1995; Edelman et al., 1996; Farr and Allisy-Roberts, 1996; Higgins et al., 1997).

2.2.7 Image generation

2.2.7.1 Cartesian co-ordinate system

MRI is superior to any other imaging technique in that it does not employ any form of ionizing radiation and, in addition, several images can be obtained simultaneously in a number of planes, at any angle without the need for moving the patient or experimental specimen (Newhouse and Wiener, 1991; Brown and Semelka, 1995; English and Moore, 1995; Edelman et al., 1996; Farr

and Allisy-Roberts, 1996; Higgins et al., 1997). It is possible to define these planes by using the conventional three-dimensional Cartesian coordinate system. By convention, the Z-axis runs along the long axis of the MRI magnet. The X-axis is horizontal and goes from side to side where as the Y-axis is vertical. The X and Y-axes define the trans-axial plane. On the other hand, the coronal and the sagittal planes are defined by the Z and X-axes and the Y and Z-axes respectively.

2.2.7.2 Slice selective excitation and the slice-selecting gradient

In order to image a particular slice in a patient, a one-dimensional linear magnetic field gradient called a slice-selecting gradient is deliberately applied in the direction perpendicular to the plane of the slice to be imaged. This slice-selecting gradient (Figure 2.10) is switched on during the period that the RF pulse is transmitted (Newhouse and Wiener, 1991; Brown and Semelka, 1995; English and Moore, 1995; Edelman et al., 1996; Farr and Allisy-Roberts, 1996; Higgins et al., 1997). The application of this magnetic field gradient is of particular importance as it allows selective excitation of protons in a particular plane through the patient. As gradient fields can be superimposed on the main magnetic field in any direction by simply activating the appropriate gradient coils, images can be obtained simultaneously in a number of planes, at any angle without the need for moving the patient.

A transverse slice can be obtained by applying an RF pulse with the slice-selecting magnetic field gradient in the Z-direction. With a slice-selecting gradient applied in the Y-direction a coronal slice is obtained whereas when it is applied in the X-direction a sagittal slice is selected.

The application of the slice–selecting gradient causes protons at different sites along its axis to precess at different precessional frequencies according to the effective magnetic field strengths to which they are exposed. The protons in the selected slice will precess with a narrow range of frequencies. In order for the RF pulse to excite these protons and to exchange energy with them, the RF transmitter should be accurately tuned to generate an RF pulse that contains a small range of frequencies (a narrow band width) that essentially match the range of frequencies of the protons in the selected slice i.e. the RF pulse and the protons in the selected slice should be in resonance (Newhouse and Wiener, 1991; Brown and Semelka, 1995; English and Moore, 1995; Edelman et al., 1996; Farr and Allisy-Roberts, 1996; Higgins et al., 1997). This ensures that only protons in the selected slice will be excited and only those protons will flip and eventually produce an MR signal.

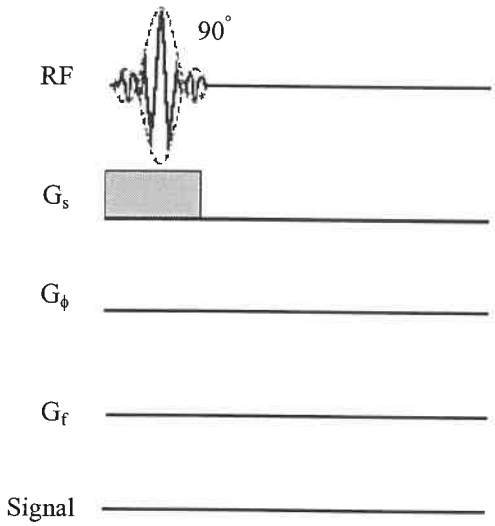

Figure 2.10: Diagrammatic representation of the slice-selecting gradient (G_s). The slice-selecting gradient is applied with the RF pulse to excite the protons from a single slice selectively.

2.2.7.3 Frequency-encoding, read-out or X-axis gradient

After slice selection, in order to generate an MRI image for that selected slice and to determine which voxel each portion of the emitted RF signal comes from, two other magnetic field gradients are applied, the frequency-encoding and the phase-encoding gradients. These two gradients are applied across the edges of the selected slice perpendicular to one another.

The frequency-encoding gradient is activated during the time that an MRI signal echo is being received and hence it is also called the read-out gradient (Figure 2.11). The application of the frequency-encoding gradient is very important for spatial-encoding as it identifies lines or columns of pixels within the selected slice (Newhouse and Wiener, 1991; Brown and Semelka, 1995; English and Moore, 1995; Edelman et al., 1996; Farr and Allisy-Roberts, 1996; Higgins et al., 1997).

With a transverse slice, the frequency-encoding gradient is usually applied in the X-direction during the detection or acquisition of the MR signal. This produces a magnetic field gradient from side to side, in the X-direction. Accordingly, protons in each different column of voxels along the X-direction will effectively experience different magnetic field strengths from other columns but protons within each particular column of voxels will experience the same magnetic field strength, and emit MR signals of the same frequency (Figure 2.12) (Newhouse and Wiener, 1991; Brown and Semelka, 1995; English and Moore, 1995; Edelman et al., 1996; Farr and Allisy-Roberts, 1996; Higgins et al., 1997).

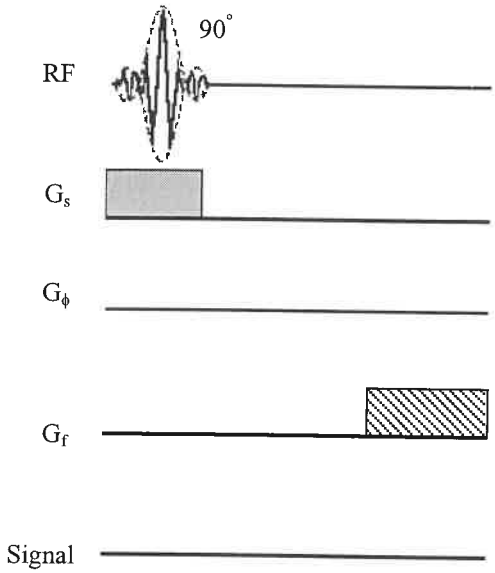

Figure 2.11: Diagrammatic representation of the frequency-encoding gradient (read-out gradient) (G_f). G_ϕ is the phase-encoding gradient described in section 2.3.7.4.

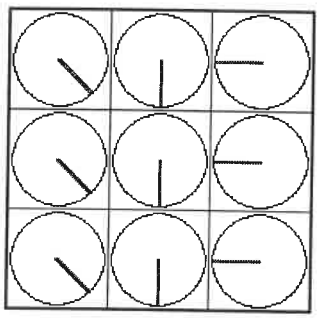

Figure 2.12: Diagram represents columns of transversal magnetic vectors, each precessing with different frequencies. As a result of the application of the frequency-encoding gradient during the detection of the MRI signal, spatial position along the X-axis is encoded into the frequency content of the signal.

2.2.7.4 Phase-encoding or Y-axis gradient

The frequency-encoding gradient performs spatial-encoding in only one axis of the imaged slice and this, understandably, will not be sufficient to generate an MRI image. This necessitates the application of another magnetic field gradient across the selected slice plane in the direction perpendicular to the frequency-encoding gradient. This magnetic field gradient is referred to as the phase-encoding gradient and is switched on in the time between slice excitation and signal collection (Figure 2.13), i.e. after the excitation of the slice but before the frequency-encoded readout (Newhouse and Wiener, 1991; Brown and Semelka, 1995; English and Moore, 1995; Edelman et al., 1996; Farr and Allisy-Roberts, 1996; Higgins et al., 1997).

With a transverse slice with the frequency-encoding gradient applied in the X-direction, the phase-encoding gradient is applied in the Y-direction. This produces a magnetic field gradient from the front to the back of the patient, in the Y-direction across the other edge of the selected slice. The result is that protons would precess at different frequencies in the Y-direction during the application of the phase-encoding gradient. Consequently, the protons will accumulate a net phase shift at the end of the phase-encoded pulse. Immediately after the phase-encoding gradient is turned off the protons begin once again to precess according to the magnetic field strength to which they are exposed. The application of the phase-encoding gradient is repeated a number of times, with the strength of the gradient increased a little each time (Newhouse and Wiener, 1991; Brown and Semelka, 1995; English and Moore, 1995; Edelman et al., 1996; Farr and Allisy-Roberts, 1996; Higgins et al., 1997). In this case, the result of the subsequent application of the frequency-encoding gradient during the acquisition of the MR signal is that protons in the different columns of voxels along the X-direction will precess at different frequencies. However, protons in each particular column will effectively precess at the same frequency but at different phases. This is particularly important is order to achieve spatial-encoding for all the constituent voxels of the selected slice.

The total acquisition time is directly related to number of the phase-encoding steps. Other factors that determine the total acquisition time include the repeat time (TR) and the number of signal averages (NSA) (Newhouse and Wiener, 1991; Brown and Semelka, 1995; English and Moore, 1995; Edelman et al., 1996; Farr and Allisy-Roberts, 1996; Higgins et al., 1997).

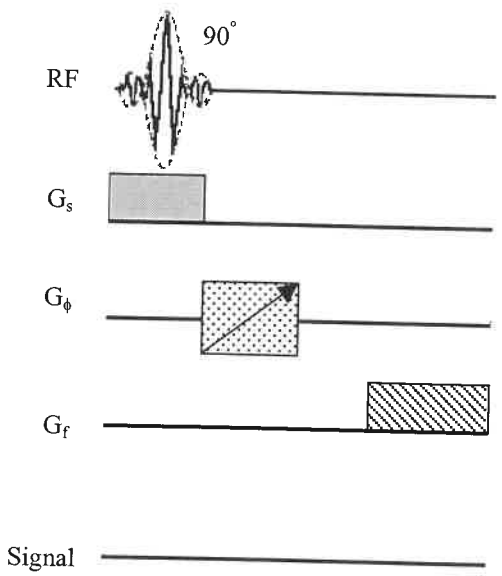

Figure 2.13: Diagrammatic representation of the phase-encoding gradient (G_ϕ). The phase-encoding gradient is applied many times during imaging depending on image matrix. Different phase-encoding steps use different gradient amplitude.

2.2.7.5 Fourier transformation

With the application of the phase encoding and frequency encoding gradients, the MR signal emitted by the constituent voxels of the selected slice is actually a multitude of spectrum of phases as well as frequencies. This complex MR signal is sampled and analyzed by a computer using a mathematical process called Fourier transform (FT). This is of crucial importance in spatial-encoding in order to determine the exact location in the body from which each portion of the emitted radio frequency signal comes from. The FT is, therefore, applied to each frequency-encoded line of data (Newhouse and Wiener, 1991; Brown and Semelka, 1995; English and Moore, 1995; Edelman et al., 1996; Farr and Allisy-Roberts, 1996; Higgins et al., 1997).

2.2.8 MRI pulse sequences

2.2.8.1 Spin echo (SE) sequence

The spin echo pulse sequence is the most commonly used pulse sequence. As previously mentioned (2.3.5.1.1), because of the inevitable inhomogeneity of both the external magnetic field and the deliberately applied magnetic field gradients, the protons lose phase coherence more quickly than would be the case if these magnetic fields were completely homogeneous (Newhouse and Wiener, 1991; Brown and Semelka, 1995; English and Moore, 1995; Edelman et al., 1996; Farr and Allisy-Roberts, 1996; Higgins et al., 1997). As a result of that, the MR or "free induction decay" (FID) signal decays very quickly with the time constant T_2* and cannot be measured in practice. It is possible to compensate for the inhomogeneity of the static magnetic field and thus to overcome the effect of T_2* by using a spin echo (SE) pulse sequence when performing an MR scan. However, SE will not eliminate the effect of the inhomogeneity of the internal magnetic environment of the protons that causes the T_2 effect i.e. decay of the signal with the time constant T_2.

In the SE pulse sequence (Figure 2.14), each 90° pulse is followed by a 180° pulse after a time (t) seconds. The idea of using the 180° pulse is to rephase the protons, therefore it is often called the rephasing or refocusing pulse (Newhouse and Wiener, 1991; Brown and Semelka, 1995; English and Moore, 1995; Edelman et al., 1996; Farr and Allisy-Roberts, 1996; Higgins et al., 1997). As a result, M_{xy} and the MR signal re-grow. After a further and equal time (t) seconds, M_{xy} and the MR signal will be at their peak as it is after this time that the protons would be once again completely in phase coherence. The time interval between the application of the 90° RF pulse and complete rephasing of the protons in the SE pulse sequence is known as the echo time or TE, which is equal to 2 *t*. The time between consecutive 90° pulses is the repeat time (TR). As

the SE pulse sequence does not eliminate the T_2 effect, the protons fall out of phase again, and M_{xy} and the MR signal decay with the time constant T_2.

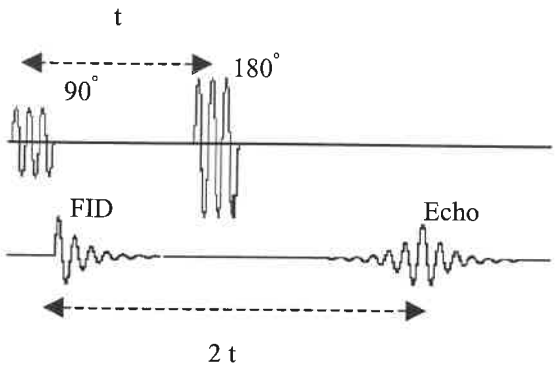

Figure 2.14: Diagrammatic representation of one cycle of the SE pulse sequence. After a 90°-excitation RF pulse, a 180° rephasing pulse is applied after a time t. A spin echo occurs at TE, which is equal to 2 t.

2.2.8.1.1 Tissue contrast and weighted images

In the SE pulse sequence, it is possible to obtain spin-echo MR images that are T_1-weighted, T_2-weighted or proton density-weighted by manipulating the TR and TE (Newhouse and Wiener, 1991; Brown and Semelka, 1995; English and Moore, 1995; Edelman et al., 1996; Farr and Allisy-Roberts, 1996; Higgins et al., 1997). This is simply because the different tissues of the body have different proton densities and T_1 and T_2 relaxation times. A short TR is one that is about as short as the shortest T_1 in which we are interested. A long TR is approximately three times as long as a short TR. In practice, a TR of less than 500 ms is considered to be short and a TR of more than 1500 ms to be long. A short TE is one that is as short as possible and a long TE is about 3 times as long. A TE of less than 30 ms is considered to be short and a TE greater than 80 ms is considered to be long in a clinical setting.

A fairly short TR produces maximum contrast between tissues of different T_1. A fairly short TE (30 ms) is also used in order to minimize the effect of T_2 on contrast. In general, the shorter is T_1, the stronger the signal and the brighter the pixel will be in the image (Newhouse and Wiener, 1991; Brown and Semelka, 1995; English and Moore, 1995; Edelman et al., 1996; Farr and Allisy-Roberts, 1996; Higgins et al., 1997).

In contrast, a fairly long TE produces maximum contrast between tissues of different T_2. However, TE must not be so long that the signal is so small as to be obscured by background noise. A fairly long TR is also used in order to minimize the effect of T_1 on contrast. In general, the longer is T_2, the stronger the signal and the brighter the pixel will appear in the image

(Newhouse and Wiener, 1991; Brown and Semelka, 1995; English and Moore, 1995; Edelman et al., 1996; Farr and Allisy-Roberts, 1996; Higgins et al., 1997).

Finally, a fairly long TR and a TE as short as possible produce maximum contrast between tissues of different poroton densities. This practically eliminates the effects of T_1 and T_2 and image contrast is then principally due to differences in the proton densities of the tissues. In general, the greater the proton density, the stronger the signal and the brighter the pixel will appear in the image (Newhouse and Wiener, 1991; Brown and Semelka, 1995; English and Moore, 1995; Edelman et al., 1996; Farr and Allisy-Roberts, 1996; Higgins et al., 1997).

2.2.8.2 Inversion recovery (IR) sequence

The IR pulse sequence is a very useful way of accentuating T_1-weighting. In this sequence, an initial 180° RF pulse is used (Newhouse and Wiener, 1991; Brown and Semelka, 1995; English and Moore, 1995; Farr and Allisy-Roberts, 1996; Higgins et al., 1997). This rotates the net tissue's longitudinal magnetization away from the main magnetic field by an angle of 180° i.e. M_0 is reversed. Immediately after the 180° RF pulse is switched off the excited protons begin to lose energy to the surrounding and return from the high-energy state to the low-energy state as a result of the T_1 effect. M_0 will then recover and reverse its direction (Farr and Allisy-Roberts, 1996). After a variable time called time to inversion (TI), a 90° RF pulse is applied (Figure 2.15). This causes the available M_0 to rotate away from the main field by 90° degrees and as a result, the net magnetization will be transverse (M_{xy}). When the 90° RF pulse is over, the M_{xy} vector so produced continues for a while to rotate in the transverse XY plane, producing an MR signal that will decay because of the T_2 effect. To generate an echo signal, a second 180° pulse is then used.

In the IR pulse sequence, the signal obtained depends on the strength of the longitudinal magnetization immediately before the application of the 90° pulse, which in turn is dependent on T_1. So the result is a T1-weighted image (Newhouse and Wiener, 1991; Brown and Semelka, 1995; English and Moore, 1995; Farr and Allisy-Roberts, 199; Higgins et al., 1997).

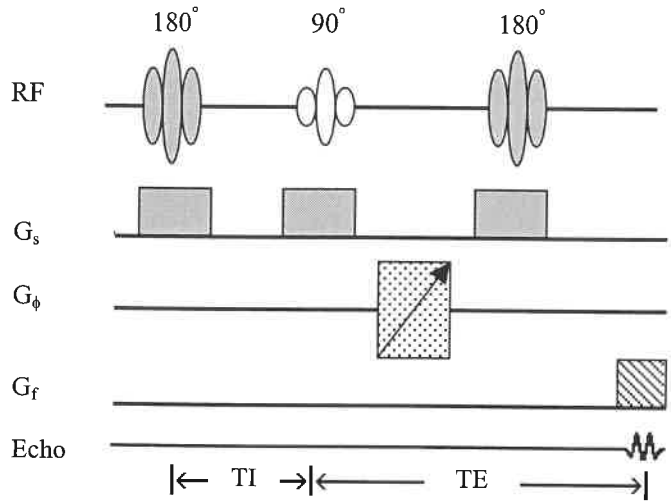

Figure 2.15: Diagrammatic representation of one cycle of the IR pulse sequence. A 180° RF pulse is used to invert M_0. Soon after the 180° is terminated, M_0 recovers with a time constant T_1. After TI, a 90° RF pulse is applied to rotate the available M_z 90°, thus converting it into transverse magnetization. A 180° refocusing pulse is then used. In IR sequence, TE is the time interval between the application of the 90° RF pulse and the acquisition of the MR signal.

2.2.8.3 Short-TI inversion recovery (STIR) sequence for fat suppression

This pulse sequence is particularly useful for fat suppression (Farr and Allisy-Roberts, 1996). The initial 180° pulse is followed after a short interval by a 90° pulse. The 180° pulse temporarily reverses the net magnetic vector M_0 of both fat and water protons. When this RF pulse is over, the excited protons begin to lose energy to the surroundings and return from the high-energy state to their original low energy state and M_0 recovers. Because of the shorter T_1 of fat the M_0 recovers more quickly in fat than in water. After about 120 ms approximately half the protons in fat would have reverted to the parallel position, and accordingly its $M_0 = 0$ (Farr and Allisy-Roberts, 1996). In contrast, after this particular time, few of the protons in water would have reverted to the parallel orientation. Thus, after that particular time, water will still have some inverted M_0. The application of a 90° pulse at this instant, understandably, produces a signal from water and other tissues but none from fat.

2.3.8.4 Gradient (recalled) echo sequence (GRE)

In GRE, 90° RF pulses are not usually used, rather RF pulses that cause "flip angles" smaller than 90° are used (Figure 2.16) (Newhouse and Wiener, 1991; Brown and Semelka, 1995; English and Moore, 1995; Edelman et al., 1996; Farr and Allisy-Roberts, 1996; Higgins et al., 1997). With flip angles smaller than 90°, the longitudinal magnetization is not totally abolished.

Accordingly, there will be always a substantial amount of longitudinal magnetization left, that can be "tilted" by the next pulse. Further, a magnetic field gradient rather than a 180° RF pulse is used to refocus the dephasing protons. This is switched on for a very short time. Then it is switched off, and after a short time turned back on with the same strength, but in opposite direction. With GRE, the TR's are thus shortened making imaging faster.

In the GRE, increasing the flip angle leads to an increase in the amount of longitudinal magnetization that must recover an as recovery of longitudinal magnetization is T_1-dependent, increasing the flip angle thus increases any differences that might be due to tissues having different T_1 values. Lowering the flip angle has opposite effects. It, therefore, follows that the flip angle controls the degree of T_1 contrast in gradient echo pulse sequences.

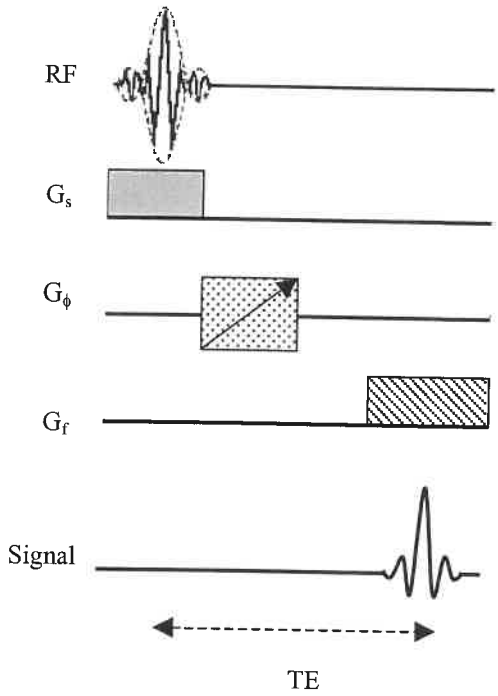

Figure 2.16: Diagrammatic representation of one cycle of the GRE pulse sequence. For standard gradient echo sequences, a single RF pulse with a reduced flip angle is used. The idea is to obtain transverse magnetization and to maintain a substantial amount of M_z at the same time to be tilted by the next pulse.

2.2.9 Characteristics of the magnetic resonance image

2.2.9.1 Signal to noise ratio (S/N ratio)

The S/N ratio is a measure of how grainy the MRI image appears. The greater the noise the smaller the MR signal appears and the more grainy the image will be. Noise has a deleterious effect on the quality of the MRI image as it reduces and obscures contrasts between tissues

(Newhouse and Wiener, 1991; Brown and Semelka, 1995; English and Moore, 1995; Edelman et al., 1996; Farr and Allisy-Roberts, 1996; Higgins et al., 1997).

In nearly all clinical scanners, most of the noise results from the presence of the patient. The so called white noise actually results from currents having a wide range of radiofrequencies induced in the receiver coils by the thermal motion of the hydrogen atoms in the tissues being imaged. Noise may also be due to machine factors.

The S/N ratio can be improved by either increasing the signal or reducing the noise or both.

The signal can be increased by:

(a) Increasing voxel size by increasing the field of view or slice thickness;
(b) Decreasing TE;
(c) Increasing TR;
(d) Increasing the flip angle; or
(e) Using a machine with higher field strength (Farr and Allisy-Roberts, 1996).

The noise can be decreased by:

(a) Increasing the number of averages (the number of excitations, NEX); or
(b) Reducing the bandwidth of the receiver so that it picks up less of the spectrum of the noise frequencies (Farr and Allisy Roberts, 1996).

2.2.9.2 Resolution

Spatial resolution is a measure of how "sharp" the MRI image looks (Newhouse and Wiener, 1991; Brown and Semelka, 1995; English and Moore, 1995; Edelman et al., 1996; Farr and Allisy-Roberts, 1996; Higgins et al., 1997). Low resolution is indicated by either fuzzy edges or a pixelly appearance to the image.

In MRI, spatial resolution is usually defined by the following equation:

$$\text{Pixel} = \text{Field of views (FOV)/matrix} \tag{2.2}$$

2.2.9.3 Time

The acquisition time for a conventional SE or Gradient echo sequence is, understandably, the product of the TR, phase-encoding steps, and number of averages (TR X phase steps X NEX)

(Newhouse and Wiener, 1991; Brown and Semelka, 1995; English and Moore, 1995; Edelman et al., 1996; Farr and Allisy-Roberts, 1996; Higgins et al., 1997).

In nearly all clinical scanners, most of the noise results from the presence of the patient. The so called white noise actually results from currents having a wide range of radiofrequencies induced in the receiver coils by the thermal motion of the hydrogen atoms in the tissues being imaged. Noise may also be due to machine factors.

The S/N ratio can be improved by either increasing the signal or reducing the noise or both.

The signal can be increased by:

(a) Increasing voxel size by increasing the field of view or slice thickness;
(b) Decreasing TE;
(c) Increasing TR;
(d) Increasing the flip angle; or
(e) Using a machine with higher field strength (Farr and Allisy-Roberts, 1996).

The noise can be decreased by:

(a) Increasing the number of averages (the number of excitations, NEX); or
(b) Reducing the bandwidth of the receiver so that it picks up less of the spectrum of the noise frequencies (Farr and Allisy Roberts, 1996).

2.2.9.2 Resolution

Spatial resolution is a measure of how "sharp" the MRI image looks (Newhouse and Wiener, 1991; Brown and Semelka, 1995; English and Moore, 1995; Edelman et al., 1996; Farr and Allisy-Roberts, 1996; Higgins et al., 1997). Low resolution is indicated by either fuzzy edges or a pixelly appearance to the image.

In MRI, spatial resolution is usually defined by the following equation:

$$\text{Pixel} = \text{Field of views (FOV)/matrix} \tag{2.2}$$

2.2.9.3 Time

The acquisition time for a conventional SE or Gradient echo sequence is, understandably, the product of the TR, phase-encoding steps, and number of averages (TR X phase steps X NEX)

(Newhouse and Wiener, 1991; Brown and Semelka, 1995; English and Moore, 1995; Edelman et al., 1996; Farr and Allisy-Roberts, 1996; Higgins et al., 1997).

2.2.9.4 Relaxation effects

T1 and T2 relaxation rates affect the S/N ratio in an MRI image. Increasing the TR up to about 3-5 T1 times improves S/N ratio, as the longitudinal magnetization would have time to recover. On the other hand increasing the TE decreases the S/N ratio secondary to T_2 effects in SE sequences, and T_2* effects in gradient echo sequences (Newhouse and Wiener, 1991; Brown and Semelka, 1995; English and Moore, 1995; Edelman et al., 1996; Farr and Allisy-Roberts, 1996; Higgins et al., 1997).

CHAPTER 3
CARDIOVASCULAR CONSEQUENCES OF DIABETES MELLITUS

3.1 Introduction

Diabetes mellitus represents a heterogeneous group of chronic metabolic disorders of high prevalence all over the world. It is characterized by a persistent inappropriate hyperglycaemia, in which the blood glucose level is persistently elevated above the normal range. Diabetes occurs as a result of either an absolute deficiency of secreted insulin (Type I or insulin-dependent diabetes mellitus; IDDM) or a relative insulin deficiency and an insulin resistance (Type II or non-insulin-dependent diabetes mellitus; NIDDM) (Weir, et al 1981). In addition to the persistent hyperglycaemia, diabetes is also associated with a wide range of metabolic abnormalities. These range from the acute development of ketoacidosis when there is a severe lack of insulin, to longer-term alterations of lipid and protein turnover. Diabetes mellitus is thus considered to be a multi-component hereditary disease involving all aspects of intermediary metabolism including carbohydrates, proteins, and fats. Nevertheless, a clinical diagnosis of diabetes is based upon demonstration of a persistent hyperglycaemia.

Prolonged diabetes mellitus is associated with many systemic complications that remain its major cause of morbidity and mortality despite modern advances in management. This constellation of abnormalities involving various organs is thought to accumulate through the years of diabetic life and culminate in the late diabetic syndrome.

3.2 Diabetic vascular disease

Epidemiological studies demonstrate that diabetes mellitus is an important risk factor predisposing to the development of premature and accelerated disorder of large blood vessels, a condition known as macrovascular disease. Several reports have confirmed that diabetes is

associated with a substantial increase in the susceptibility to coronary artery disease (Crall and Roberts, 1978; Jarrett 1979; Kannel, 1985).

Although a great deal of information is available about diabetes mellitus and its complications, there is some disagreement about the precise nature of the large vessel disease in diabetes. Some investigators have suggested that atherosclerosis simply is the predominant large vessel disturbance seen among patients with diabetes (Schwartz et al., 1992). Heickendorff et al. (1994) have more recently suggested that the macrovascular disease seen in diabetic patients is not simply synonymous with atherosclerosis. They suggest that a specific diabetic macroangiopathy coexists with the atherosclerosis itself even if enhanced atherosclerosis and its sequelae might remain the main cause for clinically manifest macrovascular disease among diabetic patients.

Nevertheless, it is noteworthy that diabetes is associated with marked quantitative increase in the extent of atherosclerosis. The Framingham study demonstrates a substantially increased susceptibility in diabetic patients to atherosclerotic disease of the heart, legs, and brain (Kannel and McGee, 1979). Diabetics were found to have a twofold to threefold increased risk of clinical atherosclerotic disease. Moreover, macroangiopathy tends to become clinically obvious at an earlier age. Of particular interest is that the excess risk of experiencing clinical atherosclerotic disease and dying from a coronary heart disease event is substantially greater in diabetic women (Jarett, 1977; Kannel and McGee, 1979). This contrasts with the fact that male sex is one of the best-documented and most consistent risk factors for coronary atherosclerosis.

There is also the important question as to whether patients with IDDM and NIDDM differ in their predisposition to macrovascular disease. Unfortunately, most studies do not always distinguish IDDM from NIDDM. Nevertheless, it is worthy noting that variations in susceptibility to macrovascular disease with diabetes mellitus may have a genetic basis and may reflect differences in the nature of the underlying metabolic disturbances. In addition, the increased prevalence of vascular disease with diabetes is strongly reinforced by many additional risk factors. A number of these; namely obesity, hypertension, hyperlipidaemia, and cigarette smoking have become well established to be related to the incidence of clinical vascular disease in epidemiological studies. Many of the modern views of these risk factors stem from the Framingham heart study (Kannel and McGee, 1979). An eventual understanding of the pathogenesis of diabetic macrovascular disease would greatly help in providing the correct basis for improving its prevention and management.

Diabetes mellitus is also known to be associated with an increased incidence of small vessel disease (microangiopathy) seen as retinopathy, nephropathy and neuropathy. The end results of diabetic retinopathy and nephropathy are blindness and renal failure (Stehouwer et al., 1997).

One very important observation is the fact that the extent of microangiopathy in both IDDM and NIDM appears to be primarily related to the severity and duration of hyperglycemia and that meticulous glycaemic control markedly reduces its progression (Hanseen et al., 1986). In contrast, there is relatively little information concerning the relationship between effectiveness of diabetic control and the extent and progression of macrovascular disease. Lemp et al. (1987), in their retrospective study exploring the relation between the severity of diabetes and the risk of significant coronary artery disease, found that patients treated with insulin had the highest risk of coronary artery disease followed by patients treated by oral hypoglycaemic drugs and lastly patients treated with diet alone. Thus, severity of diabetes was an important predictor of coronary artery disease. In contrast, no correlation was found between the age at onset or duration of diabetes and the risk of significant coronary artery disease.

3.3 Diabetic cardiac disease

Ischaemic heart disease as consequence of coronary artery atherosclerosis is by far the most important cardiac complication of diabetes. Diabetes mellitus appears to increase the risk of ischaemic heart disease independently of the usual cardiovascular risk factors for coronary artery disease (Kannel, 1985). However, diabetes also leads to myocardial dysfunction and cardiac autonomic neuropathy. Diabetes has also been associated with the existence of a specific heart disease, termed diabetic cardiomyopathy (Goodwin and Oakley, 1972; Rubler et al., 1972; Hamby et al., 1974; Kannel et al., 1974).

Most of the information we have concerning the prevalence and severity of coronary artery disease in patients with diabetes mellitus come from the Framingham heart study, which was a large population study initiated in 1948 and involved a cohort of 5209 diabetic men and women from the Tecumseh and Framingham communities in the U.S.A. The patients involved in this study were aged 30-62 years at the initial examination and were followed up biennially for cardiovascular events, which were related to prior evidence of diabetes (Kannel and McGee, 1979). The Framingham study identified macrovascular disease as the chief cause of morbidity and mortality among diabetics. Such diabetics; in particular females, showed increased incidences of cardiovascular diseases and greater risk of congestive heart failure and

cardiovascular disease death (Kannel and McGee, 1979). Furthermore, this higher risk was independent of the usual risk factors for coronary heart disease (Kannel, 1985).

However, several reports (Rubler et al., 1972) have reported that cardiomegaly and congestive heart failure can occur in diabetics with normal coronary arteries. Such abnormalities have been attributed to a diabetic cardiomyopathy (Rubler et al., 1972; Hamby et al., 1974) that has been also termed a "diabetic specific cardiac muscle disorder" (Goodwin and Oakley, 1972).

Finally, diabetes impairs function in both peripheral and autonomic nerves leading to several clinical manifestations, collectively referred to as diabetic neuropathy. This may occur in as many as 40 % of diabetic patients (Ewing and Clarke, 1986). There is increasing evidence that the risk for cardiovascular autonomic neuropathy is associated with the HLA-DR3/4 genotype in insulin-dependent diabetes mellitus. There thus may exist a genetic predisposition (Barzilay et al., 1992). Furthermore, symptomatic autonomic neuropathy, although uncommon, is more frequent in IDDM as opposed to NIDDM (Neil et al., 1989).

3.3.1 Ischaemic heart disease in diabetic patients

It is well recognized that the major cause of myocardial infarction is occlusive thrombosis on an atheromatous plaque in a coronary artery. As already mentioned, the incidence of coronary artery disease and the risk of dying from a coronary artery disease event is greater in diabetics when compared with age matched non-diabetics (Jarrett, 1977; Kannel and McGee, 1979). Patients with coronary artery disease associated with diabetes also have been reported to have a higher incidence of silent ischaemia when compared with non-diabetic patients (Nesto et al., 1988). This incidence probably is even higher among diabetic patients with accompanying peripheral vascular disease (Nesto et al., 1990). Thus, angina is not a reliable index of myocardial ischaemia in diabetic patients with coronary artery disease (Nesto et al., 1988). Diabetics may also suffer a higher incidence of silent myocardial infarction (Margolis et al., 1973). However, both these observations contrast with other findings of no increase in the incidence of silent myocardial infarctions in patients with diabetes mellitus (Smith et al., 1983). The reasons for these differences are unclear and require resolution.

In addition to the increased risk of myocardial infarction, patients with diabetes mellitus show a higher mortality following such acute myocardial infarction (Kereiakes, 1985). Explanations for this increased mortality are currently incomplete. The incidence of congestive heart failure and cardiogenic shock is higher among patients with diabetes following myocardial infarction (Kereiakes, 1985). Larger infarcts have been reported among patients with diabetes (Rennert et

al., 1985). In contrast, Jaffe et al. (1984) reported a smaller infarct size among diabetics who nevertheless had an increased incidence of congestive heart failure post-infarction. Orlander et al. (1994) also reported no difference in infarct size between diabetic and non-diabetic Mexican-American and non-Hispanic whites. Weitzman et al. (1982) reported an increased incidence of anterior myocardial infarction among patients with diabetes and observed that the combination of diabetes and anterior myocardial infarction predicts the highest mortality rate. Anterior wall myocardial infarction frequently involves more heart muscle and affects ventricular function more adversely than infarctions in other areas of the heart.

Hyperglycaemia has also been thought to contribute to the increased mortality. Poor glycaemic control may correlate with increased mortality (Oswald et al., 1984). In contrast, good glycaemic control with intravenous infusion of insulin during the period immediately following myocardial infarction has been associated with decreased mortality (Clark et al., 1985). Finally, diabetic ketoacidosis frequently occurs in association with acute myocardial infarction. This serious situation has been associated with markedly increased mortality (Husband et al., 1985).

The increased mortality in diabetic patients following myocardial infarction has also been attributed to the high fatty acid levels seen in diabetics with acute myocardial infarction, possibly associated with post-infarction arrhythmias (Oliver et al., 1968).

3.3.2 Diabetic cardiomyopathy

It was suggested in the early 1970s that diabetes is associated with a specific cardiomyopathy. The Framingham study reported that the higher incidence of congestive cardiac failure in diabetics could not be accounted for by their high incidence of coronary atherosclerosis, hypertension, or cardiac autonomic neuropathy (Kannel et al., 1974). Hamby et al. (1974) came to a similar conclusion and noted that the heart muscle can be independently involved in diabetic patients without large coronary artery involvement. A range of independent reports have supported this suggestion and reported that diabetics show abnormalities of left ventricular function despite the absence of obvious clinical heart disease (Ahmed et al., 1975; Sanderson et al., 1978). Furthermore, the significantly increased incidence of congestive heart failure and the greater mortality and morbidity among diabetics following acute myocardial infarction may be related to cardiac dysfunction associated with diabetic cardiomyopathy (Stone et al., 1989; Bell, 1995).

CHAPTER 4
THE PATHOLOGY OF DIABETIC CARDIOMYOPATHY

The term cardiomyopathy implies any structural or functional abnormality of the ventricular myocardium. However, practically, all cardiac diseases can affect myocardial structure and function. Accordingly, the term cardiomyopathy is limited to conditions that primarily affect the myocardium as opposed to changes that are secondary to narrowing of extramural coronary arteries, systemic hypertension, anatomical valvular heart disease or congenital abnormalities of the heart and vessels.

The suggestion of a specific diabetic cardiomyopathy as a separate pathological entity independent of coronary artery disease has prompted a large number of clinical and experimental studies to explore for possible underlying pathological processes. However, the pathogenesis and functional significance of diabetic cardiomyopathy and the factors that cause the associated deterioration of cardiac performance resulting in clinical heart failure are still obscure (Airaksinen et al., 1984a, b). Diabetic patients show a spectrum of left ventricular abnormalities ranging from normal through incoordinate or delayed relaxation, to heart failure. However, whether they result from a single common aetiology or from a range of differing disorders is unknown (Shapiro et al., 1981a, b; Shapiro, 1982).

Furthermore, there is relatively little information as to whether the severity and duration of diabetes influence the development of left ventricular dysfunction and chronic heart failure or whether hypoglycaemic therapy influences progression. Sanderson et al. (1978), D'Eila et al. (1979), Fein et al. (1980), Friedman et al. (1982), and Vered et al. (1984) did not detect an association between myocardial dysfunction and the duration of diabetes even though the latter does influence the progression of the microvascular complications. In contrast, Shapiro et al. (1981b) reported that the abnormalities in left ventricular function they observed among diabetic patients were related to the severity and duration of diabetes with a higher prevalence where there were severe microvascular complications. Furthermore, Shapiro et al. (1981a) reported a higher tendency to have more abnormal left ventricular function among diabetic

patients requiring insulin when compared with patients taking oral hypoglycaemic drugs or treated with diet alone.

4.1 Vascular abnormalities

4.1.1 Microangiopathy

Diabetics, especially those with severe microvascular complications, have small vessel involvement of the coronary microcirculation analogous to those of retina and kidney (Ledet, 1968, 1976). Three forms of microvascular disease of the myocardium are recognized in diabetes mellitus: intramural artery abnormalities, capillary basal laminar thickening, and arteriolar and capillary microaneurysms.

4.1.1.1 Intramural artery abnormalities

Blumenthal et al. (1960) reported endothelial cell proliferation and deposition of colloid fibrils and periodic acid-Schiff-positive (PAS-positive) material in the walls of medium-sized myocardial blood vessels of two thirds of hearts from diabetic patients but in less than one third of hearts from non-diabetic patients. Crall and Roberts (1978) observed similar histological changes in the diabetic heart.

Ledet (1968, 1976) also found periodic acid-Schiff-positive (PAS-positive) material in the smallest intramural coronary arteries of diabetics. Rubler et al. (1972) reported four diabetic patients, who presented with congestive heart failure of unknown cause with associated glomerulosclerosis. They found small-vessel disease in one case characterized by thickening of the wall and narrowing of the lumen caused by sub-endothelial thickening as a result of deposition of a periodic acid-Schiff-positive (PAS-positive) material in the sub-endothelial layers. There was also hypertrophy of the tunica media. Hamby et al. (1974) in their series of 73 patients with the idiopathic form of primary myocardial disease found that 16 were diabetic. Three of these came to necropsy and all had small-vessel changes in the myocardium characterized by proliferation of endothelial lining cells. There was also myocardial hypertrophy and interstitial fibrosis. Additionally, Zoneraich et al. (1980) found abnormalities in small coronary arteries (20-150 μm in diameter) in 36 of 50 diabetic patients in the form of endothelial proliferation, sub-endothelial fibrosis, and deposits of hyaline in the intima. They also reported atheromatous thickening in these arteries. It is noteworthy, however, that Rubler et al. (1972) and Hamby et al. (1974) reported absence of major coronary artery disease. At

necropsy, Seneviratne (1977) also found that some of the intramural coronary arteries showed narrowing of their lumina due to focal deposition of mucopolysaccharide material in the sub-endothelial layers in one diabetic patient who died after bronchopneumonia one and half years after the initial study.

The above-mentioned studies thus suggest that the specific diabetic cardiomyopathy might be caused by the micoangiopathy seen in the myocardium in diabetes rather than the metabolic defect. The clinical echocardiographic study of Sanderson et al. (1978) also supports the microvascular disease theory. Most of the examined patients had evidence of small-vessel disease in their retinae.

4.1.1.2 Capillary basal laminar thickening

The thickening of capillary basement-membrane associated with diabetic retinopathy and nephropathy is well-documented (Williamson and Kilo, 1976). One quantitative light microscopy study of diabetic hearts reported that diabetic microangiopathy in the heart was limited to arterioles (defined as vessels with a tunica media containing at least two cell layers) and that the myocardial capillaries were spared and their walls were not thickened or more PAS-positive in diabetics, in striking contrast to other organs (Ledet, 1976). However, Williamson and Kilo (1976) reported that structural alterations affected most, if not all, of the capillaries of the diabetic.

In a detailed study of capillaries in skeletal muscle from diabetic and non-diabetic subjects, it has been suggested that the basal laminar thickening actually consists of successive layers or lamellae of the basal lamina concentrically arranged around capillaries. This gives the appearance of laminations that might reflect remnants of repeatedly degenerating and regenerating capillary components (Vracko and Beditt, 1970). In contrast, Fischer et al. (1979) observed that endothelial cells or pericytes did not show such degenerative changes and that the myocardial capillary wall thickening was only rarely multi-lamellar in nature. However, Fischer et al. (1979) reported a significant increase in the thickness of capillary basal lamina in biopsied myocardial tissue obtained from overt diabetics. However, the average thickness of basal laminae in myocardial capillaries was narrower than that reported in capillaries within skeletal muscles.

4.1.1.3 Arteriolar and capillary microaneurysms

Typical diabetic capillary microaneurysms have been reported in organs such as the eye and kidney, which together with thickening of the capillary basement membrane are the hallmarks of diabetic microangiopathy. In addition, a post-mortem injection study of 6 diabetic patients and 8 non-diabetic subjects revealed typical saccular and fusiform microaneurysms involving the arterioles and capillary limbs in the hearts of 3 diabetic patients and in none of the controls (Factor et al., 1980). These microaneurysms were similar to those observed in the retinal vessels of diabetic patients. The saccular aneurysms appeared as nodular expansions with irregular surfaces, usually along one side of the vessel wall away from a branch point. Their diameter was frequently two to three times that of the vessel from which they arose.

4.2 Metabolic, myocyte and interstitial changes

There has been considerable interest over recent years in the myocardial cellular changes as well as the mechanisms producing the possible abnormalities in myocardial contraction and relaxation in diabetes. Recent evidence has suggested changes in myocardial cell function. Factor et al. (1981) in their study of four groups of rats with either no disease (control), streptozotocin-induced diabetes mellitus, renovascular hypertension, or a combination of diabetes and hypertension reported that diabetes mellitus alone produced no morphologic light microscopic changes in the myocardium of diabetic rats. In contrast, the diabetic-hypertensive rats had relative cardiac hypertrophy and significantly increased interstitial fibrosis when compared with the other three groups. Furthermore, although the hypertensive rats showed less myocardial damage than the diabetic-hypertensive rats, they had significantly more perivascular fibrosis and vascular sclerosis than the diabetic-hypertensive animals, despite similar systolic blood pressure levels during life.

It is possible that diabetes is associated with alterations in myocardial cells themselves and that this in turn contributes to cardiac dysfunction in untreated diabetics. A number of factors may contribute to the primary myocardial changes in diabetes. First, some evidence suggests that associated metabolic changes may play a part. Several prospective studies have reported frequent abnormalities of left ventricular function in diabetics with uncontrolled hyperglycaemia, which improved with restoration of metabolic control (Shapiro et al., 1980; Uusitupa et al., 1983).

Shapiro et al. (1981a) have also reported more abnormalities of left ventricular function in patients, who at the time of the investigation required insulin than in those taking oral hypoglycaemic agents or treated with diet alone.

Weir et al. (1981) treated Wistar rats with streptozotocin at 2 days of age resulting in a diabetic model that developed chronic hyperglycaemia at about 6 weeks of age. The diabetic state was not sever and therefore did not require insulin treatment and in this respect resembled human non-insulin-dependent diabetes mellitus. Schaffer et al. (1985) injected Wistar rats with streptozotocin at 3 days of age. These rats developed marked glucose intolerance by 6 weeks of age as determined by intraperitoneal glucose tolerance test (2 g/kg). However, the rats had fasting and non-fasting blood glucose levels at or near normal. These rats also developed a cardiomyopathy that resembled the condition in human non-insulin-dependent diabetes mellitus. This condition was progressive and involved both contractile and metabolic functions.

Changes in myocardial fatty acid metabolism leading to triglyceride accumulation in the myocardium may also be involved in the pathogenesis of diabetic cardiomyopathy (Paulson and Crass, 1980).

Secondly, Fischer et al. (1979) reported that the most frequently observed morphological abnormalities in biopsied myocardial tissue obtained from over diabetics were myocardial cell hypertrophy and varying degrees of interstitial fibrosis. Other studies have also demonstrated hypertrophy of the myocardium (Rubler et al., 1972).

Thirdly, diabetes is associated with abnormalities in calcium transport processes in ventricular myocytes. The cardiac sarcoplasmic reticulum is the source of activating calcium in the heart (Solaro and Briggs, 1974). Alteration in its function could also affect mechanical relaxation (Dhalla et al., 1998). The cardiac sarcoplasmic reticular ATP-dependent calcium transport (Ca^{2+} pump) was significantly depressed in streptozotocin-induced diabetic rats (Ganguly et al., 1983).

Ganguly et al. (1983) also reported depressed Ca^{2+}-stimulated ATPase activities of cardiac myofibrils. They went on to demonstrate that the defect in sarcoplasmic reticular calcium transport develops gradually through the disease process. Thus, depressed sarcoplasmic reticular ATP-dependent calcium uptake was not evident despite highly elevated blood glucose levels for up to 28 days after streptozotocin injection. These changes were reversed by insulin treatment. Thus, Ganguly et al. (1983) provided evidence that the depression in sarcoplasmic reticular

calcium accumulation might result from insulin deficiency and its associated chronic metabolic changes. Insulin replacement therapy has similarly been observed to restore papillary muscle contractile performance to normal during chronic diabetes (Fein et al., 1981).

Fourthly, the diffusion distance of oxygen to myocardial mitochondria in streptozotocin-induced diabetic rats with a 40-50 day diabetes was significantly increased when compared to control rats, thereby reducing the oxygen supply to the underlying mitochondria. This could lead to myocardial functional abnormalities (Warley et al., 1995).

Finally, the myocardial interstitium may also alter in diabetes. Warley et al. (1995) reported a threefold increase in extracellular components of the left ventricle of streptozotocin-induced diabetic rats. This often takes the form of interstitial fibrosis (Rubler, 1972; Regan et al., 1981).

4.3 Role of angiotensin II

Angiotensin II has been reported to induce cardiac growth responses in isolated adult rat hearts (Schunkert et al., 1995). Angiotensin II also induces proliferation of fibroblasts isolated from the rat heart (Schorb et al., 1993). It has thus been suggested that angiotensin II is responsible for the increased myocardial and blood vessel fibrosis observed in some forms of cardiac hypertrophy and cardiomyopathy through an intracardiac renin-angiotensin system (Dostal et al., 1992a, b). Rösen et al. (1995) recently reported that the renin-angiotensin system is activated in diabetes leading to an enhanced production of angiotensin II. Therefore, angiotensin II may well cause the myocardial interstitial fibrosis that in turn leads to the increase in myocardial stiffness in diabetics.

The beneficial effects of angiotensin-converting enzyme inhibitors in the treatment of hypertension and congestive heart failure is well known (Cohn and Levine, 1982). Angiotensin-converting enzyme inhibitors have also been shown to induce regression of left ventricular mass in essential hypertension (Dunn et al., 1984). Finally, streptozotocin-diabetic rats have been found to have increased levels of angiotensin converting enzyme (ACE) in their left ventricular tissue and a decrease in left ventricular developed pressure. These changes were prevented by treatment with the angiotensin converting enzyme inhibitor enalapril (Goyal et al., 1998). It was the latter findings that prompted the inclusion of MRI examination of the effect of captopril in the present study.

CHAPTER 5
PHYSIOLOGICAL STUDIES OF CARDIAC FUNCTION IN DIABETES

Impaired left ventricular function has frequently been detected in diabetics without clinical heart disease (Shapiro et al., 1980, 1981a, b; Shapiro, 1982). Thus, diabetic cardiomyopathy may well pass through an asymptomatic phase when left ventricular function is nevertheless impaired. Cardiac function in diabetes has been evaluated both in humans and animals by several techniques.

5.1 Experimental animal studies

A number of measurements of cardiac performance have been made in experimental animal models of diabetes. Haemodynamic studies of dogs made mildly diabetic for 11 months with alloxan suggested an increased diastolic stiffness of left ventricular muscle (Regan et al., 1974). Two methods were used to characterize left ventricular function. First, angiotensin infusion produced moderate elevations in aortic diastolic pressure, thus, resulting in a moderate increase in afterload. This led to a significant rise in end-diastolic and stroke volumes in normal control dogs. In contrast, there was no increase in end-diastolic volume in diabetic dogs. Secondly, the dogs were infused with normal saline via a catheter in the left ventricle. This produced a significantly higher rise in end-diastolic pressure in the diabetic dogs, which was twice that in the control dogs. These abnormalities might have resulted from altered wall compliance or impaired ventricular relaxation.

Studies of isolated perfused hearts from diabetic rats demonstrated decreased peak systolic pressures (Miller, 1979). There have also been a number of studies of isolated papillary ventricular muscles from diabetic rats. Fein et al. (1980) reported a delayed onset and a slower rate of relaxation characterized by a prolonged time for peak developed tension to fall to 50% during isometric relaxation. The velocity of shortening was also depressed at all loads during isotonic contraction. Warley et al. (1995) have also reported significant increase in time to 75%

relaxation, which indicates prolonged relaxation. In addition, the time to peak tension was also significantly increased and the sensitivity to increased concentrations of calcium and adrenaline in the bathing medium was reduced in the isolated muscles (Warley et al., 1995).

5.2 Human studies

Many clinical studies have detected frequent abnormalities of left ventricular function that could be attributed to a pre-clinical cardiomyopathy in diabetic patients without clinically obvious heart disease. Thus, subtle abnormalities may exist in the course of diabetes in persons previously considered free of chronic cardiac complications. Some of the clinical studies performed were non-invasive and used systolic time intervals and echocardiography to detect the early abnormalities in left ventricular function. Invasive studies by the use of ventriculography were also performed to detect these abnormalities.

5.2.1 Systolic time intervals

Systolic time intervals allow timing of particular events that occur during the cardiac cycle and relate them to the mechanical state of the left ventricle. Systolic left ventricular function and abnormalities, thus, can be assessed by measurements of the systolic time intervals although these time intervals do not identify the cause. Such abnormalities have even been demonstrated in diabetics without clinically obvious heart disease.

The calculation of the systolic time intervals involves external carotid pulse recording from carotid arterial pulsations in the neck, phonocardiography and electrocardiograhy (ECG) (Katz, 1992). The upstroke of the carotid pulse correlates with the beginning of left ventricular systole. In contrast, the dicrotic notch coincides with the closure of the aortic valve at the end of proto-diastole. The ECG defines the onset of electrical systole in the left ventricle since the initial deflection of the QRS complex is produced by left ventricular depolarization. Mechanical systole in the left ventricle begins shortly before closure of the mitral valve and thus is marked by the first heart sound (S_1) in phonocardiography. Phonocardiography can also identify the end of proto-diastole, which is marked by the second heart sound (S_2).

The Q-S_2 time is one of the commonly used systolic time intervals. It is measured from the beginning of ventricular depolarization as detected by the electrocardiographic QRS complex to the end of proto-diastole marked by the high frequency vibration of S_2 in phonocardiography. Thus, it represents the total duration taken by electromechanical systole (plus proto-diastole).

This systolic time interval can be further subdivided into three phases: the Q-S_1 interval measured from the beginning of the QRS complex in the ECG to the beginning of S_1 in phonocardiography, the isovolumic contraction time measured from S_1 to onset of the rise in aortic pressure, and left ventricular ejection time (LVET) measured from the onset of carotid upstroke to the dicrotic notch. Thus, Q-S_1 is physiologically correlated to the time interval between electrical excitation and the onset of contraction, while the isovolumic contraction time and the LVET represent the rate of pressure generation within the ventricles and the time required for total ejection (plus proto-diastole) respectively.

Left ventricular pre-ejection period (PEP) is another systolic time interval in common use. It is correlated physiologically to the isovolumic contraction time plus the Q-S_1 interval and thus can be measured by subtracting the LVET from the Q-S_2.

Reduced myocardial contractility prolongs the PEP and shortens the LVET. Thus, the PEP/LVET ratio is increased in patients with left ventricular systolic dysfunction due to reduced myocardial contractility.

Seneviratne (1977) assessed left ventricular function by measuring systolic time intervals in 28 insulin-requiring diabetic patients with (n = 14 patients) and without (n = 14 patients) significant microangiopathy. Significant microangiopathy was diagnosed through the existence of either a proteinuria over 3 g/24 h or of proliferative retinopathy. The PEP/LVET ratio increased significantly in the fourteen diabetics with significant microangiopathy (all were women), indicating impaired left ventricular function. In contrast, the fourteen patients with uncomplicated diabetes had normal left ventricular function using this criterion. The strict selection of patients free of angina and previous myocardial infarction and with normal electrocardiograms and chest radiographs excluded coronary heart disease as a cause of the increase in PEP/LVET in the diabetics with microangiopathy. Seneviratne (1977) accordingly attributed these abnormalities to a specific diabetic cardiomyopathy due to microangiopathy rather than the metabolic defect.

Shapiro et al. (1980) demonstrated frequent abnormalities of left ventricular function as reflected in the systolic time intervals and echocardiography in 69 mature onset diabetics without clinically obvious heart disease before and during standard hypoglycaemic treatment. The PEP/LVET findings during the first two months of treatment identified two groups of patients. The first group had a normal or slightly raised ratio, which fell with treatment. In the second group, the ratio was significantly higher and did not alter even after four months of

treatment. The persistently high PEP/LVET ratio in the latter group suggested significant left ventricular dysfunction. Shapiro et al. (1981a, b) and Uusitupa et al. (1985) have also reported abnormal systolic time intervals among patients with diabetes suggesting that left ventricular function may become impaired early in the clinical course of diabetes.

Cellina et al. (1983) also reported a more prolonged PEP and a shorter LVET and consequently a higher PEP/LVET ratio among patients with gestational diabetes and also among pregnant women with clinical diabetes. These abnormalities were detected at the third trimester of pregnancy. Interestingly, these abnormal systolic time intervals returned to normal 5 weeks after delivery in patients with gestational diabetes but remained abnormal in patients with clinical diabetes. A good correlation was also found between the abnormal systolic time intervals seen in diabetics and the levels of glycosylated haemoglobin. This shows the importance of glycaemic control in diabetic cardiac dysfunction (Jermendy et al., 1984).

5.2.2 Echocardiography

Sanderson et al. (1978) studied 23 young diabetic patients of whom 19 had retinopathy. All patients had normal blood pressures, were in sinus rhythm, had normal chest radiographs and their electrocardiograms showed no evidence of clinically obvious heart disease. The close time relation between mitral valve movement and wall movement was lost in fourteen patients with opening of the mitral valve delayed in eight of these fourteen patients. Thus, these patients showed an abnormally prolonged left ventricular isovolumetric relaxation time reflecting abnormalities of diastolic function that may reflect sub-clinical heart disease. Other echocardiographic studies have also reported abnormally prolonged left ventricular isovolumetric relaxation times among diabetics (Shapiro et al., 1980, 1981a, b; Shapiro, 1982; Airaksinen et al., 1984a). Thus, diastolic abnormalities of left ventricular function may well occur in diabetes.

Shapiro (1982) studied left ventricular diastolic function in 142 diabetic patients free from clinically obvious heart disease, hypertension and conditions known to influence left ventricular function and derived the following measurements from simultaneous echocardiography and phonocardiography:

(1) End-diastolic posterior wall thickness (cm) and peak rate of change of posterior wall thickness in early diastole (cm/s).

(2) The duration over which the posterior wall showed rapid thinning (ms). This is arbitrarily defined as time taken for the posterior wall to stretch from its maximum thickness to 20% of that peak value.

(3) The peak rate of increase in left ventricular dimension during early diastole (cm/s).

(4) The duration over which the left ventricular dimension showed rapid increase in early diastole, arbitrarily defined as the time taken for the peak rate of increase in left ventricular dimension to become 20% of its value (ms)

(5) The time interval (ms) form the left ventricular minimal dimension to the onset of mitral valve opening (measured at cusp separation) and from the first low frequency vibrations of the second heart sound (A_2) to mitral valve opening (isovolumetric relaxation time).

(6) The change in left ventricular dimension during isovolumetric relaxation, expressed as percentage of total dimension change during the cardiac cycle.

All the diabetic patients in this study had a normal wall thickness. The diastolic parameters of left ventricular function were normal in the 12 young patients who had no diabetic complications. The remaining diabetic patients showed a significantly delayed mitral valve opening relative to time at which the left ventricular dimension was at its minimum dimension and this could be attributed to a prolonged isovolumetric relaxation. The patients with severe complications showed significant abnormalities in their peak rates and duration of posterior wall thinning. Thus, the primary myocardial abnormality in diabetes is a prolonged duration and reduced rate of posterior wall thinning combined with impaired left ventricular relaxation.

Friedman et al. (1982) studied 33 children with IDDM (only one of them had retinopathy and none had proteinuria, hypertension or clinical evidence of neuropathy). Computerized methods were used to derive velocities of left ventricular circumferential fibre and minor axis shortening from echocardiographic data. Left ventricular volumes were also computed and ejection fractions were calculated from these data. Many of the diabetic children showed abnormal myocardial performance. Patients and control subjects showed indistinguishable left ventricular end-diastolic volumes. In contrast, the diabetics had larger left ventricular end-systolic volumes, lower left ventricular ejection fractions and minor axis shortening, and higher ratios of left ventricular end-systolic dimension to left ventricular systolic wall thickness (LVESD/LVSWT). Since the diabetics had normal left ventricular wall thicknesses, their increased LVESD/LVSWT could not be related to differences in wall thickness. The mean velocity of circumferential fiber shortening was less in diabetics than in the normal children. The increased end-systolic dimension reflecting incomplete emptying of the ventricle during systole together

with the decreased ejection fraction indicate a myocardial dysfunction that may reflect subclinical cardiomyopathy early in the disease, that precedes the appearance of small vessel abnormalities. Lababidi and Goldstein (1983) also reported a decrease in myocardial contractility in diabetic children. Additionally, they detected interventricular septal hypertrophy in their adolescent population.

However, there are a number of conflicting reports arising from echocardiography concerning cardiac dimensions and function in diabetes. First, one group of studies reported normal or modest dilatation of the left ventricle (Shapiro et al., 1981a; Friedman et al., 1982; Fisher et al., 1989). In contrast, Airaksinen et al. (1984a, 1987) reported a reduction in left ventricular size among diabetics. Secondly, whereas some reported an increase in left ventricular thickness in diabetics (Airaksinen et al., 1984a, 1987), Friedman et al. (1982), Shapiro et al. (1981a), and Fisher et al. (1989) reported no changes in the thickness of the posterior wall of the left ventricle. Thirdly, whereas several echocardiographic studies reported a depressed left ventricular function with advanced diabetic complications as described above (Shapiro et al., 1981a, b, Uusitupa et al., 1985), other investigators have reported a normal left ventricular systolic function (Airaksinen et al., 1984b; Fisher et al., 1989). Surprisingly, Thuesen et al. (1988) reported an enhanced systolic function in insulin-dependent patients developing microvascular complications.

5.2.3 Radionuclide ventriculography

D'Elia et al. (1979) studied fifteen juvenile onset diabetics with severe nephropathy who were free of significant coronary artery disease using cardiac catheterization, coronary angiography and ventriculography. Their myocardial function fell into three groups. Four patients showed a cardiomyopathy with a diffusely abnormal ventriculography, reduced ejection fraction, and elevated left ventricular end-diastolic pressure. Four patients showed an elevated left ventricular end-diastolic pressure as the sole abnormality. The remaining seven showed normal myocardial function.

Other investigators, also using radionuclide ventriculography, have reported normal resting left ventricular ejection fractions with an abnormal response to dynamic exercise (Vered et al., 1984; Fisher et al., 1985, 1986; Arvan et al., 1988). In contrast, Zola et al. (1986) reported significant reductions in mean left ventricular ejection fractions in diabetics with cardiac autonomic neuropathy at rest as well as after maximal exercise.

5.2.4 Cardiac magnetic resonance imaging

It is thus clear that a range of techniques can be used to identify and quantify cardiac changes in diabetes. However, until recently no single non-invasive technique has been able to characterize all the structural and the functional-dependent features of the myocardium in diabetic cardiomyopathy.

Until recently, magnetic resonance imaging (MRI) was not a feasible physiological tool for studying cardiac function because of its inherently long imaging times and motion artefacts associated with contraction of the heart. Recent innovations in magnetic resonance system hardware and pulse sequences have overcome these limitations and allowed rapid imaging to offer exceptional opportunities to obtain reliable cardiac images amenable to quantitative measurements of anatomical and functional characteristics of the heart (Herfkens et al., 1983; Crooks et al., 1984; Higgins, 1986). In addition, cine magnetic resonance of the heart offers a sensitive approach to detecting blood in the chambers of the heart and has been reported to measure accurately left ventricular volumes and to detect dysfunctional myocardium using spin or gradient echo sequences (Higgins, 1986). Both techniques have also proved useful for accurate measurement of right and left ventricular volumes and for qualitative and quantitative evaluation of right and left ventricular anatomy and function (Higgins, 1986; Stratemeier et al., 1986; Markiewicz et al., 1987; Sechtem et al., 1987; Semelka et al., 1990).

Many of the MRI-derived anatomical and functional parameters of the left ventricle have been validated by many investigators (Stratemeier et al., 1986; Sechtem et al., 1987; Semelka et al., 1990).

Additionally, MRI can provide complete anatomical reconstruction of both ventricles and characterize changes through the cardiac cycle. Finally the non-invasive nature of the MRI allows serial experimental animal studies to be performed.

It would therefore appear that MRI offers an excellent method for assessing qualitative and quantitative biventricular morphology and function in diabetes. Yet, no such MRI studies have been performed on diabetic patients or diabetic animals aiming at characterizing the morphological and functional alterations of the left and right ventricles associated with diabetic cardiomyopathy. Furthermore, most if not all of the studies done so far on diabetic patients or diabetic animals using other techniques to identify and quantify cardiac changes in diabetes have concentrated on evaluating the morphology and function of the left ventricle only.

CHAPTER 6
MATERIALS AND METHODS

6.1 Experimental animals

All animal procedures used protocols approved by the Home Office, UK, and were in accordance with the Animal Procedures Act (1986). The experiments studied a total of 20 male fully conditioned, healthy, and pathogen-free Wistar rats (6-week old), obtained from Harlan, UK. These were reared in the animal facilities of the Central Biomedical Service of the University of Cambridge under standard housing conditions and fed a normal animal chow with water ad libitum. The animals were divided at random into 5 groups. Diabetes was induced in animals in 4 of the groups (each n = 4) with a single intraperitoneal injection of streptozotocin (STZ 65 mg/kg body weight, Sigma-Aldrich Co., Poole, Dorset, UK) as described below. The fifth group (n = 4) was kept as a control group. Two groups of the test animal were made diabetic at the age of 7 weeks and the other 2 groups were made diabetic at the ages of 10 and 13 weeks respectively.

All the animals, including the 4 in the control group, were scanned at the age of 16 weeks. The experimentally induced diabetic state accordingly was maintained for a duration of 3 weeks before scanning in the group made diabetic at the age of 13 weeks and for 6 weeks and 9 weeks for the groups made diabetic at the ages of 10 weeks and 7 weeks respectively. For the purpose of simplicity, these groups will be referred to as the 3-, 6-, and 9-week diabetic groups respectively. Since diabetes was induced at the age of 7 weeks in 2 experimental groups, this work, thus, involved two 9-week diabetic groups. For one of these 2 groups, chosen at random, immediately after induction of diabetes, commercially available captopril (Sigma-Aldrich Co., Poole, Dorset, UK) was added to the drinking water of that group at a concentration of 2 g/l. The rats of this experimental group were kept on captopril-containing drinking water till they were scanned at the age 16 weeks. Since the rats in the control group were imaged at the same age of 16 weeks as the rats in the 4 diabetic groups were scanned, this would serve as an age and sex matched control for all the 4 diabetic groups. The 4 different diabetic groups accordingly provided controlled diabetic groups in which the disease state had developed for 3

different durations. They thus provided an indication of the time course of the appearance and development of the possible effects of diabetes on the structural and functional parameters of the left and right ventricles. Furthermore, the 9-week captopril-treated diabetic group was used to evaluate the beneficial therapeutic effects of captopril in the prevention of the anatomical and the pathophysiological changes in the cardiac cycle produced by diabetic cardiomyopathy.

The ages at induction of diabetes used in this study were selected on the basis of previous findings with the STZ-diabetic rat model (Rodrigues et al., 1997). In all the animals, body weight was monitored every 3 days and blood glucose every 2 weeks using a glucometer.

6.2 Induction of diabetes

The experiments thus used the widely used experimental model of STZ-induced diabetes (Warley et al., 1995). The rats in each of the 4 experimental groups made diabetic were first anaesthetized using 1-2 % halothane (Sigma-Aldrich Co. Poole, Dorset, UK) in oxygen (British Oxygen Gas, UK); their blood glucose levels were then measured using a blood glucometer. This was followed by a single intraperitoneal injection of streptozotocin (STZ 65 mg/kg body weight; Sigma-Aldrich Co. Poole, Dorset, UK) dissolved in 0.1 ml citrate buffer (Sigma-Aldrich Co. Poole, Dorset, UK), pH 4.5. The control rats received sham injections of the citrate buffer when they were 7 weeks old. STZ at a moderate dose of 55 – 65 mg/kg body weight is known to produce a stable diabetes of modest severity that would nevertheless eventually lead to structural and functional myocardial abnormalities in Wistar rats (Warley et al., 1995; Rodrigues et al., 1997). Hyperglycaemia (blood glucose level>13 mmol/l) ensued 48 h post-STZ. Blood glucose levels measured 2 weeks after injection always exceeded 13 mmol/l.

Figure 6.1 (next page): **Diagrammatic representation of the experimental design.**

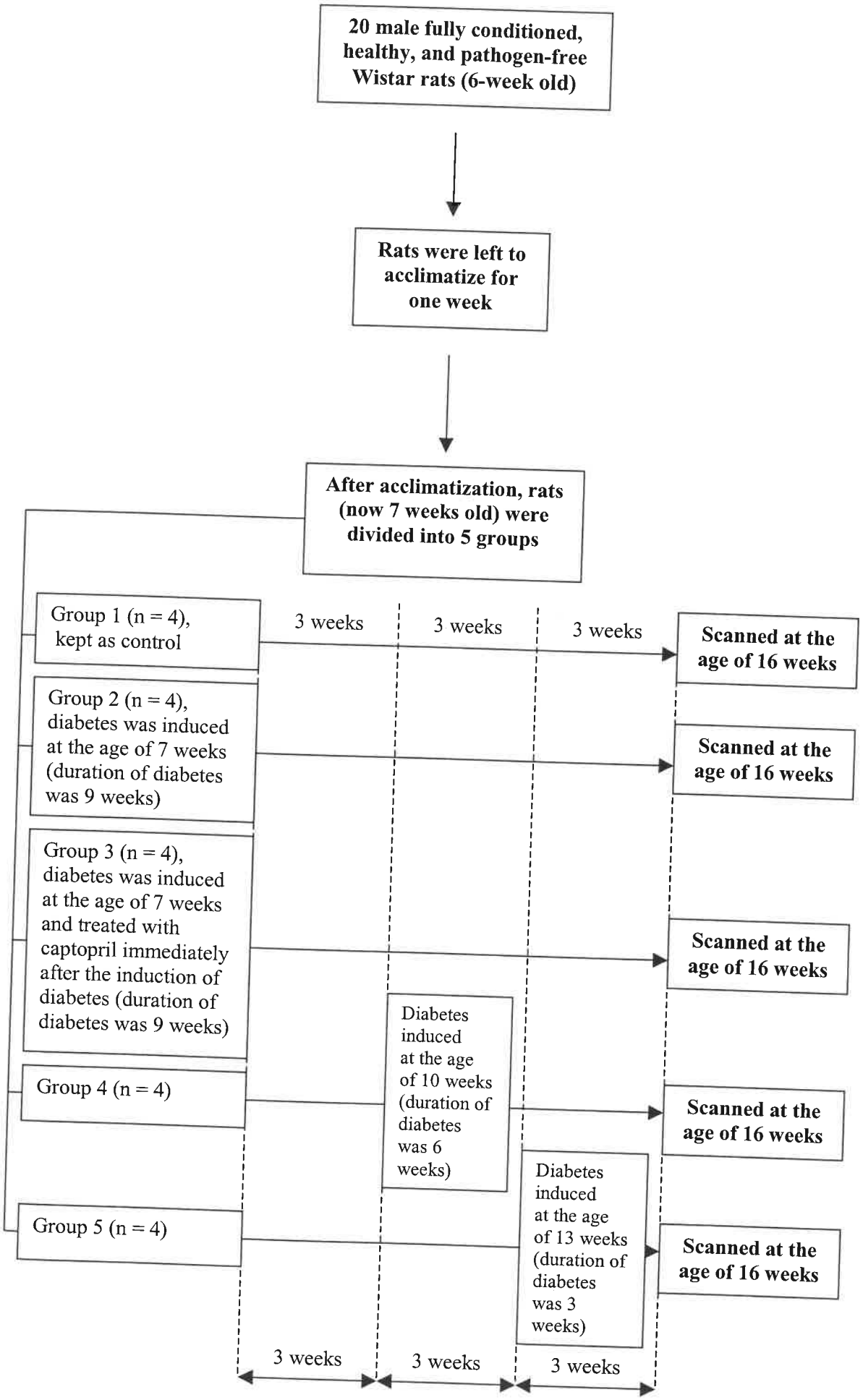
20 male fully conditioned, healthy, and pathogen-free Wistar rats (6-week old)
Rats were left to acclimatize for one week
After acclimatization, rats (now 7 weeks old) were divided into 5 groups
Group 1 (n = 4), kept as control
Group 2 (n = 4), diabetes was induced at the age of 7 weeks (duration of diabetes was 9 weeks)
Group 3 (n = 4), diabetes was induced at the age of 7 weeks and treated with captopril immediately after the induction of diabetes (duration of diabetes was 9 weeks)
Group 4 (n = 4)
Group 5 (n = 4)
3 weeks
3 weeks
3 weeks
Diabetes induced at the age of 10 weeks (duration of diabetes was 6 weeks)
Diabetes induced at the age of 13 weeks (duration of diabetes was 3 weeks)
Scanned at the age of 16 weeks
Scanned at the age of 16 weeks
Scanned at the age of 16 weeks
Scanned at the age of 16 weeks
Scanned at the age of 16 weeks
3 weeks
3 weeks
3 weeks

6.3 Physiological monitoring

Prior to each imaging session, rats were anaesthetized using 1-2 % halothane (Sigma-Aldrich Co. Poole, Dorset, UK) in oxygen (British Oxygen Gas, UK). Their systolic blood pressures were then measured using a non-invasive rat-tail blood pressure monitor (Harvard Apparatus, Edenbridge, Kent, UK). Tables 7.1 and 7.2 summarizes such systolic blood pressure values for the 5 study groups. This measurement was repeated soon after MRI to confirm that the systolic blood pressure remained stable within reasonable physiological limits.

Shielded subcutaneous electrodes were used for electrocardiographic (ECG) recording and display using a Tektronix 2225 oscilloscope (Tektronix, Harpenden, Herts). These signals enabled imaging acquisition to be synchronized or gated to the QRS complex of the electrocardiogram (ECG). The ECG signals also enabled a continuous monitoring of the heart rate throughout the imaging sessions.

Following establishment of stable ECG trigger signal (Figure 6.2), the anaesthetized animal was then placed in a specially designed home-built half sine-spaced birdcage radiofrequency probe.

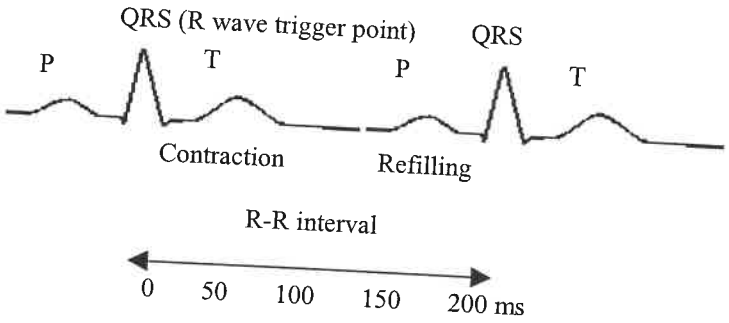

Figure 6.2: **Diagrammatic representation of the ECG waves displayed during cardiac imaging in the rat.** With an average heart rate of 300 beats Min^{-1}, the duration of the cardiac cycle represented by the R-R interval is 200 ms. End-diastole coincides with the R wave of the electrocardiographic QRS complex representing ventricular depolarization. Signal was acquired at twelve time-points through the cardiac cycle with a delay of 8, 21, 34, 47, 60, 73, 86, 99, 112, 125, 138, and 151 ms after the trigger, taken from the R wave of the ECG, thus covering the whole systole and most of diastole. P and T represent atrial depolarization and ventricular repolarization waves respectively.

6.4 Radiofrequency (RF) probe

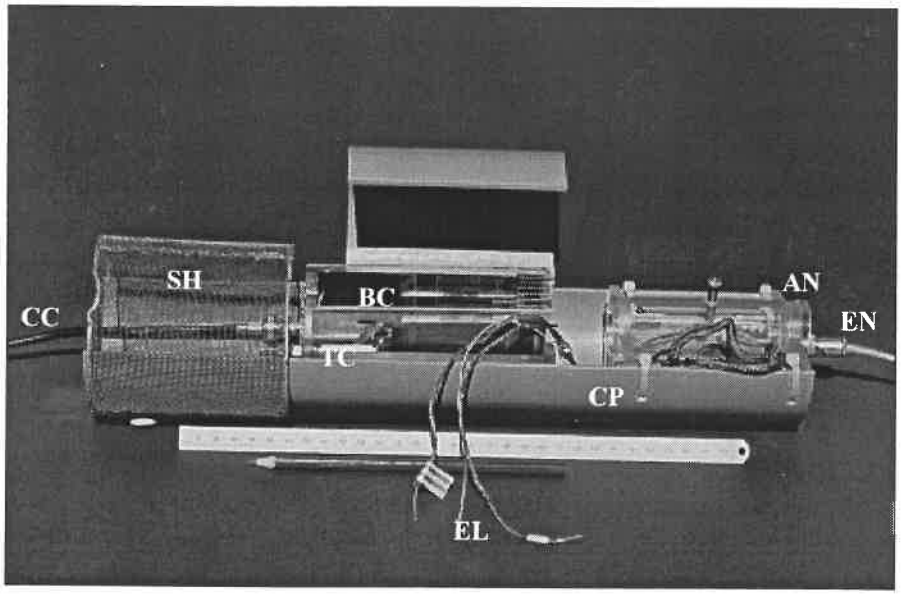

Figure 6.3: **An assembly containing a half sine spaced birdcage radiofrequency (RF) probe.** This assembly was built at the Herchel Smith Laboratory for Medicinal Chemistry, Cambridge University, and was designed to fit inside a gradient set of an internal diameter of 11 cm. It was contained within a cylindrical plastic holder (CP) and included the RF probe unit, which is made up of an RF probe (BC), which was approximately half cylindrical in shape with open ends, an RF shield (SH) consisting of a cylinder of copper gauze surrounding and sliding over the birdcage, a tuning capacitor (TC), and a coaxial cable (CC) to carry the RF. This assembly also included the ECG leads (EL), attachment plugs for the ECG leads (EN) and a unit to anchor anaesthetic delivery tubes near the nose of the animal (AN). The ruler in the foreground is 30 cm long.

The home-built radiofrequency probe was approximately half cylindrical in shape, of 4.5 cm internal diameter and with both ends open (Figure 6.3). It was designed to fit inside the bore of a gradient set of 11cm internal diameter. It incorporated delivery tube assemblies that delivered the anaesthetic gases and additionally provided secure attachments for the ECG leads. It therefore provided a self-contained assembly for the physiological monitoring of the animal lying in the half cylinder that was inserted into the magnet bore for magnetic resonance imaging.

6.5 Magnetic resonance imaging

6.5.1 Imaging hardware and pulse sequence

All the experiments were performed in a 2 Tesla Oxford instrument superconducting magnet with a horizontal internal bore of 31 cm. A home built gradient set of 11cm internal diameter designed to fit in the 31cm bore of the 2-Tesla horizontal magnet was used for imaging. The radiofrequency coil was a home built half sine-spaced birdcage probe of internal diameter of 4.5 cm as described above.

The imaging sessions acquired ECG triggered images. They characterized both left and right ventricular anatomy through systole and diastole. For this purpose, they typically used 12 imaging slices that were taken perpendicular to the principal cardiac axis and extended through the entire length of the 2 ventricles from the base of the heart to its apex (Figure 6.4). Each image slice was imaged at typically 12 time-points covering the entire systole and most the diastole. Successful imaging was achieved despite the high intrinsic heart rates in rats, which reached about 350 beats/min.

Images were obtained using a gated cine protocol by synchronizing imaging to set times following the electrocardiographic QRS complex and repeating the acquisition at the same slice position with the same phase encoding at different times, through the cardiac cycle. Each slice was imaged at typically 12 times through the cardiac cycle as mentioned above. The effective repeat time (TR) was approximately 13 ms. A short echo-time (TE) of 4.3 ms was used in this study.

The field of view used was typically 4.0–5.0 cm depending on the size of the animal. The image matrix used was 128X128 pixels, thus giving a nominal pixel resolution of 390–313 μm. Slice thickness was typically 1.37–1.75 mm. Two signal averages for each image were used in most of the imaging sessions.

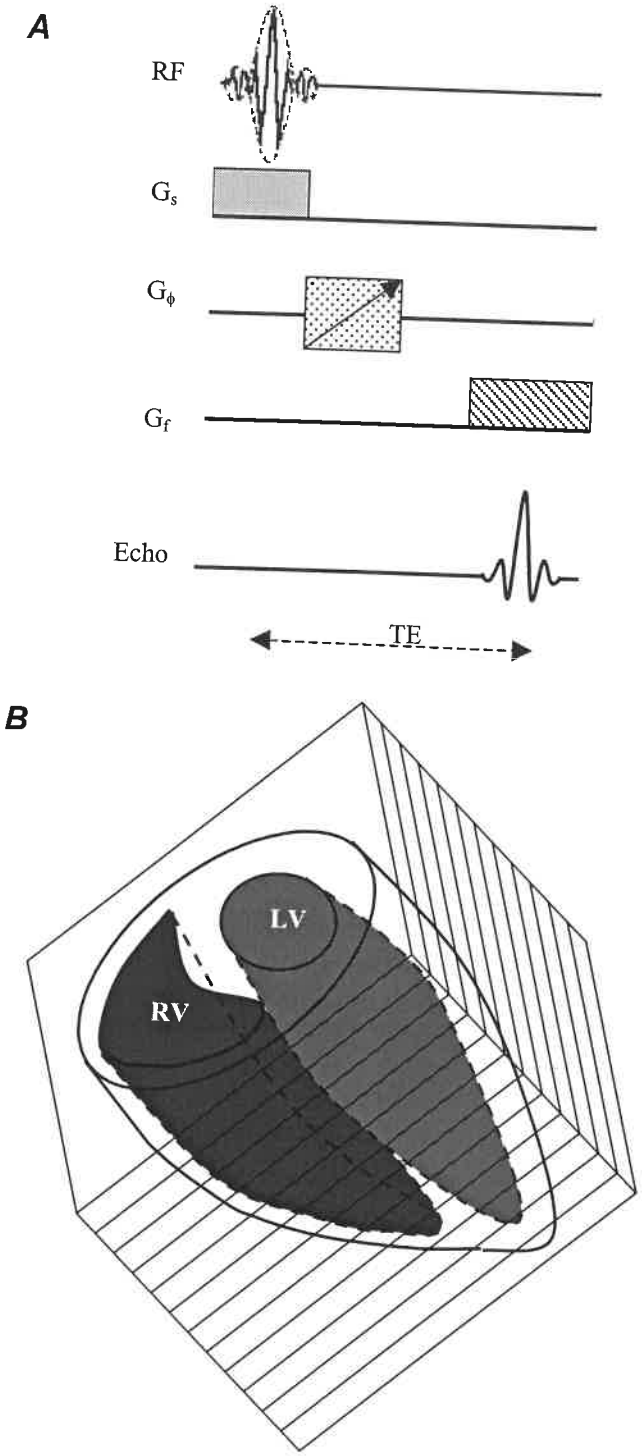

Figure 6.4: **Gradient echo pulse sequence (A), diagrammatic representation of the right and left ventricles of the rat heart (B).** Typically 12 transverse image slices taken perpendicular to the principal cardiac axis were acquired contiguously covering both ventricles. Each transverse cardiac slice was typically imaged at 12 time-points through the cardiac cycle using a gated cine protocol. The pulse sequence was thus applied 12 times during each particular cardiac cycle. Full data set with MR images at the 12 time-points was obtained from each particular slice before imaging other slices. Thus, the effective repeat time (TR) was 13 ms. Echo time TE=4.3 ms. LV and RV indicate left and right ventricles respectively.

6.5.2 Consistent image slice positioning

A repeatable and consistent image slice positioning protocol ensured that the 12 imaged transverse cardiac slices of the heart of each experimental rat were perpendicular to the principal cardiac axis that joins the cardiac apex and the aortic valve. The rat lying prone in the radiofrequency probe was first positioned horizontally in the bore of the magnetic resonance imaging gradient set with its craniocaudal axis along the main magnetic field axis of the superconducting magnet. Its thoracic cavity was then imaged using a set of typically 9 sagittal planes. The sagittal image, which offered the clearest representation of the heart, was then used as a pilot image to derive transverse coronal multi-slice images. Finally, the transverse-coronal image with the clearest representation of the heart was used as a pilot image to position a definitive set of typically 12 imaging planes (transverse cardiac slices or sections) with their geometrical planes perpendicular to the principal cardiac axis and covering the whole left and right ventricles. The selected 12 slices covered the entire length of both ventricles. Epicardial and endocardial borders of both ventricles in all the selected slices at all the 12 time-points derived form the resulting magnetic resonance images could be used for accurate and consistent quantitative analysis that was comparable between different animals became possible.

6.5.3 Temporal synchronisation of image acquisition

The first image of each of the 12 transverse cardiac sections was typically acquired 8 ms after the trigger pulse from the R wave of the ECG. The effective repeat time (TR) in the gated cine protocol used in the present study was typically 13 ms as mentioned above. The next image of the selected sections accordingly was obtained at typically 21 and the third at typically 34 ms after the trigger pulse from the R wave of the ECG and so on. However, it should be noted that the actual repeat time was 26 ms as image acquisition was gated from every alternate heart beat rather than imaging every cardiac cycle.

As each transverse cardiac section was imaged at 12 time-points during the cardiac cycle, the pulse sequence used was typically repeated 12 times during each cardiac cycle with the same phase encoding. Giving that the image matrix used was 128X128 pixels, to acquire complete magnetic resonance images for one transverse cardiac section at the selected 12 time-points, 128 cardiac cycles would be required with the strength of the phase encoding gradient increased with each consecutive cardiac cycle. However, since each image was derived from two signal averaged acquisitions and image acquisition was gated from every alternate heart beat rather than imaging every cardiac cycle, a total of 128X2X2 cardiac cycles were required to image any particular transverse cardiac section at the 12 time-points required. It, thus, follows that in order

to obtain a complete data sets for all the transverse cardiac sections with complete coverage of the heart and at the different 12 time-points through the cardiac cycle, a total number of 12X128X2X2 cardiac cycles, with the pulse sequence repeated 12 times during each alternate cardiac cycle, were required.

6.5.4 Image processing

For quantitative analysis, image data were transferred from the MRI console by means of in-house hardware and software to remote UNIX workstations. The borders of both ventricles in each transverse image slice were interactively defined using in-house software based on CaMReS libraries (CaMReS, Dr N J Herrod, University of Cambridge). This used the blood/myocardial wall contrast for defining the endocardial borders and the myocardial wall/thoracic cavity contrast for drawing the epicardial borders. The pixel numbers enclosed within each border were then converted into units of mm^2 using the field of view (FOV). The epicardial and endocardial borders of both ventricles were independently drawn 4 times for all the images of the 12 selected slices. This analysis was performed for images obtained from all 12 time-points through the cardiac cycle for each of the selected 12 transverse cardiac sections. Left and right ventricular epicardial and endocardial volumes were then calculated. The mean of each of the calculated 4 volumes, was then taken to represent the empirical volume. Myocardial volumes of both ventricles were also derived at each of the studied 12 time-points by subtracting the endocardial volume from the corresponding epicardial volume. The resulting intra-observer variability was very small as evidenced by the very small standard errors of the mean volumes calculated.

The left ventricles in the images were circularly symmetrical in transverse sections from all the rats (Figures 8.1-8.5). Accordingly the geometrical analysis treated the interventricular septum as part of the left ventricle in agreement with earlier protocols (Crowley et al., 1997; Wise et al., 1998). In contrast, the right ventricle was defined as the crescent-shaped cardiac chamber with its myocardial wall meeting the left ventricular myocardial wall close to the diameter of the left ventricle (Figure 6.5).

Figure 6.5 (next page): **A Typical Transverse cardiac MRI section.** A typical transverse cardiac MRI section obtained from the heart of a 3-week diabetic male Wistar rat weighing 330 g and aged 16 weeks with the outlines of both left and right ventricles drawn (A) and without drawn outlines (B). The heart rate was continuously monitored throughout the imaging session giving an intrinsic heart rate of 304±4 beats min^{-1}. The section was taken perpendicular to the principal cardiac axis. The time indicated in the upper left-hand corner of the image corresponds to the delay after the trigger, taken from the R-wave of the electrocardiogram (ECG), at which the signal was acquired. LV endo- and RV endo- indicate left and right ventricular endocardial outlines respectively, whereas LV epi- and RV epi- indicate left and right ventricular epicardial outlines respectively. Slice thickness was 1.44 mm. Field of view (FOV) was 4.5 cm and with an image matrix of 128X128 pixels, the nominal in-plane resolution was approximately 351.6 μm $pixel^{-1}$. The effective repeat-time (TR) was approximately 13 ms. The left ventricle shows circularly symmetry in transverse sections at all time-points through the cardiac cycle. Thus, the interventricular septum was considered as part of the left ventricle for subsequent geometrical analysis. In contrast, the right ventricle was defined as the crescent-shaped cardiac chamber with its wall meeting the left ventricular wall close to the diameter of the left ventricle.

A

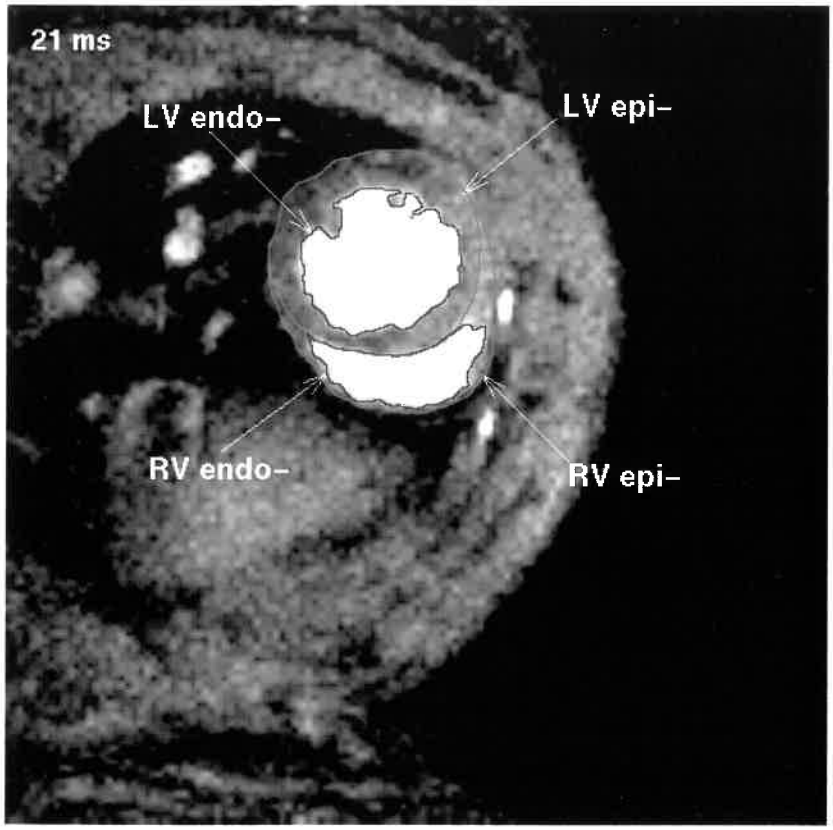

B

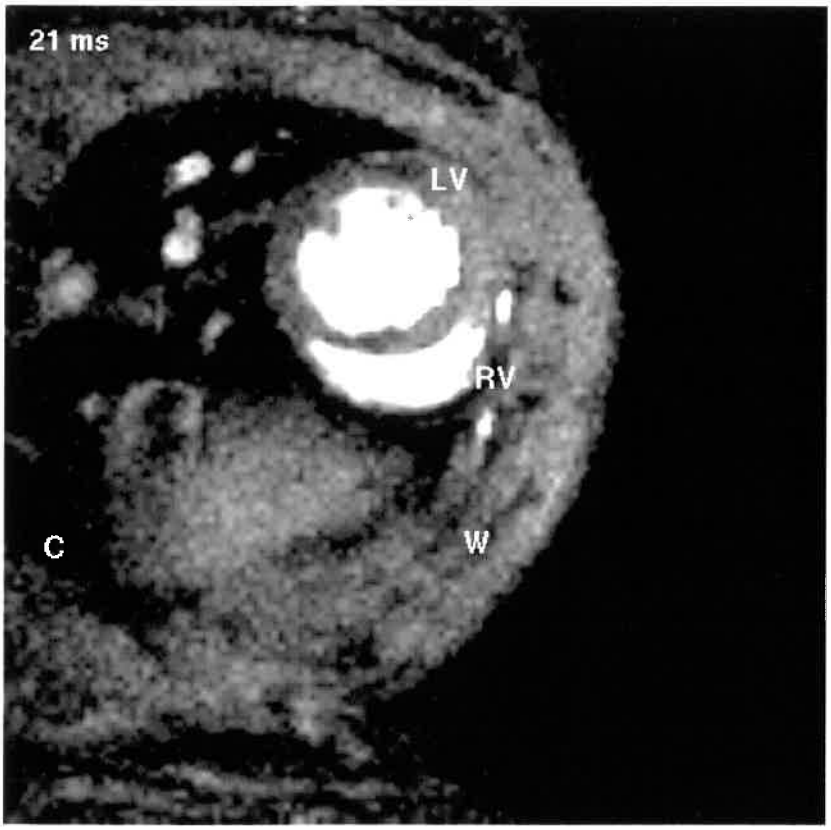

6.6 Post-mortem examination

For post-mortem examination and weighing of the left and right ventricular muscles, the animals were sacrificed after the magnetic resonance imaging using an overdose of euthetal (Schedule One method, Animal Scientific Procedures Act 1986) and their hearts were removed and placed in 3.7% phosphate buffered formaldehyde (BDH laboratory supplies, Poole, UK) for approximately 15 minutes, after which the hearts were removed from the fixative and blotted dry. The 2 atria were then removed and rings of the myocardium of both ventricles of 1–2 mm thick were cut perpendicular to the long axis of the heart. The right and left ventricular muscles were then separated from each other and weighed, then fixed in 3.7% phosphate buffered formaldehyde for an additional 24-48 hours.

6.7 Statistical analyses

Results are presented as means ± standard error of the means (SEM). As already mentioned (4.1), the main objectives of this study were: (1) to characterize left and right ventricular anatomical and functional myocardial changes associated with experimental diabetes, (2) to find out whether the duration of diabetes has an effect on these changes, and finally (3) to evaluate the therapeutic effects of captopril on ameliorating these abnormalities. Thus, statistical evaluation was first performed with the one-way analysis of variance (One-Way ANOVA) in comparison of the control group and the three untreated diabetic groups (the 3-, 6- and 9-week diabetic groups). This was followed by another One-Way ANOVA involving the control group and the two 9-week diabetic groups (the untreated group and the captopril-treated one). When there was a statistically significant difference, pair-wise multiple comparison procedures were performed using Tukey's Honestly Significant Difference (HSD) test. Differences were considered significant at $p<0.05$. The statistical significance of differences in the structural and functional parameters between the left and right ventricles in each of the five experimental groups was determined by the *t*-test and differences were considered significant at $p<0.05$. Pearson correlation coefficient (r) was used to test for correlations between measured or calculated quantities.

CHAPTER 7
BASIC PHYSIOLOGICAL PARAMETERS IN CONTROL AND DIABETIC ANIMALS

Tables 7.1-7.4 compare basic physiological parameters of control and diabetic animals 3-, 6- and 9-weeks following streptozotocin administration as well as the corresponding parameters in the 9-week captopril-treated diabetic animals. In addition to blood glucose concentrations, they summarize body weight, heart rate, systolic blood pressure as well as some baseline cardiac characteristics. The latter included both absolute left and right ventricular and total cardiac weight and the same values normalized to body weight. The findings were comparable with earlier studies of the diabetic heart (Maeda et al., 1995; Hicks et al., 1998).

7.1 Changes in blood glucose level

Tables 7.1 and 7.2 show that STZ-treatment produces a significant (five to six-fold) elevation in blood glucose compared to findings in control group confirming a successful induction of experimental diabetes mellitus. Furthermore, the STZ and captopril-treated group also showed similarly elevated blood glucose levels. It is also noticed that once induced, blood glucose levels remained elevated at stable levels throughout the experimental period.

7.2 Effects on systolic blood pressure and heart rate

Tables 7.1 and 7.2 demonstrate that the 6- and the 9-week but not the 3-week diabetic rats showed reduced heart rates and systolic blood pressures compared with the control animals, in agreement with previous studies (Maeda et al., 1995; Hicks et al., 1998). However, systolic blood pressure was not significantly reduced in the 6-week diabetic group compared with the control group. In contrast, the systolic blood pressures and the heart rates of the captopril-treated 9-week diabetic group were comparable with those of the control group and were accordingly significantly higher than corresponding values in the 9-week untreated diabetic

group. Table 7.1 also shows that the differences in the heart rate and systolic blood pressure between the 6- and the 9-week untreated groups were insignificant.

7.3 Effect on body weight

Tables 7.1 and 7.2 show lower weights in all diabetic animals including those treated with captopril compared with normal animals. Differences in the body weight were significant between the control group and the 6-week ($p<0.05$), the 9-week untreated ($p<0.05$), and the 9-week captopril-treated ($p<0.05$) diabetic groups. The body weights of the 3-week diabetic group were similar to those of the normal group ($p>0.05$). Furthermore, body weight fell significantly between 6 and 9 weeks of diabetes ($p<0.05$). These findings corresponded to a 4.6% reduction in body weight between the control group and the 3-week diabetic group, 15.7% between 3 weeks to 6 weeks, and 16.8% between 6 to 9 weeks.

7.4 Effects on absolute and normalized heart weight

The absolute heart weights of all the diabetic rats were decreased in comparison with those of the normal rats. However, in the absence of captopril treatment diabetic rats showed higher heart weights when these were normalized to the corresponding body weight, thus confirming earlier studies (Hicks et al., 1998). This relative hypertrophy was significant in the 6- week ($p<0.05$) and the 9-week ($p<0.05$) but not the 3-week diabetic group ($p>0.05$) relative to the control group; there was a significant progression of this hypertrophy between 6 and 9 weeks but the greatest change took place between 3 to 6 weeks (11.4%) rather than 6 to 9 weeks (9.5%). In contrast, no such relative cardiac hypertrophy in captopril-treated rats even at 9 weeks.

7.5 Effects on absolute and normalized left and right ventricular weights

Tables 7.1 and 7.2 also demonstrates in all the diabetic animals a reduced left and right ventricular weights compared to the normal animals. However, this corresponded to a relative hypertrophy when normalized to body weight in both left and right ventricles in the rats not treated with captopril.

It was not possible to calculate the mean percentage change in the absolute and normalized left and right ventricular weights following the different experimental periods as the study was not a serial one, involving a single experimental group examined serially following the different experimental periods, but rather it involved different experimental groups. Thus, the mean values of the absolute and normalized left and right ventricular weights in Tables 7.1 and 7.2 were used to calculate the percentage increase (+) or decrease (-) in these parameters following 3 and 6 weeks of diabetes without captopril treatment and following 9 weeks of diabetes without as well as with captopril treatment (Table 7.3). Thus, the mean value of each parameter of the control group was used as a reference value for calculating the percentage increase or decrease in the parameter following the different periods of experimental diabetes. Table 7.3, thus, shows, first, whether the changes occurred in these parameters over 3 weeks of diabetes were statistically significant and compares these changes with those occurred over 6 and 9 weeks of diabetes with and without captopril treatment. Secondly, it compares the changes occurred over 6 weeks of diabetes with those occurred over 9 weeks of diabetes with and without treatment. Finally, it demonstrates the effects of captopril treatment in ameliorating the abnormalities caused by diabetes by comparing the changes following 9 weeks of diabetes without captopril treatment with those following 9 weeks of diabetes without captopril treatment. The statistical significance of differences in the changes in each parameter following the different experimental periods is indicated by the same *p*-values obtained from Tukey's Honestly Significance Difference test while performing pair-wise multiple comparisons (Tables 7.1 and 7.2). The increase in normalized left ventricular weights thus was not significant at 3 weeks (2.1%) but became marked at 6 weeks (15.3%) and significantly more marked at 9 weeks (24.9%) greater than control respectively. In the absence of captopril treatment, the normalized right ventricular weights also increased 3.3%, 10%, and 25.0% over 3, 6, and 9 weeks of diabetes respectively when compared with the control group, with the differences at 6 and 9 but not 3 weeks of diabetes being significant against the control and the increase between 6 and 9 weeks also being significant.

In contrast, the normalized left ventricular weight actually decreased by 0.5% in the 9-week diabetic rats treated with captopril. Similarly, their normalized right ventricular weights were not significantly different from those of the control.

Table 7.4 completes this analysis by comparing the fractional deteriorations in the ventricular weights through each period of experimental diabetes. The mean value of each weight parameter was used to calculate its percentage increase (+) or decrease (-) respectively between 0 and 3, 3 and 6, and 6 and 9 weeks of diabetes without captopril treatment. The mean value of

each parameter of the control group was used to calculate its percentage increase or decrease between 0 and 3 weeks of diabetes without captopril treatment. The statistical significance of the deterioration in each parameter is indicated by the same *p*-value obtained when comparing the data obtained from the 3-week group with the data obtained from the control group, while performing pair-wise multiple comparisons using Tukey's Honestly Significance Difference test (Tables 7.1 and 7.2). Similarly, the *p*-values shown for each parameter between 3 and 6 and between 6 and 9 weeks of diabetes without captopril treatment are those obtained when comparing the data obtained from the 6-week group with the data obtained from the 3-week group and when comparing the data obtained from the 9-week group with the data obtained from the 6-week group respectively, also while performing pair-wise multiple comparisons using Tukey's Honestly Significance Difference test (Tables 7.1 and 7.2). The percentage increase in such normalized weights in the left ventricles were 2.1%, 13% and 8.3% between 0 and 3, 3 and 6 and 6 and 9 weeks respectively and the corresponding increases in normalized right ventricular weights were 3.3%, 6.5% and 13.6% respectively. Thus, the left ventricles showed the greatest changes between 3-6 weeks and the right ventricles the greatest changes later (6-9 weeks) in the condition.

Parameter	Control (n = 4)	3-week diabetic (n = 4)	6-week diabetic (n = 4)	9-week untreated diabetic (n = 4)	One-Way ANOVA	
					F	*P*-value (all levels)
Body weight (g)	351.3 ± 9.7 [c, d]	335 ± 8.4 [c, d]	282.5 ± 6.6 [a, b, d]	235 ± 8.4 [a, b, c]	40.095	<0.001
Blood glucose (mM)	5.2 ± 0.2 [b, c, d]	29.8 ± 1.5 [a]	30.3 ± 1.8 [a]	30.9 ± 1.4 [a]	88.323	<0.001
Systolic BP (mmHg)	143.8 ± 6.3 [d]	137.5 ± 7.2 [d]	112.5 ± 7.2	93.8 ± 12 [a, b]	7.455	0.004
Heart rate (beat/min)	322 ± 9 [c, d]	318 ± 7 [c, d]	280 ± 7 [a, b]	280 ± 6 [a, b]	9.593	0.002
Heart weight (g)	0.87 ± 0.01 [d]	0.85 ± 0.02 [d]	0.8 ± 0.03	0.73 ± 0.03 [a, b]	6.546	0.007
Heart weight/body weight (%)	0.249 ± 0.003 [c, d]	0.255 ± 0.001 [c, d]	0.284 ± 0.003 [a, b, d]	0.311 ± 0.003 [a, b, c]	99.176	<0.001
Left ventricular weight (g)	0.663 ± 0.01 [d]	0.645 ± 0.01 [d]	0.615 ± 0.02	0.555 ± 0.03 [a, b]	5.632	0.012
Left ventricular weight/body weight (%)	0.189 ± 0.002 [c, d]	0.193 ± 0.001 [c, d]	0.218 ± 0.003 [a, b, d]	0.236 ± 0.003 [a, b, c]	74.031	<0.001
Right ventricular weight (g)	0.21 ± 0.004 [d]	0.208 ± 0.005 [d]	0.188 ± 0.006	0.176 ± 0.006 [a, b]	8.894	0.002
Right ventricular weight/body weight (%)	0.06 ± 0.001 [c, d]	0.062 ± 0.001 [c, d]	0.066 ± 0.001 [a, b, d]	0.075 ± 0.0004 [a, b, c]	46.890	<0.001

Table 7.1: **General non-MRI derived features of the control and the three untreated diabetic groups.**

All values expressed as mean ± standard error of the mean (SEM). One-way analysis of variance (One-Way ANOVA) was used in comparison of the control and the three untreated diabetic groups followed by Tukey's Honestly Significant Difference test for pair-wise multiple comparisons. A value of $p<0.05$ was considered statistically significant.

[a] Significantly different from the control group.

[b] Significantly different from the 3-week diabetic group.

[c] Significantly different from the 6-week diabetic group.

[d] Significantly different from the 9-week untreated diabetic group.

Parameter	Control (n = 4)	9-week untreated diabetic (n = 4)	9-week captopril-treated diabetic (n = 4)	One-Way ANOVA	
				F	*P*-value (all levels)
Body weight (g)	351.3 ± 9.7 $^{+,\S}$	235 ± 8.4 *	247.5 ± 15.5 *	30.317	<0.001
Blood glucose (mM)	5.2 ± 0.2 $^{+,\S}$	30.9 ± 1.4 *	29.4 ± 1.2 *	185.699	<0.001
Systolic BP (mmHg)	143.8 ± 6.3 $^{+}$	93.8 ± 12 *,§	137.5 ± 7.5 $^{+}$	9.334	0.006
Heart rate (beat/min)	322 ± 9 $^{+}$	280 ± 6 *	311 ± 10	6.653	0.017
Heart weight (g)	0.87 ± 0.01 $^{+,\S}$	0.73 ± 0.03 *,§	0.61 ± 0.03 $^{*,+}$	22.437	<0.001
Heart weight/body weight (%)	0.249 ± 0.003 $^{+}$	0.311 ± 0.003 *,§	0.247 ± 0.01 $^{+}$	38.431	<0.001
Left ventricular weight (g)	0.663 ± 0.01 $^{+,\S}$	0.555 ± 0.03 *,§	0.463 ± 0.02 $^{*,+}$	20.206	<0.001
Left ventricular weight/body weight (%)	0.189 ± 0.002 $^{+}$	0.236 ± 0.003 *,§	0.188 ± 0.009 $^{+}$	24.403	<0.001
Right ventricular weight (g)	0.21 ± 0.004 $^{+,\S}$	0.176 ± 0.006 *,§	0.148 ± 0.008 $^{*,+}$	22.822	<0.001
Right ventricular weight/body weight (%)	0.06 ± 0.001 $^{+}$	0.075 ± 0.0004 *,§	0.06 ± 0.0005 $^{+}$	104.350	<0.001

Table 7.2: **General non-MRI derived features of the control and the two 9-week diabetic groups.**

All values expressed as mean ± standard error of the mean (SEM). One-way analysis of variance (One-Way ANOVA) was used in comparison of the control and the two 9-week diabetic groups followed by Tukey's Honestly Significant Difference test for pair-wise multiple comparisons. A value of $p<0.05$ was considered statistically significant.

*Significantly different from the control group.

$^{+}$ Significantly different from the 9-week untreated diabetic group.

§ Significantly different from the 9-week captopril-treated diabetic group.

Parameter	Change following 3 weeks of diabetes without captopril treatment	Change following 6 weeks of diabetes without captopril treatment	Change following 9 weeks of diabetes without captopril treatment	Change following 9 weeks of diabetes with captopril treatment
LV weight (g)	-2.7% [d]	-7.2%	-16.3% [a, b, §]	-30.2% [a, d]
RV weight (g)	-1.0% [d]	-10.5%	-16.2% [a, b, §]	-29.5% [a, d]
LV weight/ body weight (%)	+2.1% [c, d]	+15.3% [a, b, d]	+24.9% [a, b, c, §]	-0.5% [d]
RV weight/ body weight (%)	+3.3% [c, d]	+10.0% [a, b, d]	+25.0% [a, b, c, §]	0.0% [d]

Table 7.3: **The effect of the duration of diabetes on left and right ventricular weights and its modification by captopril treatment.**

LV weight: left ventricular weight and RV weight: right ventricular weight respectively.

The (-) and the (+) signs indicate a decrease and an increase in absolute and normalized left and right ventricular weights with diabetes respectively.

The symbols **a, b, c, d, and §** repeat the results obtained from Tukey's Honestly Significant Difference test while performing pair wise-multiple comparisons in Tables 7.1 and 7.2.

Parameter	Between 0 and 3 weeks of diabetes	Between 3 and 6 weeks of diabetes	Between 6 and 9 weeks of diabetes
LV weight (g)	-2.7%	-4.7%	-9.8%
RV weight (g)	-1.0%	-9.6%	-6.4%
LV weight/ body weight %	+2.1%	+13.0% [b]	+8.3% [c]
RV weight/ body weight %	+3.3%	+6.5% [b]	+13.6% [c]

Table 7.4: **Fractional deterioration in left and right ventricular weights through the experimentally induced diabetic state without captopril treatment.**

LV weight: left ventricular weight and RV weight: right ventricular weight respectively.

The (-) and the (+) signs indicate a decrease and an increase in absolute and normalized left and right ventricular weights with diabetes respectively.

The symbols **a, b, and c** repeat the results obtained from Tukey's Honestly Significant Difference test while performing pair wise-multiple comparisons in Tables 7.1 and 7.2. They only indicate that the deterioration was significant.

CHAPTER 8
CHANGES IN MYOCARDIAL ANATOMY IN EXPERIMENTAL DIABETES

8.1 Transverse MRI cardiac sections

The MRI sessions obtained complete sets of transverse MRI cardiac sections in order to characterize and compare the dynamic changes occurring in both ventricles through the cardiac cycle between the 4 experimental diabetic groups, including the 9-week captopril-treated group and control group. In addition to being used for qualitative analysis of ventricular geometry and measuring left and right ventricular myocardial volumes, the sets of transverse sections were also used to derive endocardial, epicardial, and myocardial volume curves for both ventricles. These made it further possible to reconstruct the kinetics of both left and right ventricular contraction and relaxation. These data provided the basis for further quantitative descriptions of these events in terms of the left and right ventricular systolic and diastolic dV/dt through the cardiac cycle.

Figures 8.1-8.5 display typical transverse cardiac sections through intact beating hearts in the control and the 3-, 6-, 9-week untreated, and the 9-week captopril-treated diabetic rats respectively. Images of twelve transverse contiguous slices of the same thickness perpendicular to the principal cardiac axis were typically obtained from the heart of each animal studied. All sections were positioned perpendicular to the principal cardiac axis and taken together fully covered the two ventricles from their apices to their outlets. This made it possible to reconstruct their geometry for subsequent quantitative analysis. In order to characterize temporally both systolic and diastolic events, each slice in turn was typically imaged at twelve time-points during the cardiac cycle.

The cine imaging protocol provided high quality anatomical images in all the experimental groups and proved particularly useful in demonstrating blood as a bright intensity within the

cardiac chambers. This achieved a clear demarcation of myocardium from blood and therefore accurately defined the endocardial borders of both ventricles. This facilitated reliable quantitative estimation of the end-diastolic and end-systolic volumes.

The left ventricles of the hearts of all the experimental rats resembled that of the human heart in the consistent circular symmetry of their epicardial and endocardial borders in transverse sections throughout the cardiac cycle. This feature made it convenient to regard the inter-ventricular septum as part of the left ventricle in quantitative measurements of left and right ventricular anatomy. Similarly, normal and diabetic right ventricles resembled the right ventricle of the human heart in their crescent-shaped transverse section and thinner walls. These similarities with the human heart would expedite use of the rat heart as a disease model for MRI studies.

The frames in Figures 8.1-8.5 are separated in time by 13 ms, the TR in the imaging protocol used; thus provided a sufficiently close temporal resolution of left and right ventricular geometry for identification of both end-diastole and end-systole points in the cardiac cycle. The first frames in Figures 8.1-8.5 showed images acquired typically 8 ms after the trigger pulse from the R-wave of the ECG and demonstrated fully dilated ventricles at end-diastole. The succeeding frames in Figures 8.1, 8.2, and 8.5, obtained from a typical normal, a typical 3-week diabetic and a typical 9-week captopril-treated diabetic rats respectively then follow a prompt development of systole in which both the left and right ventricular walls thickened and their cavities contracted. End-systole corresponding to the minimum cross section in both ventricular cavities was reached synchronously at about 100 ms after the trigger pulse in the control, the 3-week diabetic and the 9-week captopril treated groups. This was followed by a rapid diastolic refilling of both the left and right ventricular cavities accompanied by a relative thinning of the ventricular walls. In contrast, in the 6- and 9-week diabetic rats, which were not treated with captopril, the first few frames showing early systole indicated a significant lag in the myocardial thickening and contraction process until approximately 34 ms after the trigger pulse from the R-wave of the ECG. End-systole was not reached until approximately 112 ms after the trigger pulse. These changes suggest significant changes in left and right ventricular systolic function in these 2 groups of rats. Both the left and right ventricles of the 6- and 9-week diabetic rats also showed a retarded diastolic refilling.

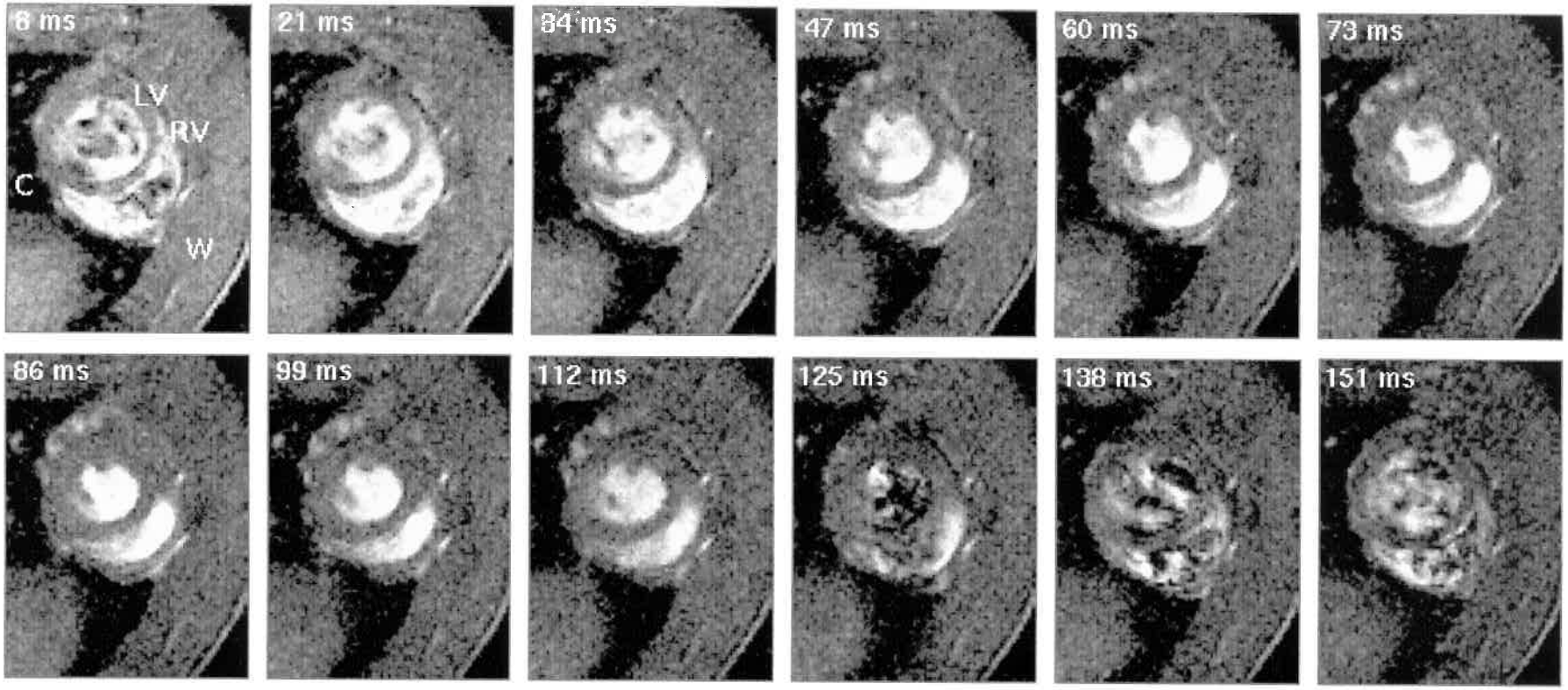

Figure 8.1: **Typical transverse sections obtained from the heart of a normal control rat.** A series of typical transverse MR sections obtained from the heart of a typical normal 16 weeks old male Wistar rat weighing 340 g. The heart rate was continuously monitored throughout the imaging session giving an intrinsic heart rate was 315 ± 4 beats min^{-1}. The sections were taken perpendicular to the principal cardiac axis at one spatial slice at typically twelve time points during the cardiac cycle. These time points are indicated in the upper left-hand corner of each panel and correspond to the delay after the trigger, taken from the R-wave of the electrocardiogram (ECG), at which the signal was acquired. Each image is the average of two signals obtained at corresponding points in the cardiac cycle following the R wave. LV and RV indicate left and right ventricles respectively and C and W indicate chest cavity and chest wall respectively. Slice thickness was 1.50 mm. Field of view (FOV) was 5 cm and with an image matrix of 128 pixel square, the nominal in-plane resolution was approximately 390.6 μm $pixel^{-1}$. The effective repeat-time (TR) was approximately 13 ms.

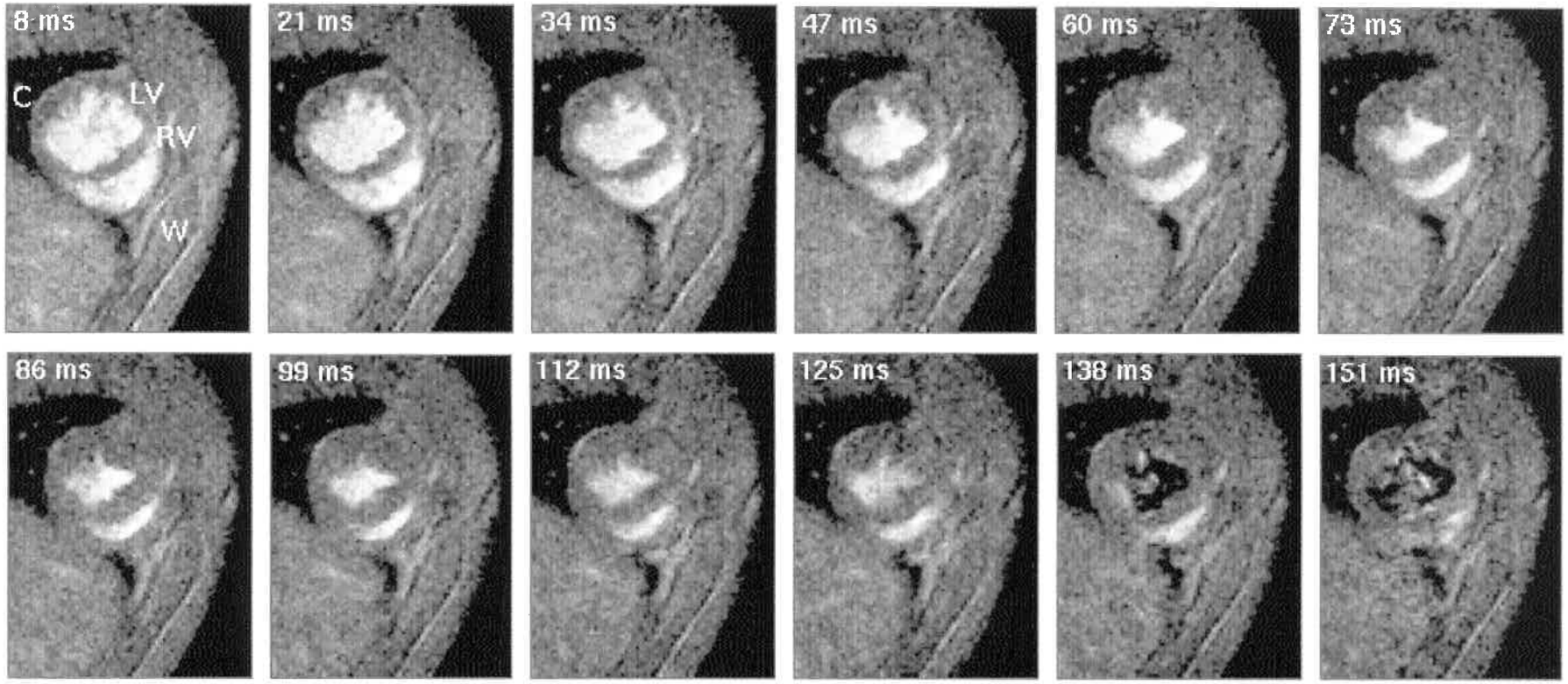

Figure 8.2: **Typical transverse sections obtained from the heart of a 3-week diabetic rat.** A series of typical transverse MR sections obtained from the heart of a typical 3-week diabetic male Wistar rat weighing 330 g and aged 16 weeks. The heart rate was continuously monitored throughout the imaging session giving an intrinsic heart rate was 307 ± 4 beats min^{-1}. The sections were taken perpendicular to the principal cardiac axis at one spatial slice at typically twelve time points during the cardiac cycle. These time points are indicated in the upper left-hand corner of each panel and correspond to the delay after the trigger, taken from the R-wave of the electrocardiogram (ECG), at which the signal was acquired. Each image is the average of two signals obtained at corresponding points in the cardiac cycle following the R wave. LV and RV indicate left and right ventricles respectively and C and W indicate chest cavity and chest wall respectively. Slice thickness was 1.44 mm. Field of view (FOV) was 4.5 cm and with an image matrix of 128 pixel square, the nominal in-plane resolution was approximately 351.6 μm $pixel^{-1}$. The effective repeat-time (TR) was approximately 13 ms.

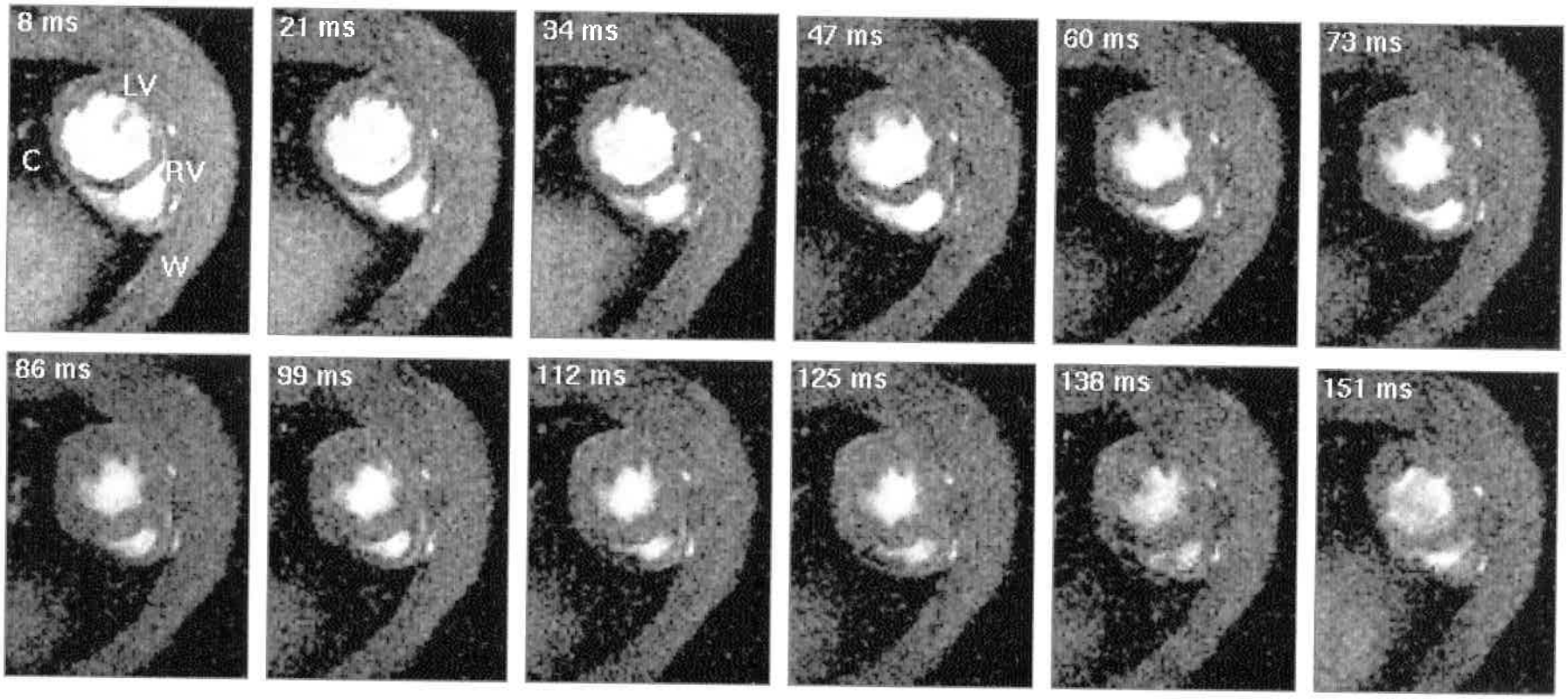

Figure 8.3: **Typical transverse sections obtained from the heart of a 6-week diabetic rat.** A series of typical transverse MR sections obtained from the heart of a typical 6-week diabetic old male Wistar rat weighing 275 g and aged 16 weeks. The heart rate was continuously monitored throughout the imaging session giving an intrinsic heart rate was 300 ± 6 beats min^{-1}. The sections were taken perpendicular to the principal cardiac axis at one spatial slice at typically twelve time points during the cardiac cycle. These time points are indicated in the upper left-hand corner of each panel and correspond to the delay after the trigger, taken from the R-wave of the electrocardiogram (ECG), at which the signal was acquired. Each image is the average of two signals obtained at corresponding points in the cardiac cycle following the R wave. LV and RV indicate left and right ventricles respectively and C and W indicate chest cavity and chest wall respectively. Slice thickness was 1.44 mm. Field of view (FOV) was 4.5 cm and with an image matrix of 128 pixel square, the nominal in-plane resolution was approximately 351.6 μm $pixel^{-1}$. The effective-repeat time (TR) was approximately 13 ms.

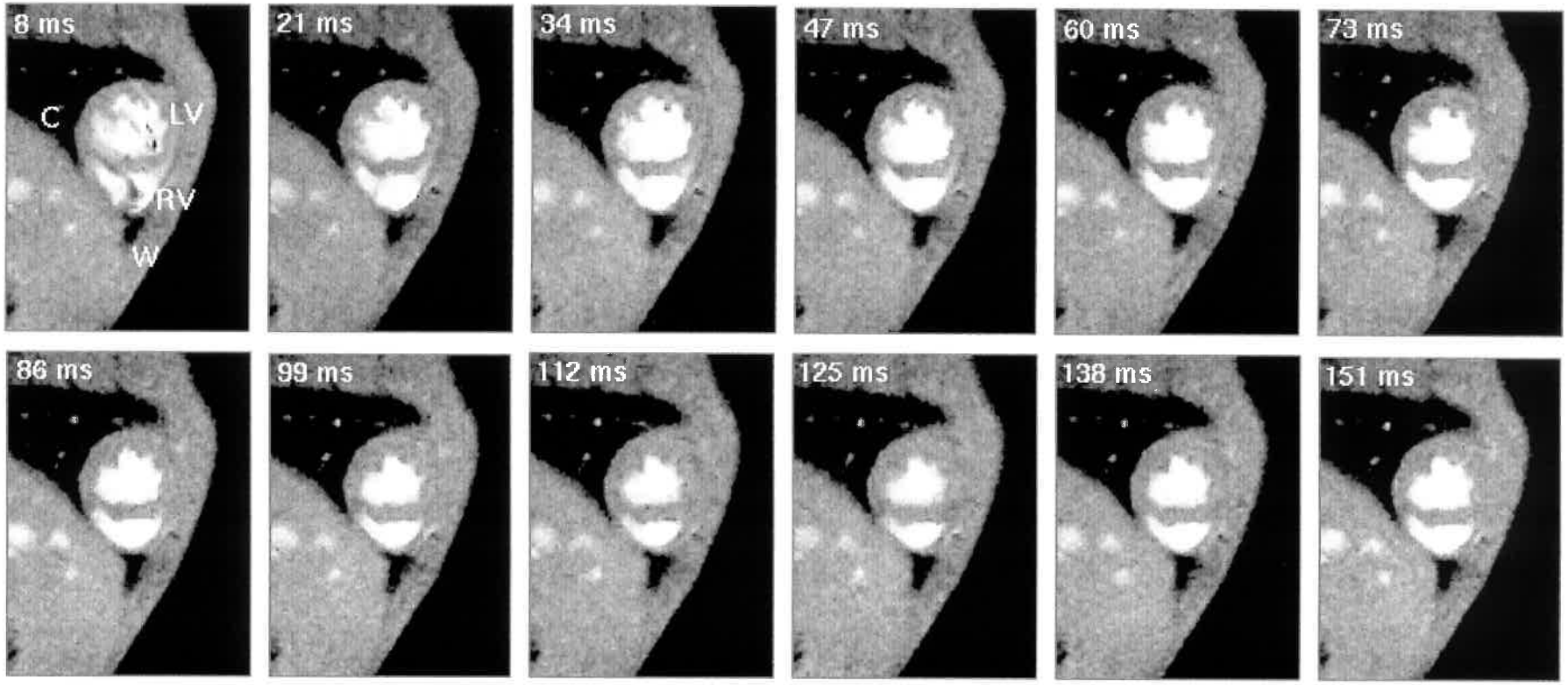

Figure 8.4: **Typical transverse sections obtained from the heart of a 9-week diabetic rat.** A series of typical transverse MR sections obtained from the heart of a typical 9-week diabetic old male Wistar rat weighing 230 g and aged 16 weeks. The heart rate was continuously monitored throughout the imaging session giving an intrinsic heart rate was 290 ± 4 beats min^{-1}. The sections were taken perpendicular to the principal cardiac axis at one spatial slice at typically twelve time points during the cardiac cycle. These time points are indicated in the upper left-hand corner of each panel and correspond to the delay after the trigger, taken from the R-wave of the electrocardiogram (ECG), at which the signal was acquired. Each image is the average of two signals obtained at corresponding points in the cardiac cycle following the R wave. LV and RV indicate left and right ventricles respectively and C and W indicate chest cavity and chest wall respectively. Slice thickness was 1.44 mm. Field of view (FOV) was 4.5 cm and with an image matrix of 128 pixel square, the nominal in-plane resolution was approximately 351.6 μm $pixel^{-1}$. The effective-repeat time (TR) was approximately 13 ms.

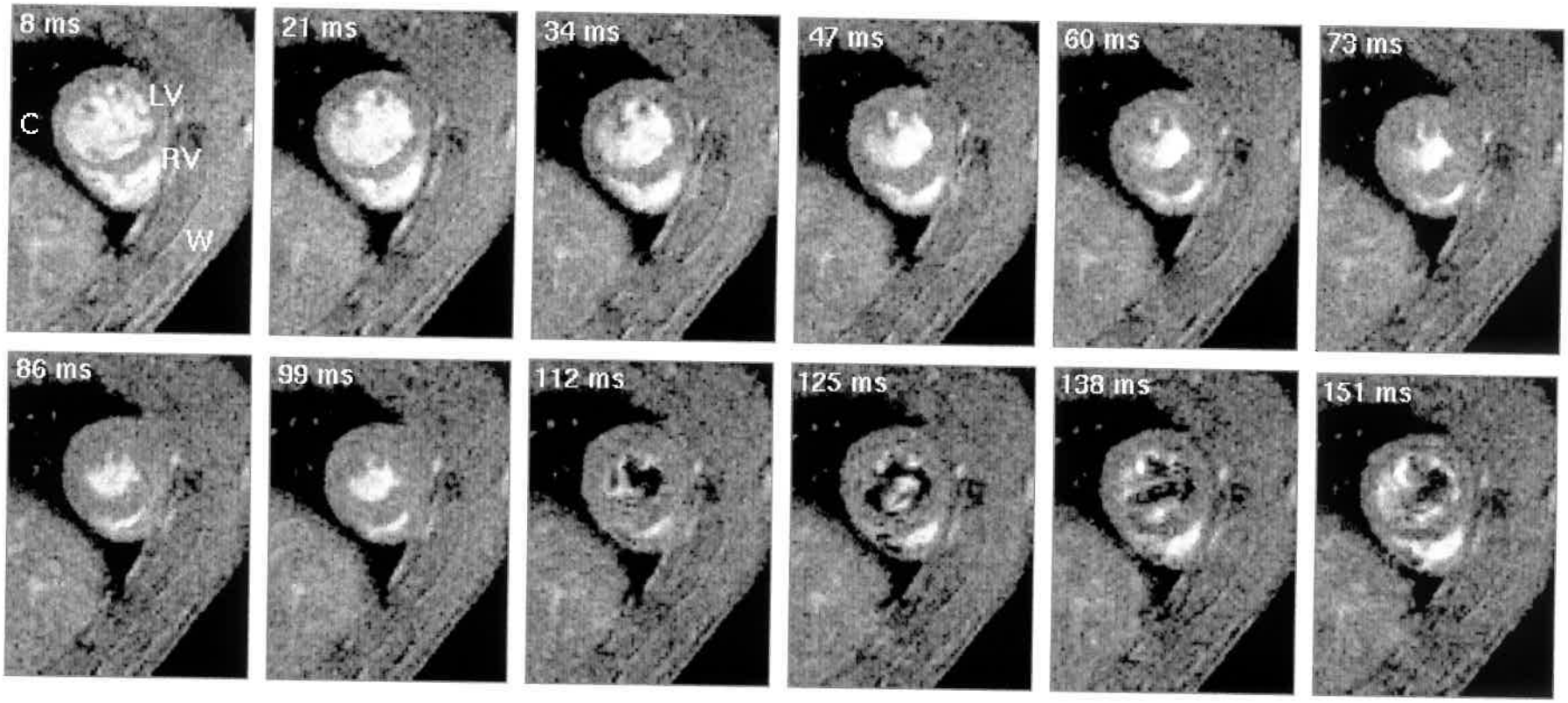

Figure 8.5: **Typical transverse sections obtained from the heart of a captopril-treated 9-week diabetic rat.** A series of typical transverse MR sections obtained from the heart of a typical captopril-treated 9-week diabetic male Wistar rat weighing 245 g and aged 16 weeks. The heart rate was continuously monitored throughout the imaging session giving an intrinsic heart rate was 300 ± 4 beats min^{-1}. The sections were taken perpendicular to the principal cardiac axis at one spatial slice at typically twelve time points during the cardiac cycle. These time points are indicated in the upper left-hand corner of each panel and correspond to the delay after the trigger, taken from the R-wave of the electrocardiogram (ECG), at which the signal was acquired. Each image is the average of two signals obtained at corresponding points in the cardiac cycle following the R wave. LV and RV indicate left and right ventricles respectively and C and W indicate chest cavity and chest wall respectively. Slice thickness was 1.44 mm. Field of view (FOV) was 4.5 cm and with an image matrix of 128 pixel square, the nominal in-plane resolution was approximately 351.6 μm $pixel^{-1}$. The effective-repeat time (TR) was approximately 13 ms.

8.2 Ventricular myocardial volumes measured by MRI

Myocardial volumes of both ventricles of the five experimental groups, both diabetic and control, were obtained from the corresponding transverse cardiac MRI sections. To assess the internal consistency of such MRI-based measurements, both the left and right ventricular myocardial volumes during systole were compared with the corresponding volumes during diastole for all the experimental rats. Finally, the left and right ventricular myocardial volumes of all the five experimental groups were compared with their corresponding left and right ventricular myocardial masses obtained at post-mortem. The derived left and right ventricular myocardial densities were then compared with previous reports.

Tables 8.1-8.4 demonstrate that the use of MRI to derive absolute and normalized myocardial volumes gave results that agreed with the post-mortem determinations (Tables 7.1-7.4).

Table 8.3 uses the mean value of the absolute and normalized left and right ventricular myocardial volumes in Tables 8.1 and 8.2 to calculate the percentage increase (+) or decrease (-) in these parameters following 3 and 6 weeks of diabetes without captopril treatment and following 9 weeks of diabetes both without and with captopril treatment. The mean value of each parameter of the control group was used as a reference value for calculating its percentage increase or decrease. Thus, Table 8.3 shows whether the changes occurred in these parameters following the different periods of experimental diabetes were significant and compares the effect of the different experimental periods on these parameters. It also confirms the beneficial therapeutic effects of captopril in ameliorating the abnormalities caused by diabetes. The statistical significance of differences in the changes in each parameter following the different periods of experimental diabetes is indicated by the same p-values obtained from Tukey's Honestly Significance Difference test while performing pair-wise multiple comparisons (Tables 8.1 and 8.2).

Tables 8.1-8.3, thus, show that the absolute left ventricular myocardial volumes measured by MRI showed relatively little change at 3 weeks (a reduction of 2.4% when compared with the control group), but progressive decreases of 7.8% at 6 weeks and 17.6% and 31.3% at 9 weeks of diabetes without and with captopril treatment respectively compared with the control group. Significant differences were only observed between the control group and both the 9-week untreated ($p<0.05$) and the 9-week captopril-treated ($p<0.05$) diabetic groups respectively. In addition, the 9-week captopril-treated diabetic rats had significantly lower left ventricular myocardial volumes than the 9-week untreated diabetic rats ($p<0.05$).

Tables 8.1-8.3 also show that both the 9-week diabetic groups, the untreated group and the one treated with captopril, but not the 3-week or the 6-week diabetic groups had significantly smaller absolute right ventricular myocardial volumes compared with the normal group.

Tables 8.1 and 8.2 also summarize left and right ventricular myocardial volumes of the five experimental groups normalized to their corresponding body weights. Consistent with the post-mortem findings, these values increased in the 6- and the 9-week untreated groups but not the 3-week, or the 9-week captopril-treated group.

Thus, without captopril treatment, the normalized left ventricular myocardial volume increased by 2.2%, 14.5% and 23.1% over 3, 6 and 9 weeks of diabetes respectively over the control group (Table 8.3). The corresponding right ventricular values were 1.7%, 10.3% and 24.1% respectively. In both the left and right ventricles, there was a significant increase in the normalized myocardial volume even between 6 and 9 weeks. In contrast, the normalized right ventricular myocardial volumes increased by only 1.7% and the normalized left ventricular myocardial volumes decreased by 2.2% with captopril treatment (Table 8.3).

Table 8.4 completes this analysis by summarizing the fractional deteriorations in left and right ventricular myocardial volumes through each of the experimental periods. As before, the mean value of each myocardial volume parameter was used to calculate its percentage increase (+) or decrease (-) respectively between 0 and 3, 3 and 6, and 6 and 9 weeks of diabetes without captopril treatment. The mean value of each parameter of the control group was used to calculate its percentage increase or decrease between 0 and 3 weeks of diabetes without captopril treatment. The statistical significance of the deterioration in each parameter between 3 and 6 weeks of diabetes without captopril treatment is indicated by the same *p*-value obtained when comparing the data obtained from the 6-week group with the data obtained from the 3-week diabetic group, while performing pair-wise multiple comparisons using Tukey's Honestly Significance Difference test (Tables 8.1 and 8.2). Similarly, the *p*-values shown for each parameter between 6 and 9 weeks of diabetes without captopril treatment are those obtained when comparing the data obtained from the 9-week group with the data obtained from the 6-week diabetic group also while applying Tukey's Honestly Significance Difference test for performing pair-wise multiple comparisons. Thus, Table 8.4 shows that without captopril treatment, any changes in the left and the right ventricular myocardial volumes that occurred over 3 weeks of diabetes were insignificant, whereas there were significant changes between 3 and 6 and between 6 and 9 weeks of diabetes. However, there were relatively larger changes in normalized left ventricular myocardial volumes between 3 and 6 weeks (12.1%) than between 6

and 9 weeks (7.5%). In the case of the right ventricle, larger changes took place between 6 and 9 weeks (12.5%) than between 3 and 6 weeks (8.5%).

8.3 Conservation of left and right ventricular myocardial volumes throughout the cardiac cycle

Figure 8.6 plots MRI-measured left and right ventricular myocardial volumes obtained from the transverse cardiac magnetic resonance sections during systole and diastole from all the experimental rats and demonstrates that both left and the right ventricular myocardial volumes were conserved throughout the cardiac cycle.

8.4 Left and right ventricular myocardial densities

Figure 8.7 plots left and right ventricular myocardial volumes determined by MRI against the corresponding directly determined left and right ventricular masses of the five experimental groups measured at post-mortem. It shows that the MRI-measured left and right ventricular myocardial volumes (μl) and the directly determined respective left and right ventricular muscle masses (mg) were almost equal in each of the five experimental groups. Furthermore, all the four diabetic groups had left and right ventricular myocardial densities almost equal to those of the control group. Thus, the left and right ventricular myocardial densities were almost equal in the five experimental groups with an average ventricular myocardial density of 1.02 ± 0.02 mg μl^{-1} and 1.03 ± 0.02 mg μl^{-1} for the left and right ventricles respectively, in agreement with previous reports (Wise et al., 1998).

Figure 8.6 (next page): **Conservation of left and right ventricular myocardial volumes throughout the cardiac cycle.** *A*, a comparative plot of the MRI-determined left ventricular (LV) myocardial volume during systole and diastole. The left ventricular myocardial volume at the 12 time points during the cardiac cycle for each rat. The left ventricular myocardial volume measured by MRI during systole, for each individual rat, was taken from the average value from all the time-points sampled during systole. Similarly the left ventricular myocardial volume measured by MRI during diastole, for each individual rat, was taken from the average value from all the time-points sampled during diastole in the cardiac cycle. These are the volumes correlated here. As displayed, there was a close correlation between the systolic and diastolic left ventricular myocardial volumes ($r = 0.91$). *B,* a comparative plot of the MRI-determined right ventricular (RV) myocardial volume during systole and diastole. The right ventricular myocardial volume at the 12 time points during the cardiac cycle for each rat. The right ventricular myocardial volume measured by MRI during systole, for each individual rat, was taken from the average value from all the time-points sampled during systole. Similarly the right ventricular myocardial volume measured by MRI during diastole, for each individual rat, was taken from the average value from all the time-points sampled during diastole in the cardiac cycle. These are the volumes correlated here. As displayed, there was a close correlation between the systolic and diastolic right ventricular myocardial volumes ($r = 0.90$).

A

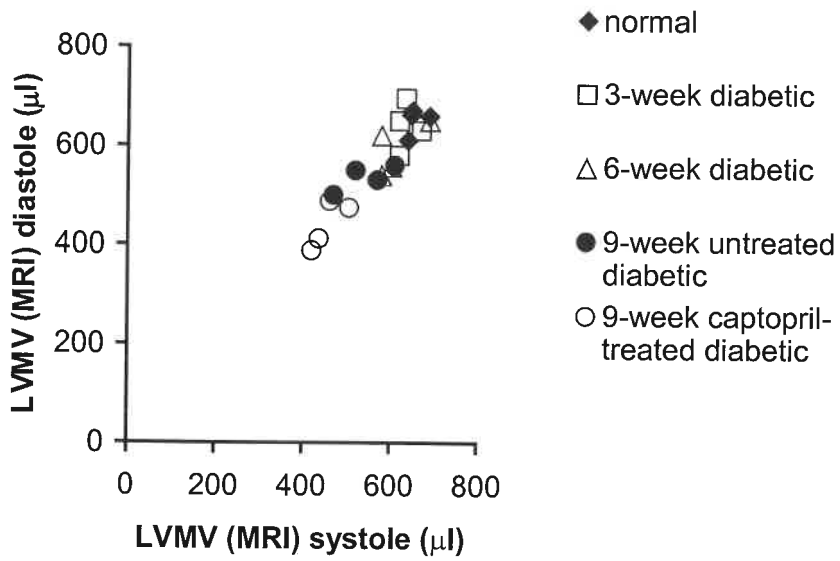
LVMV (MRI) diastole (µl)
800
600
400
200
0
0
200
400
600
800
LVMV (MRI) systole (µl)
normal
3-week diabetic
6-week diabetic
9-week untreated diabetic
9-week captopril-treated diabetic

B

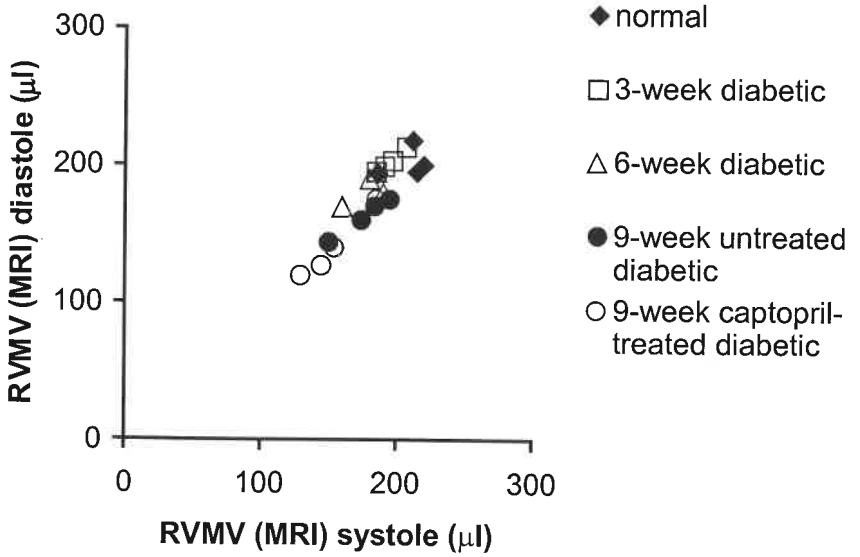
RVMV (MRI) diastole (µl)
300
200
100
0
0
100
200
300
RVMV (MRI) systole (µl)
normal
3-week diabetic
6-week diabetic
9-week untreated diabetic
9-week captopril-treated diabetic

Figure 8.7 (next page)**: Left and right ventricular muscle volumes.** *A*, a comparative plot of the MRI-determined left ventricular (LV) myocardial volumes (μl) against the corresponding directly determined left ventricular masses (mg) of the experimental groups measured at post-mortem. As displayed, the mean left ventricular myocardial volume measured my MRI (μl) was almost equal to the corresponding left ventricular mass (mg) measured directly at post-mortem in the control as well as in the four diabetic groups, giving left ventricular myocardial densities of 1.01 ± 0.004, 1.01 ± 0.002, 1.02 ± 0.005, 1.03 ± 0.01, 1.03 ± 0.03 mg μl^{-1} for the control, the 3-week, the 6-week, the 9-week untreated, and the 9-week captopril-treated diabetic groups respectively. *B*, a comparative plot of the MRI-determined right ventricular (RV) myocardial volumes (μl) against the corresponding directly determined right ventricular masses (mg) of the experimental groups measured at post-mortem. As displayed, the mean right ventricular myocardial volume measured my MRI (μl) was almost equal to the corresponding right ventricular mass (mg) measured directly at post-mortem in the control as well as the four diabetic groups, giving right ventricular myocardial densities of 1.03 ± 0.01, 1.04 ± 0.02, 1.03 ± 0.01, 1.05 ± 0.02, and 1.01 ± 0.02 mg μl^{-1} for the control, the 3-week, the 6-week, the 9-week untreated diabetic, and the 9-week captopril-treated diabetic groups respectively. *C*, a comparative plot of left ventricular myocardial density against the corresponding right ventricular myocardial density of the five experimental groups. As displayed, the average left ventricular density was almost equal to the corresponding right ventricular density in each experimental group with the difference being insignificant.

A

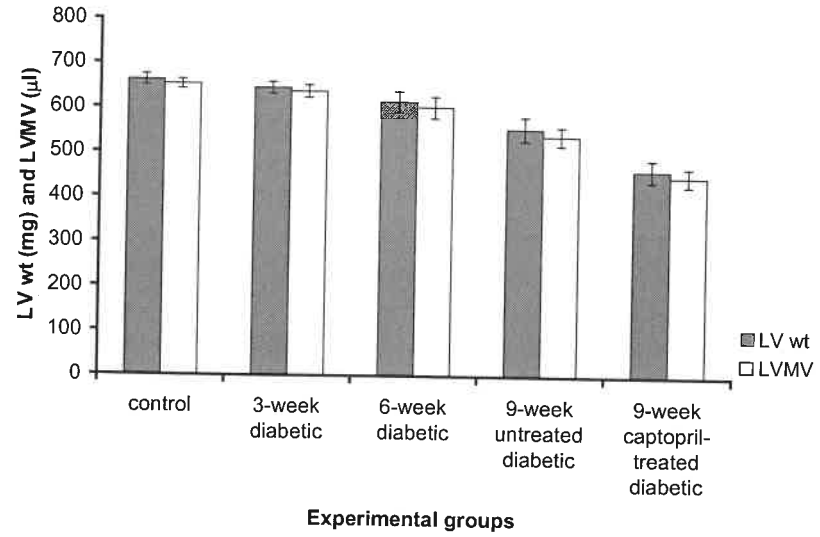
LV wt (mg) and LVMV (μl)
800
700
600
500
400
300
200
100
0
control
3-week diabetic
6-week diabetic
9-week untreated diabetic
9-week captopril-treated diabetic
LV wt
LVMV
Experimental groups

B

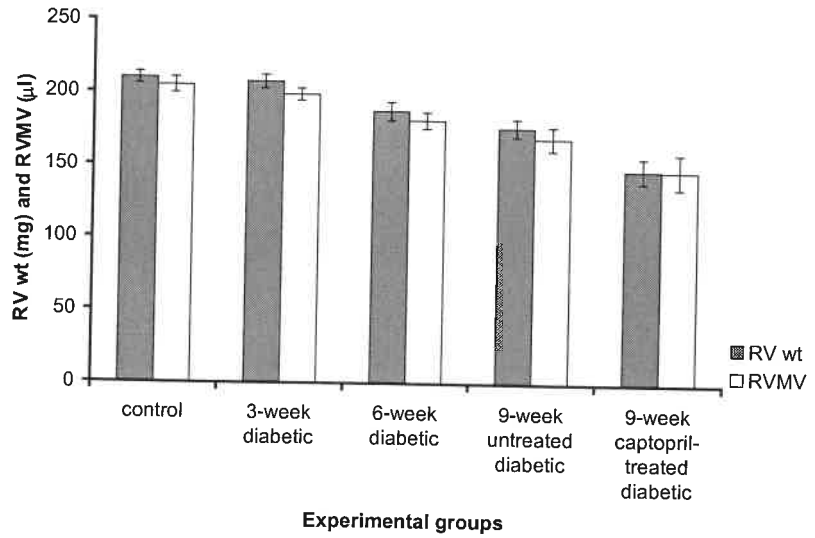
RV wt (mg) and RVMV (μl)
250
200
150
100
50
0
control
3-week diabetic
6-week diabetic
9-week untreated diabetic
9-week captopril-treated diabetic
RV wt
RVMV
Experimental groups

C

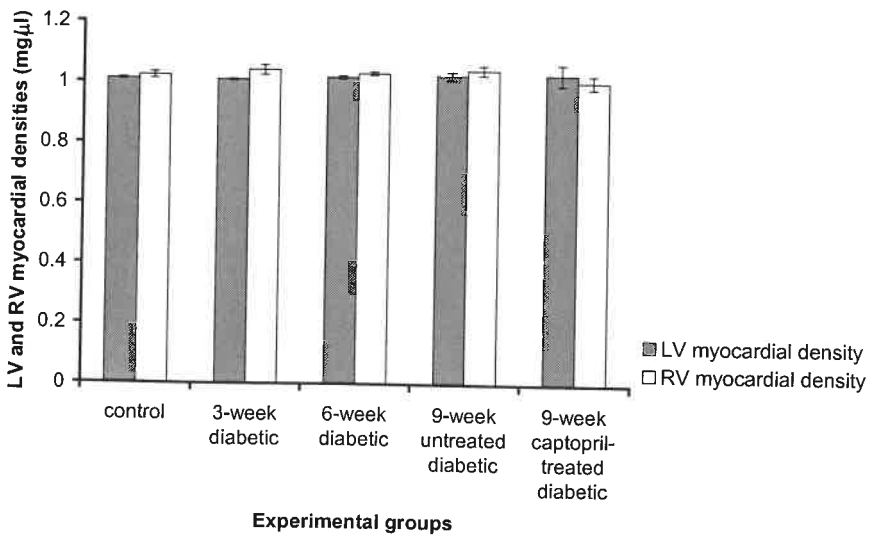
LV and RV myocardial densities (mg/μl)
1.2
1
0.8
0.6
0.4
0.2
0
control
3-week diabetic
6-week diabetic
9-week untreated diabetic
9-week captopril-treated diabetic
LV myocardial density
RV myocardial density
Experimental groups

Parameter	Control (n = 4)	3-week diabetic (n = 4)	6-week diabetic (n = 4)	9-week untreated diabetic (n = 4)	One-Way ANOVA	
					F	*P*-value (all levels)
Left ventricular myocardial volume (LVMV) (μl)	653.5 ± 10.3 [d]	637.5 ± 3.9 [d]	602.5 ± 23.9	538.8 ± 20.8 [a, b]	7.942	0.003
Right ventricular myocardial volume (RVMV) (μl)	205 ± 5.4 [d]	198.8 ± 4.3 [d]	181.3 ± 5.5	169 ± 8.2 [a, b]	7.426	0.005
LVMV/ body weight (μl/g)	1.86 ± 0.03 [c, d]	1.9 ± 0.01 [c, d]	2.13 ± 0.04 [a, b, d]	2.29 ± 0.01 [a, b, c]	68.378	<0.001
RVMV/ body weight (μl/g)	0.58 ± 0.01 [c, d]	0.59 ± 0.01 [d]	0.64 ± 0.01 [a, d]	0.72 ± 0.01 [a, b, c]	27.927	<0.001

Table 8.1: **MRI-measured left and right ventricular myocardial volumes of the control and the three untreated diabetic groups.** The left and right ventricular myocardial volume measured by MRI, for each rat, was taken form the average value from all the time-points sampled throughout the cardiac cycle. The body weight-normalized left and right ventricular myocardial volumes of the experimental rats were calculated using the corresponding body weight of the anaesthetised rat.

All values expressed as mean ± standard error of the mean (SEM). One-way analysis of variance (One-Way ANOVA) was used in comparison of the control and the three untreated diabetic groups followed by Tukey's Honestly Significant Difference test for pair-wise multiple comparisons. A value of $p<0.05$ was considered statistically significant.

[a] Significantly different from the control group.

[b] Significantly different from the 3-week diabetic group.

[c] Significantly different from the 6-week diabetic group.

[d] Significantly different from the 9-week untreated diabetic group.

Parameter	Control (n = 4)	9-week untreated diabetic (n = 4)	9-week captopril-treated diabetic (n = 4)	One-Way ANOVA	
				F	*P*-value (all levels)
Left ventricular myocardial volume (LVMV) (μl)	653.5 ± 10.3 $^{+,\S}$	538.8 ± 20.8 *,§	448.8 ± 20.1 $^{*,+}$	33.509	<0.001
Right ventricular myocardial volume (RVMV) (μl)	205 ± 5.4 $^{+,\S}$	169 ± 8.2 *	147 ± 11.9 *	10.822	0.004
LVMV/ body weight (μl/g)	1.86 ± 0.03 $^{+}$	2.29 ± 0.01 *,§	1.82 ± 0.05 $^{+}$	53.537	<0.001
RVMV/ body weight (μl/g)	0.58 ± 0.01 $^{+}$	0.72 ± 0.01 *,§	0.59 ± 0.01 $^{+}$	39.381	<0.001

Table 8.2: **MRI-measured left and right ventricular myocardial volumes of the control and the two 9-week diabetic groups.** The left and right ventricular myocardial volume measured by MRI, for each rat, was taken form the average value from all the time-points sampled throughout the cardiac cycle. The body weight-normalized left and right ventricular myocardial volumes of the experimental rats were calculated using the corresponding body weight of the anaesthetised rat.

All values expressed as mean ± standard error of the mean (SEM). One-way analysis of variance (One-Way ANOVA) was used in comparison of the control and the two 9-week diabetic groups followed by Tukey's Honestly Significant Difference test for pair-wise multiple comparisons. A value of $p<0.05$ was considered statistically significant.

*Significantly different from the control group.

$^{+}$Significantly different from the 9-week untreated diabetic group.

§Significantly different from the 9-week captopril-treated diabetic group.

Parameter	Change following 3 weeks of diabetes without captopril treatment	Change following 6 weeks of diabetes without captopril treatment	Change following 9 weeks of diabetes without captopril treatment	Change following 9 weeks of diabetes with captopril treatment
LVMV (µl)	-2.4% [d]	-7.8%	-17.6% [a, b, §]	-31.3% [a, d]
RVMV (µl)	-3.0% [d]	-11.6%	-17.6% [a, b]	-28.3% [a]
LVMV/ body weight (µl/g)	+2.2% [c, d]	+14.5% [a, b, d]	+23.1% [a, b, c, §]	-2.2% [d]
RVMV/ body weight (µl/g)	+1.7% [d]	+10.3% [a, d]	+24.1% [a, b, c, §]	1.7% [d]

Table 8.3: **The effect of the duration of diabetes on left and right ventricular myocardial volumes and its modification by captopril treatment.**

LVMV: left ventricular myocardial volume and RVMV: right ventricular myocardial volume respectively.

The (-) and the (+) signs indicate a decrease and an increase in absolute and normalized left and right ventricular myocardial volumes with diabetes respectively.

The symbols **a, b, c, d, and §** repeat the results obtained from Tukey's Honestly Significant Difference test while performing pair wise-multiple comparisons in Tables 8.1 and 8.2.

Parameter	Between 0 and 3 weeks of diabetes	Between 3 and 6 weeks of diabetes	Between 6 and 9 weeks of diabetes
LVMV (µl)	-2.4%	-5.5%	-10.6%
RVMV (µl)	-3.0%	-8.8%	-6.8%
LVMV/ body weight (µl/g)	+2.2%	+12.1% [b]	+7.5% [c]
RVMV/ body weight (µl/g)	+1.7%	+8.5%	+12.5% [c]

Table 8.4: **Fractional deterioration in left and right ventricular myocardial volumes through the experimentally induced diabetic state without captopril treatment.**

LVMV: left ventricular myocardial volume and RVMV: right ventricular myocardial volume respectively.

The (-) and the (+) signs indicate a decrease and an increase in absolute and normalized left and right ventricular myocardial volumes with diabetes respectively.

The symbols **a, b, and c** repeat the results obtained from Tukey's Honestly Significant Difference test while performing pair wise-multiple comparisons in Tables 8.1 and 8.2. They only indicate that the deterioration was significant.

CHAPTER 9
CHANGES IN THE CARDIAC CYCLE OF THE LEFT AND RIGHT VENTRICLES IN EXPERIMENTAL DIABETES

9.1 Ventricular volume curves

Closely sampled MRI data of the kind showed in Figures 8.1-8.5 made it possible to reconstruct the volume changes through the cardiac cycle of both the left and right ventricles in all the 5 experimental groups. Figures 9.1 and 9.2 plot the mean endocardial (circles), epicardial (squares), and myocardial volume curves (triangles) of the left and right ventricles respectively of the normal (A) , the 3-week (B), the 6-week (C), the 9-week untreated diabetic (D), and the 9-week captopril-treated diabetic (E) groups respectively. Twelve imaging sections were taken perpendicular to the principal cardiac axis as mentioned above (Chapters 6 and 8), each at twelve time-points during the cardiac cycle to provide full coverage of the heart of each experimental rat during systole and diastole. The transverse cardiac MRI sections were then analyzed to generate MRI-dependent volumes versus time curves. For each section, the epicardial and endocardial borders of the left and right ventricular chambers were traced 4 times at all the 12 studied time-points through the cardiac cycle using an in-house software. The total epicardial and endocardial left and the corresponding right ventricular volumes were then determined at the 12 studied time-points on the basis of the traced areas and thickness of the 12 constituent slices. The calculated volumes were then plotted against time after the electrocardiographic R wave. The volumes shown in Figures 9.1 and 9.2 are the average left and right ventricular epicardial, endocardial and myocardial volumes obtained from the five experimental groups at the studied 12 time-points in the cardiac cycle. The standard errors of the means of the volumes at the 12 studied time-points in the cardiac cycle were small in the five experimental groups and are not seen in the curves because of the size of the symbols. The ascending and descending limbs of the endo- and epicardial volume curves represent diastole and systole respectively.

Following the R-wave trigger, both the left and right endocardial volumes fell rapidly in the hearts of the normal, the 3-week and the 9-week captopril-treated diabetic rats (Figures 9.1A, B, E and 9.2A, B, E). Left and right ventricular contraction was most rapid early in systole and decreased in rate as systole progressed with end-systole being reached synchronously in both ventricles approximately 99 ms after the trigger pulse. In contrast, left and right ventricular endocardial volume curves of the 6- and the 9-week untreated diabetic rats (Figures 9.1C, D and 9.2C, and D) showed a much smaller initial rate of decline and reached their minimum volume approximately 112 ms after the R-wave trigger. Such systolic changes were followed by a more rapid diastolic filling of both left and right ventricles in the control, the 3-week, and the 9-week captopril-treated diabetic groups than in the 6-week and the 9-week untreated diabetic groups.

9.2 Functional ventricular volumes and ejection fractions

The preliminary analysis described in Chapter 7 suggested that diabetic rats show a relative left and right ventricular hypertrophy that is prevented by captopril treatment. This was confirmed by the MRI studies (Chapter 8), which went on to follow the detailed changes in the epicardial and endocardial volumes through the cardiac cycle. This provided the basis for the detailed analysis of diastolic and systolic volumes and ejection fractions of both left and right ventricles of the experimental groups presented below. Thus, the maximum values of the endocardial volume curves (Figures 9.1 and 9.2) at the end of ventricular diastolic filling and prior to systole, when the ventricles were fully dilated with blood, provided an estimate of the end-diastolic volume (EDV) in the particular ventricle. The minimum values in such endocardial volume curves represented the corresponding end-systolic volumes (ESV's) and the corresponding stroke volumes (SV's) were calculated by subtracting the EDV from the corresponding ESV.

Tables 9.1-9.4 summarize absolute values of these parameters for the left and right ventricles respectively. Tables 9.5-9.8 normalize these values to body weight.

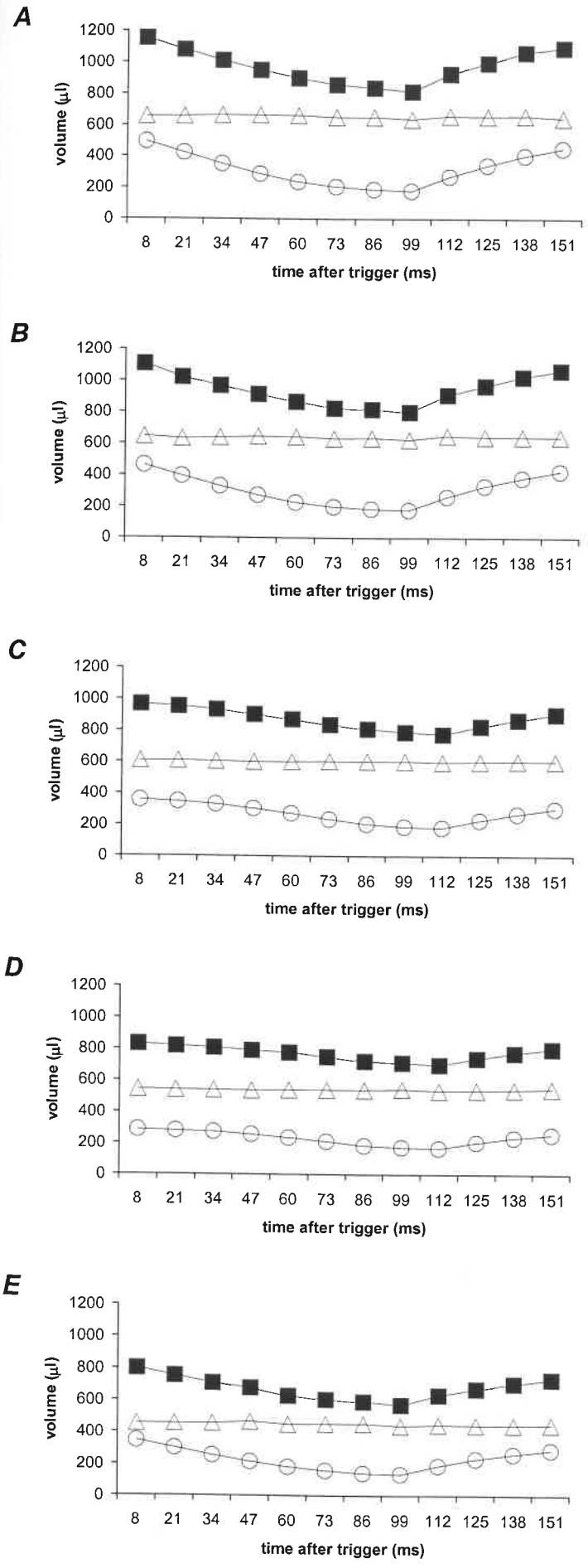

Figure 9.1: **Epicardial (squares), endocardial (circles), and myocardial (triangles) left ventricular (LV) volume curves.** Epicardial, endocardial and myocardial left ventricular (LV) volume curves obtained from the transverse MRI images of the control group (A), the 3-week diabetic group (B), the 6-week diabetic group (C), the 9-week untreated diabetic group (D), and the 9-week captopril-treated diabetic group (E). All the experimental animals were male Wistar rats aged 16 weeks at the time of scanning. The average body weight of the control group (n = 4) was 351.3 ± 9.7 g and those of the four diabetic groups were 335 ± 8.4, 282.5 ± 6.6, 235 ± 8.4, and 247.5 ± 15.5 g for the 3-week (n = 4), 6-week (n = 4), 9-week untreated (n = 4), and the 9-week captopril-treated (n = 4) diabetic groups respectively. The heart rate was continuously monitored throughout the imaging session giving average intrinsic heart rates of 322 ± 9 beats min^{-1} for the control rats and 318 ± 7, 280 ± 7, 280 ± 6, and 311 ± 10 beats min^{-1} for the 3-week, 6-week, 9-week untreated, and the 9-week captopril-treated diabetic groups respectively.

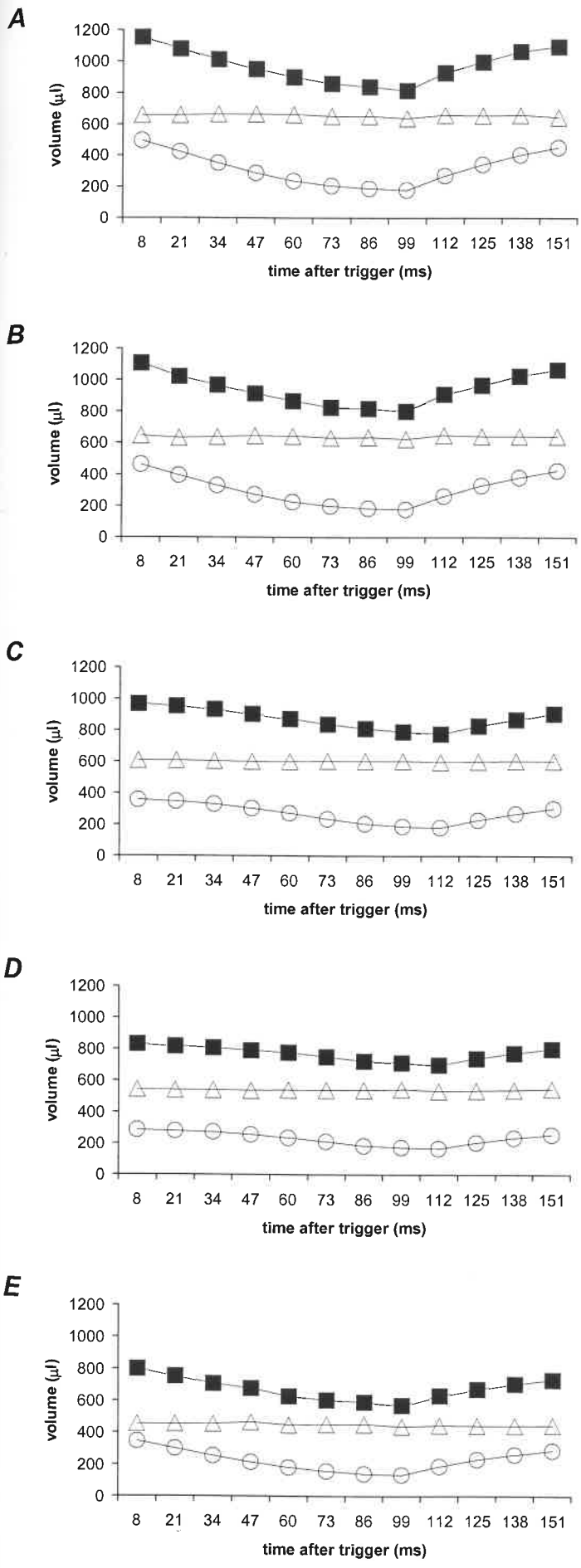

Figure 9.1: **Epicardial (squares), endocardial (circles), and myocardial (triangles) left ventricular (LV) volume curves.** Epicardial, endocardial and myocardial left ventricular (LV) volume curves obtained from the transverse MRI images of the control group (A), the 3-week diabetic group (B), the 6-week diabetic group (C), the 9-week untreated diabetic group (D), and the 9-week captopril-treated diabetic group (E). All the experimental animals were male Wistar rats aged 16 weeks at the time of scanning. The average body weight of the control group (n = 4) was 351.3 ± 9.7 g and those of the four diabetic groups were 335 ± 8.4, 282.5 ± 6.6, 235 ± 8.4, and 247.5 ± 15.5 g for the 3-week (n = 4), 6-week (n = 4), 9-week untreated (n = 4), and the 9-week captopril-treated (n = 4) diabetic groups respectively. The heart rate was continuously monitored throughout the imaging session giving average intrinsic heart rates of 322 ± 9 beats min^{-1} for the control rats and 318 ± 7, 280 ± 7, 280 ± 6, and 311 ± 10 beats min^{-1} for the 3-week, 6-week, 9-week untreated, and the 9-week captopril-treated diabetic groups respectively.

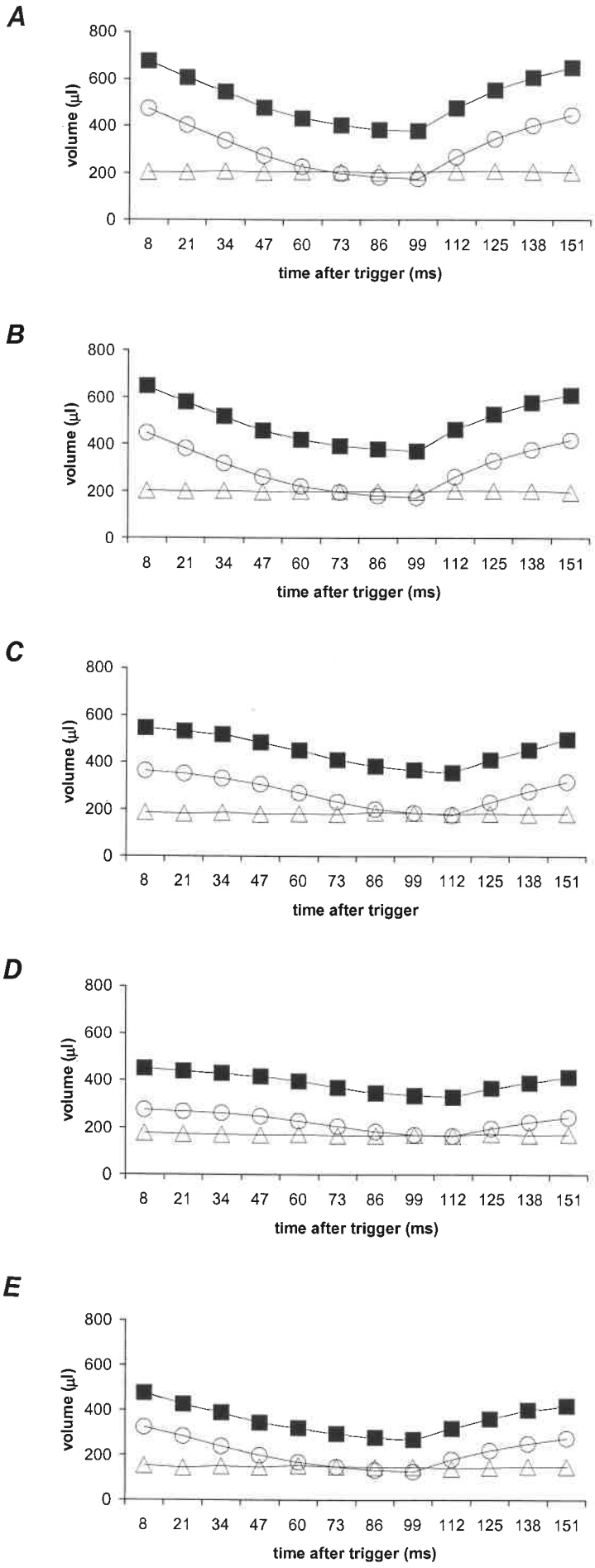

Figure 9.2: **Epicardial (squares), endocardial (circles), and myocardial (triangles) right ventricular (RV) volume curves.** Epicardial, endocardial and myocardial right ventricular (RV) volume curves obtained from the transverse MRI images of the control group (A), the 3-week diabetic group (B), the 6-week diabetic group (C), the 9-week untreated diabetic group (D), and the 9-week captopril-treated diabetic group (E). Other experimental details are summarized in legend to Figure 9.1.

Tables 9.9-9.10 summarize the statistical analysis of the left and right ventricular ejection fractions (EF's) and their absolute and normalized end-diastolic volumes (EDV's), end-systolic volumes (ESV's) and stroke volumes (SV's) . They use the mean values of these parameters in Tables 9.1-9.8 to calculate the percentage increase (+) or decrease (-) in these parameters following 3 and 6 weeks of diabetes without captopril treatment and following 9 weeks of diabetes without as well as with captopril treatment. As before, the mean value of each parameter of the control group was used as a reference value for calculating its percentage increase or decrease. The statistical significance of differences in the changes in each parameter following the different periods of experimental diabetes is indicated by the same *p*-values obtained from Tukey's Honestly Significance Difference test while performing pair-wise multiple comparisons (Tables 9.1-9.8). Tables 9.11 and 9.12 extract these as trends at different stages of the experimental disease process. Thus, they summarize the fractional deterioration in the ventricular volumes and ejection fractions through each experimental period. The mean value of each volume parameter was used to calculate its percentage increase (+) or decrease (-) respectively between 0 and 3, 3 and 6, and 6 and 9 weeks of diabetes without captopril treatment. The mean values of each parameter of the control and the 3-week diabetic groups were used to calculate its percentage increase or decrease between 0 and 3 weeks of diabetes without captopril treatment. The levels of significance shown for each parameter between 3 and 6 weeks of diabetes without captopril treatment are the same *p*-values obtained when comparing the data obtained from the 6-week with the data obtained from the 3-week diabetic group while performing pair-wise multiple comparisons using Tukey's Honestly Significance Difference test. Similarly, the levels of significance shown for each parameter between 6 and 9 weeks of diabetes without captopril treatment are the same *p*-values obtained when comparing the data obtained from the 9-week with the data obtained from the 6-week diabetic group also while using Tukey's Honestly Significance Difference test for performing pair-wise multiple comparisons.

9.2.1 Ventricular end-diastolic volumes (EDV's)

Tables 9.1-9.4 indicate that the induction of diabetes produced a progressive decrease in both the left and right ventricular EDV's. Thus, differences between the control and the diabetic rats for both the left and right ventricular EDV's were significant at 6 and 9 weeks with or without captopril treatment but not at 3 weeks, with deteriorations continuing between 6 and 9 weeks. However, the 9-week captopril-treated showed significantly higher left and right ventricular EDV's values than the corresponding untreated diabetic group.

Tables 9.9 shows that the left ventricular EDV's decreased by 6.6% over 3 weeks of diabetes and by 27.6% and 42.1% over 6 and 9 weeks of diabetes respectively without captopril treatment compared with the control rats. On the other hand, rats treated with captopril showed a 29.9% reduction in their left ventricular EDV's when compared with the control group. Similarly, right ventricular EDV's decreased by 5.9%, 23.5%, and 42.3% over the same time periods without captopril treatment whereas captopril treatment left a decrease in right ventricular EDV's of 31.7% (Table 9.10). Thus, captopril treatment reduced the fall in left and right ventricular EDV's during experimental diabetes.

Tables 9.11 and 9.12 extract the fractional deteriorations in left and right ventricular EDV's between time-points through the diabetic state without captopril treatment. They indicate that, without captopril treatment, diabetes progressively reduced EDV's with the left ventricle showing the greatest deterioration between 3 and 6 weeks and the right ventricle deteriorating most between 6 to 9 weeks. Thus, left ventricular EDV's decreased by 6.6% at 3 weeks, by 22.5% between 3 and 6 weeks and by 20.1% between 6 and 9 weeks of diabetes respectively. The corresponding decreases in right ventricular EDV's were 5.9%, 18.7% and 24.6% respectively.

Normalization of the EDV's to their corresponding body weights gave similar results (Tables 9.5-9.8). There were insignificant decreases in normalized left (2.1%) and right (1.5%) EDV's at 3 weeks and normalized right (5.2%) EDV's at 6 weeks compared to the normal rats, but significant decreases in normalized left (10.6%) EDV's at 6 weeks and normalized left (13.5%) and right (14.1%) EDV's at 9 weeks without captopril treatment with significant differences even between 6 and 9 weeks (Tables 9.9 and 9.10). In addition, normalized left and right EDV's of the 9-week captopril-treated group were similar to those of the control and significantly higher than those of the 9-week untreated group (Tables 9.6 and 9.8). The reductions in their normalized left and right ventricular EDV's were only 0.7% and 3.7% respectively when compared with the control group; these were significantly lower than the reductions observed at 9 weeks of diabetes without treatment with captopril (Tables 9.9 and 9.10).

Tables 9.11 and 9.12 show the fractional deterioration in the normalized left and right ventricular EDV's throughout the diabetic state without captopril treatment. They demonstrated that without treatment with captopril, the absolute and normalized left and the absolute but not the normalized right ventricular EDV's deteriorated significantly between 3 and 6, and 6 and 9 weeks of diabetes, but not between 0 and 3 weeks. The deterioration in left ventricular volumes was greatest between 3 and 6 weeks of diabetes; while that in the right ventricles was maximal

between 6 and 9 weeks of diabetes. Thus, normalized left ventricular EDV's decreased by 2.1%, 8.7% and 3.2% between 0 to 3, 3 to 6 and 6 to 9 weeks of diabetes in the absence of captopril treatment respectively. The corresponding values for the right ventricle were 1.5%, 3.8% and 9.4% respectively.

9.2.2 Ventricular end-systolic volumes (ESV's)

Tables 9.1-9.4 demonstrate that the control and the diabetic rats, which were not treated with captopril, had comparable left as well as right ventricular ESV's. However, the 9-week captopril-treated group had significantly lower left and right ventricular ESV's. However, the left and right ventricular ESV's normalized to their corresponding body weights (Tables 9.5-9.8) progressively increased with the duration of diabetes. Although no significant changes were observed at 3 weeks, there were significant increases at 6 and 9 weeks with demonstrable changes even between 6 and 9 weeks diabetes without captopril treatment. Thus, Tables 9.9 and 9.10 indicate increases in the normalized left ventricular ESV's of 6.0%, 28.0%, and 42% and in the corresponding normalized right ventricular ESV's of 4.1%, 26.5%, and 40.8% over the control group respectively. In contrast, the captopril-treated group showed insignificant increases in normalized left (8%) and right (2%) ventricular ESV's values over those of the control group.

9.2.3 Ventricular stroke volumes (SV's)

Tables 9.1-9.4 show that left and right ventricular SV's significantly decreased at 6 and at 9 weeks of diabetes both without and with captopril treatment and also at 3 weeks, with significant changes between both 3 and 6 and 6 and 9 weeks. Thus, Tables 9.9 and 9.10 show that the left ventricular SV's decreased by 10.7%, 44.1%, and 62.4% and the corresponding right ventricular SV's decreased by 8.9%, 37.6%, and 63.1% at 3, 6, and 9 weeks of diabetes respectively compared with the control group in the absence of captopril treatment. However, captopril treatment increased the left and right ventricular SV's significantly over those of the corresponding 9-week untreated diabetic group. Thus, left and right ventricular SV's in rats treated with captopril were decreased by 32.7% and by 33.4% compared with the control group respectively.

Tables 9.11 and 9.12 summarize the fractional deterioration in left and right ventricular SV's between times in the diabetic state without captopril treatment. The left ventricular SV's fell by 10.7%, 37.4%, and 32.7% between 0 and 3, 3 and 6, and 6 and 9 weeks of diabetes respectively. The corresponding changes in the right ventricle were decreases of 8.9%, 31.5% and 41.0%

respectively. Thus, the left ventricles showed the greatest deterioration in their SV's between 3 and 6 weeks of diabetes, whereas the deterioration in right ventricular SV's was greatest between 6 and 9 weeks of diabetes.

When normalized to body weight (Tables 9.5-9.8), the left and right ventricular SV's values were significantly decreased at 6 and 9 but not at 3 weeks of diabetes without captopril treatment with significant changes again even between 6 and 9 weeks. Thus, Tables 9.9 and 9.10 show decreases in normalized left ventricular SV's of 6.6%, 30.8%, and 44.0% and decreases in right ventricular SV's of 4.7%, 22.4%, and 44.7% at 3, 6, and 9 weeks of diabetes respectively compared with the control group. Furthermore, values in the 9-week captopril-treated diabetic group were only slightly lower than those of the control group and were significantly higher than those of the corresponding untreated group. Thus, normalized left and right ventricular SV's in captopril-treated rats decreased by only 4.4% and 5.9% respectively.

Tables 9.11 and 9.12 show the fractional deterioration in the normalized left and right ventricular SV's through successive time-points in the diabetic state without captopril treatment. The normalized left ventricular SV's decreased by 6.6%, 25.9% and 19% between 0-3, 3- 6, and 6-9 weeks of diabetes respectively. The corresponding values for the right ventricle were decreases of 4.7%, 18.5% and 28.8%. Both corresponded to significant decreases between 3-6, and 6-9 but not 0-3 weeks of diabetes. The normalized left ventricular SV's deteriorated maximally between 3 and 6 weeks whereas the right ventricles deteriorated maximally between 6 and 9 weeks of diabetes.

9.2.4 Ventricular ejection fractions (EF's)

The ejection fractions of the left and right ventricles expressed as the ratio between the left or right ventricular SV's and the corresponding EDV's. Tables 9.1-9.4 show that 6 weeks or 9 weeks of diabetes without captopril treatment significantly reduced both the left and the right ventricular EF's compared with the control rats. The 9-week diabetic group showed significantly lower EF's than those of the 6-week diabetic group. Thus, the left ventricular EF's decreased by 4.5%, 22.8%, and 35.2%, and the corresponding right ventricular EF's decreased by 3.3%, 18.5%, and 36.5% over 3, 6, and 9 weeks of diabetes respectively compared with the control group (Tables 9.9 and 9.10). These corresponded to fractional deteriorations (Tables 9.11 and 9.12) in left ventricular EF's of 4.5%, 19.2%, and 16.1% between 0-3, 3-6, and 6-9 weeks of diabetes respectively with right ventricular values of 3.3%, 15.7% and 22.1% respectively. This corresponds to significant reductions in the left and right ventricular EF's between 3-6 and between 6-9 weeks of diabetes but not between 0 and 3 weeks of diabetes.

Furthermore, the deterioration in the left ventricular EF's was greatest between 3 and 6 weeks of diabetes, while the right ventricles showed the greatest deterioration in their EF's between 6 and 9 weeks of diabetes. However, both the 3-week and the 9-week captopril-treated diabetic groups showed no significant changes. Furthermore, the left and right ventricular EF's of the 9-week captopril-treated group were significantly higher than those of the corresponding untreated group. Thus, the left and right ventricular EF's values then only decreased by 4.0% and 2.7% respectively in the 9-week captopril-treated group.

9.3 Ventricular SV's versus their EDV's

Figure 9.3A correlates the MRI-measured left ventricular SV's and EDV's of all the five experimental groups. Similarly, Figure 9.3B plots the MRI-measured right ventricular SV's of the five experimental groups against their corresponding right ventricular EDV's. It was not possible to vary the EDV within individual rats owing to the inherently non-invasive nature of the MRI investigations. Nevertheless, the plots obtained show: (i) a progressive change in EDV's with the development of diabetes, in both the left and right ventricles, (ii) the plots appearing to fall upon two approximately linear functions, one formed by data obtained by 0 and 3 weeks of diabetes, and the other by 6- and 9-week diabetic rats. This is consistent with the findings here that significant cardiac changes were obvious at 6 and 9 weeks but not at 3 weeks and are consistent not only with changes in diastole, but also alterations in systolic function with the disease, (iii) thus, the 6-week and the 9-week untreated diabetic groups had left and right ventricular systolic abnormalities, which were not directly caused by their diastolic abnormalities, and (iv) the data points in captopril-treated group fell significantly above these suggested by both the 6- and 9-week groups and were close to the function suggested by the 0- and 3-week diabetic rats. Hence these abnormalities were at least partly prevented by captopril treatment.

9.4 Matching of left and right ventricular volumes and EF's

Figure 9.4 demonstrates that (i) there was a close matching of left and right ventricular EDV's, ESV's, SV's, and EF's in the normal rat heart, and (ii) this matching appeared to persist throughout the diabetic disease process although, as previously mentioned, the left ventricle had its greatest changes between 3 and 6 weeks, while the right ventricular changes were greatest between 6 and 9 weeks of diabetes.

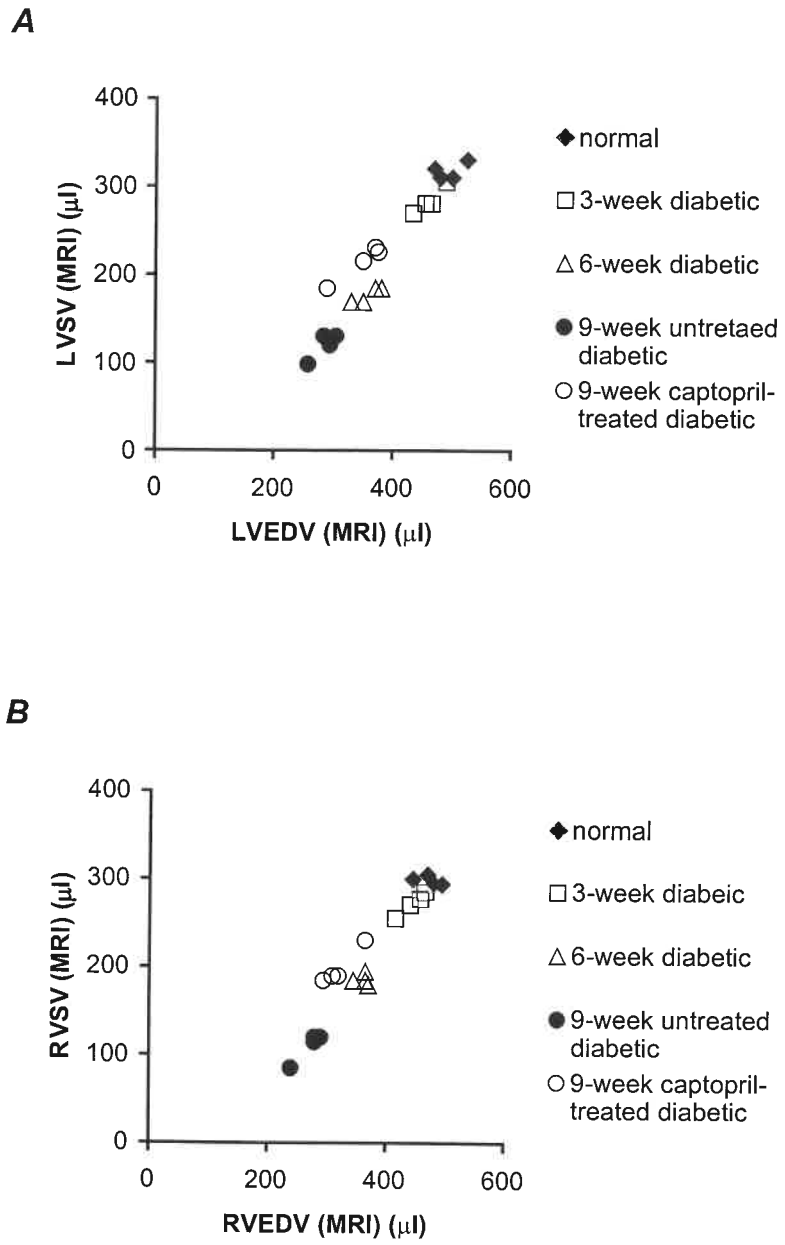

Figure 9.3: **Left ventricular (LV) end-diastolic volume (EDV) *versus* stroke volume (SV) and right ventricular (RV) end-diastolic volume (EDV) *versus* stroke volume (SV).** *A*, a comparative plot between the MRI-measured left ventricular stroke volumes (SV's) and end-diastolic volumes (EDV's) of the five experimental groups. *B*, a comparative plot between the MRI-measured right ventricular stroke volumes (SV's) and end-diastolic volumes (EDV's) of the five experimental groups. The 6- and 9-week untreated diabetic groups had impairment in left and right ventricular diastolic functions as well as impairment in left and right ventricular systolic functions.

Figure 9.4 (next page): **Left ventricular (LV) and right ventricular (RV) MRI-derived volumes and ejection fraction (EF).** *A*, a comparative plot of the MRI-measured left ventricular (LV) and right ventricular (RV) end-diastolic volumes (EDV's) of the five experimental groups. As displayed the MRI-measured left ventricular and the corresponding right ventricular EDV's were almost equal in each of the five experimental groups with the differences being insignificant. This signifies a close matching of the MRI-measured left and right ventricular EDV's of the control as well as the diabetic rats. *B*, a comparative plot of the MRI-measured left ventricular and right ventricular end-systolic volumes (ESV's) of the five experimental groups. As displayed the MRI-measured left ventricular and the corresponding right ventricular ESV's were almost equal in each of the five experimental groups with the differences being insignificant. This signifies a close matching of the MRI-measured left and right ventricular ESV's of the control as well as the diabetic rats. This plot also shows that the control and the three untreated diabetic groups had comparable Left as well as right ventricular ESV's despite the markedly smaller EDV's of the 6- and 9-week diabetic groups. *C*, a comparative plot of the MRI-measured left ventricular and right ventricular stroke volumes (SV's) of the five experimental groups. As displayed the MRI-measured left ventricular and the corresponding right ventricular SV's were almost equal in each of the five experimental groups with the differences being insignificant. This signifies a close matching of the MRI-measured left and right ventricular SV's of the control as well as the diabetic rats. *D*, a comparative plot of the MRI-measured left ventricular and right ventricular ejection fractions (EF's) of the five experimental groups. As displayed the MRI-measured left ventricular and the corresponding right ventricular EF's were almost equal in each of the five experimental groups with the differences being insignificant. This signifies a close matching of the MRI-measured left and right ventricular EF's of the control as well as the diabetic rats. The left ventricular ejection fraction of each rat was calculated using the formula: Left ventricular ejection fraction = (left ventricular stroke volume /left ventricular end-diastolic volume) x 100. Similarly, the right ventricular ejection fraction of each rat was calculated by a similar formula: Right ventricular ejection fraction = (right ventricular stroke volume /right ventricular end-diastolic volume) x 100.

Figure 9.4 (next page): **Left ventricular (LV) and right ventricular (RV) MRI-derived volumes and ejection fraction (EF).** *A*, a comparative plot of the MRI-measured left ventricular (LV) and right ventricular (RV) end-diastolic volumes (EDV's) of the five experimental groups. As displayed the MRI-measured left ventricular and the corresponding right ventricular EDV's were almost equal in each of the five experimental groups with the differences being insignificant. This signifies a close matching of the MRI-measured left and right ventricular EDV's of the control as well as the diabetic rats. *B*, a comparative plot of the MRI-measured left ventricular and right ventricular end-systolic volumes (ESV's) of the five experimental groups. As displayed the MRI-measured left ventricular and the corresponding right ventricular ESV's were almost equal in each of the five experimental groups with the differences being insignificant. This signifies a close matching of the MRI-measured left and right ventricular ESV's of the control as well as the diabetic rats. This plot also shows that the control and the three untreated diabetic groups had comparable Left as well as right ventricular ESV's despite the markedly smaller EDV's of the 6- and 9-week diabetic groups. *C*, a comparative plot of the MRI-measured left ventricular and right ventricular stroke volumes (SV's) of the five experimental groups. As displayed the MRI-measured left ventricular and the corresponding right ventricular SV's were almost equal in each of the five experimental groups with the differences being insignificant. This signifies a close matching of the MRI-measured left and right ventricular SV's of the control as well as the diabetic rats. *D*, a comparative plot of the MRI-measured left ventricular and right ventricular ejection fractions (EF's) of the five experimental groups. As displayed the MRI-measured left ventricular and the corresponding right ventricular EF's were almost equal in each of the five experimental groups with the differences being insignificant. This signifies a close matching of the MRI-measured left and right ventricular EF's of the control as well as the diabetic rats. The left ventricular ejection fraction of each rat was calculated using the formula: Left ventricular ejection fraction = (left ventricular stroke volume /left ventricular end-diastolic volume) x 100. Similarly, the right ventricular ejection fraction of each rat was calculated by a similar formula: Right ventricular ejection fraction = (right ventricular stroke volume /right ventricular end-diastolic volume) x 100.

A

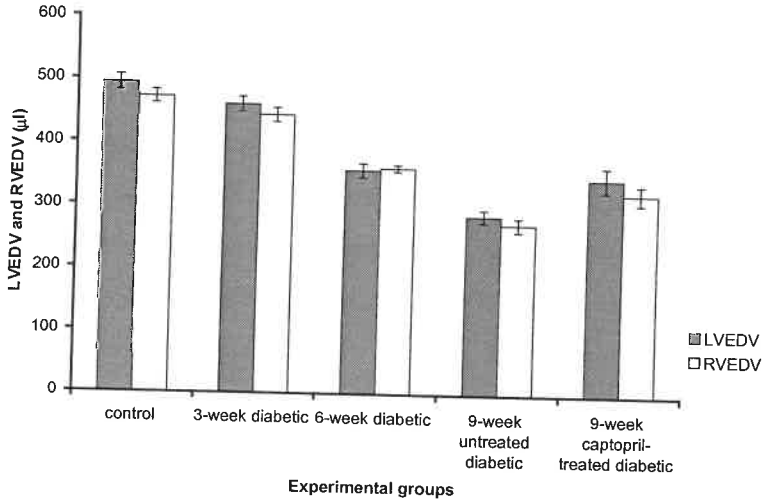
LVEDV and RVEDV (µl)
600
500
400
300
200
100
0
control
3-week diabetic
6-week diabetic
9-week untreated diabetic
9-week captopril-treated diabetic
Experimental groups
LVEDV
RVEDV

B

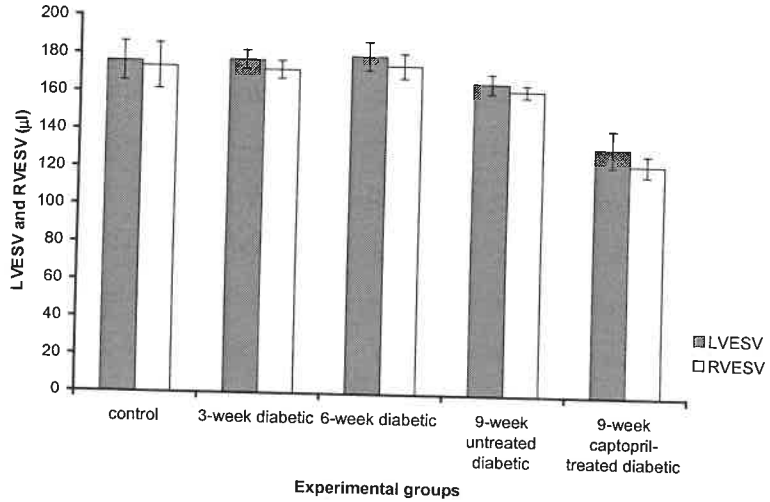
LVESV and RVESV (µl)
200
180
160
140
120
100
80
60
40
20
0
control
3-week diabetic
6-week diabetic
9-week untreated diabetic
9-week captopril-treated diabetic
Experimental groups
LVESV
RVESV

C

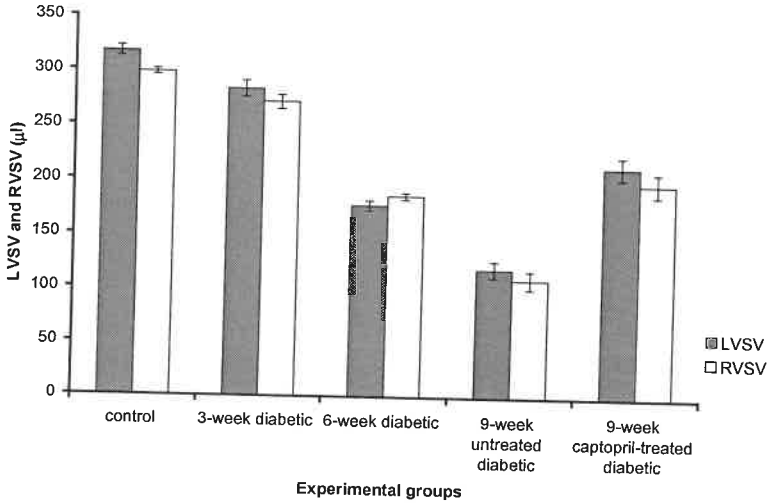
LVSV and RVSV (µl)
350
300
250
200
150
100
50
0
control
3-week diabetic
6-week diabetic
9-week untreated diabetic
9-week captopril-treated diabetic
Experimental groups
LVSV
RVSV

D

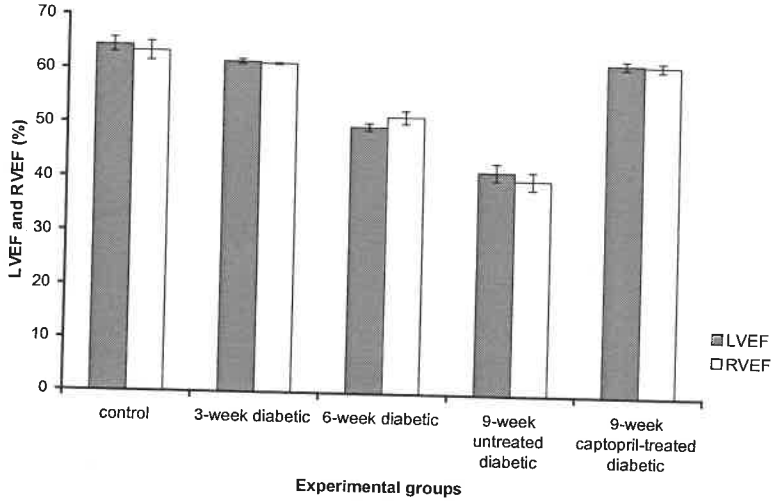
LVEF and RVEF (%)
70
60
50
40
30
20
10
0
control
3-week diabetic
6-week diabetic
9-week untreated diabetic
9-week captopril-treated diabetic
Experimental groups
LVEF
RVEF

9.5 Systolic and diastolic indices

Tables 9.13-9.16 summarize values for two indices, for systolic contraction and diastolic relaxation. These are the systolic and the diastolic time periods required for the left and right ventricles of the five experimental groups to pump 25% of their SV's and to be filled with 25% of their diastolic filling volumes (DFV's) respectively. These tables also summarize the rates of left and right ventricular ejection and filling during early systole and early diastole respectively.

Since end-diastole was considered to be represented by images typically acquired 8 ms after the R wave trigger in almost all the experimental rats, the exact time taken by the ventricles to eject 25% of their SV's were calculated by subtracting 8 ms from the time after the R wave trigger taken by the ventricles to eject 25% of their SV's. The ventricles of the normal, the 3-week diabetic and the captopril-treated 9-week diabetic rats reached their end-systole approximately 99 ms and those of the 6- and 9-week diabetic rats approximately 112 ms after the R wave trigger. Accordingly, the exact time taken by the ventricles of the normal, the 3-week and the captopril-treated 9-week diabetic rats to be filled with 25% of their DFV's were calculated by subtracting 99 ms and those of the ventricles of the 6-and 9-week diabetic rats were calculated by subtracting 112 ms from the time after the R wave trigger taken by their ventricles to be filled by 25% of their DFV's. The rates of ejection during early systole were calculated by dividing the 25% SV of each ventricle by the exact time taken by that particular ventricle to eject 25% of its SV. Similarly the rates of filling during early diastole were calculated by dividing the 25% DFV of each ventricle by the exact time taken by that ventricle to get filled by its 25% DFV. As the average diastolic filling volume (DFV) is normally equal to the average SV, the 25% DFV was consistently taken to be equal to the 25% SV. Accordingly, the 3-, 6-, 9-week untreated and the 9-week captopril-treated diabetic groups, all had significantly smaller left and right ventricular SV's, had smaller 25% SV's and 25% DFV's values compared with the control group. These values were also significantly different between the 6- and 9-week untreated diabetic groups. In contrast, the 9-week captopril-treated diabetic group had significantly higher left and right ventricular 25% SV's and 25% DFV's than those of the corresponding untreated group.

Despite these diminished values of left and right ventricular 25% SV's of the 6- and 9-week diabetic groups, times required for both their left and their right ventricles to eject 25% of their respective SV's were much longer than those of the left and right ventricles of the control group. In contrast, corresponding values in captopril-treated rats were close to those of normal. These findings similarly indicate that 6 and 9 weeks of untreated diabetes sharply reduce the

initial rate of systolic ejection. In contrast, although the captopril-treated diabetic group showed significantly slower values than those of the control group, they were improved over the rates of the corresponding untreated group.

The rates of left and right ventricular filling during early diastole in the 6- and 9-week untreated diabetic groups were similarly much slower than those of the control group. The 9-week captopril-treated diabetic group also showed slower rates of early diastolic filling when compared with the control group, which were, however, significantly faster than the rates of the corresponding 9-week untreated diabetic group.

9.6 Rate of left and right ventricular volume changes, dV/dt's

Figure 9.5 plots the instantaneous rates of change of left (filled bars) and right (clear bars) ventricular endocardial volumes, dV/dt's, for each experimental group derived from comparing endocardial volumes at successive time-points obtained over the cardiac cycle. Values of dV/dt's are represented as negative during systole, while left and right ventricular volumes are decreasing with time and the diastolic dV/dt's values are represented as positive owing to filling of the left and right ventricles.

The left and right ventricles showed synchronized patterns and comparable values of volume change through both systole and diastole in the normal and the 3-week diabetic rats (Figure 9.5A & 9.5B). Systolic dV/dt was greatest in early part of systole and diastolic dV/dt greatest early in diastole; in both cases values then subsequently declined.

The left ventricles of the 9-week captopril-treated group also showed similar dV/dt's to those of their corresponding right ventricles through both systole and diastole (Figure 9.5E). The qualitative temporal patterns of volume change in both left and right ventricles of the 9-week captopril-treated group were similar to those of the control and the 3-week groups; contraction began early in systole and relaxation began early in diastole with both events synchronized in the left and right ventricles. However, the systolic and diastolic left and right ventricular dV/dt's were quantitatively smaller than those of the control group, though better than those of the 6- and 9-week untreated diabetic groups (see below).

Left and right ventricles of the 6- and 9-week untreated diabetic groups both showed contrasting systolic and diastolic patterns to those of the control, 3- and 9-week captopril-treated diabetic

groups (Figure 9.5C and 9.5D). Thus, dV/dt was relatively small early in systole, and only gradually increased in magnitude into the middle part of systole before declining. The initial values of both the left and right ventricular systolic dV/dt's were thus smaller than those shown by the normal, the 3-, and the 9-week captopril-treated diabetic groups. However, from mid-systole, the dV/dt's values of the 6- and 9-week untreated diabetic groups were similar to the corresponding rates calculated for the control, the 3- and the 9-week captopril treated groups. The diastolic left and right ventricular dV/dt's were also significantly compromised in the 6- and 9-week untreated diabetic group.

Both left and right ventricular dV/dt's of the 6-week and 9-week untreated diabetic groups also showed similar patterns throughout the cardiac cycle. Thus, left and right ventricular values were closely matched through all time-points in all the 5 experimental groups. Both ventricles reached both their limits of end-systole and end-diastolic refilling at approximately the same time during the cardiac cycle. The former typically took place at about 99 ms after the R-wave trigger in the control, the 3- and the 9-week captopril-treated groups and at approximately 112 ms in the 6- and the 9-week untreated diabetic groups.

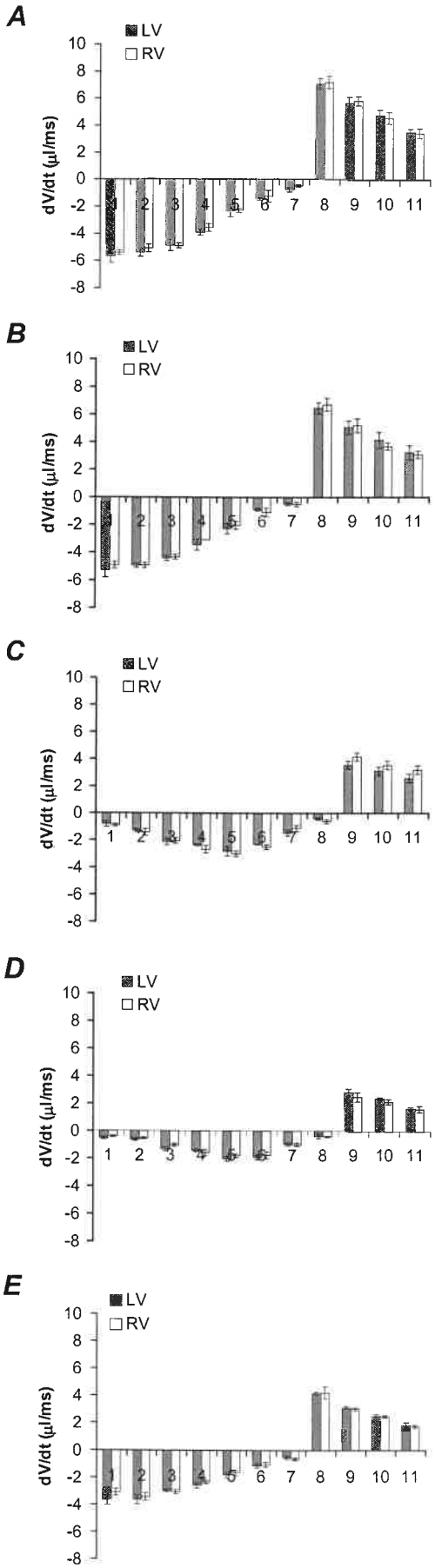

Figure 9.5: **Left and right ventricular dV/dt.** Block diagram displaying left (filled bars) and right (clear bars) ventricular volume changes with respect to time during the 12 studied time points through the cardiac cycle obtained from the normal control group (A), the 3-week diabetic group (B), the 6-week diabetic group (C), the 9-week untreated diabetic group (D), and the 9-week captopril-treated diabetic group (E) (see legend to Fig. R.7). Data points derived from obtaining the slopes between adjacent points in the left ventricular (LV) and right ventricular (RV) volume curves obtained from individual groups themselves summarized in Figures R.7, 8 respectively. Each bar represents the average dV/dt ± SEM between 2 consecutive time points through the cardiac cycle. Negative dV/dt's represent contraction of the cardiac walls during systole and positive dV/dt's represent their relaxation. The bar **1** represents dV/dt between the 1st and 2nd studied time points during the cardiac cycle with the first point timed typically 8 ms after the trigger pulse from the electrocardiographic R wave and 21 ms for the second point. Points **2** to **11** represent dV/dts between volume points successively obtained 21, 34, 47, 60, 73, 86, 99, 112, 125, 138, and 151 ms following the R wave.

Parameter	Control (n = 4)	3-week diabetic (n = 4)	6-week diabetic (n = 4)	9-week untreated diabetic (n = 4)	One-Way ANOVA	
					F	*P*-value (all levels)
End-diastolic volume (EDV) (µl)	493.8 ± 12.1 [c, d]	461 ± 11.6 [c, d]	357.5 ± 11.1 [a, b, d]	285.8 ± 10.1 [a, b, c]	71.874	<0.001
End-systolic volume (ESV) (µl)	176.3 ± 10.3	177.5 ± 4.8	180 ± 7.4	166.3 ± 5.2	0.697	0.572
Stroke volume (SV) (µl)	317.5 ± 4.8 [b, c, d]	283.5 ± 7.6 [a, c, d]	177.5 ± 4.3 [a, b, d]	119.5 ± 7.5 [a, b, c]	215.864	<0.001
Ejection fraction (EF) %	64.4 ± 1.3 [c, d]	61.5 ± 0.5 [c, d]	49.7 ± 0.7 [a, b, d]	41.7 ± 1.6 [a, b, c]	87.424	<0.001

Table 9.1: **Absolute (non-normalized) MRI-derived diastolic and systolic volumes and ejection fractions (EF) of the left ventricles of the control and the three untreated diabetic groups.**

All values expressed as mean ± standard error of the mean (SEM). One-way analysis of variance (One-Way ANOVA) was used in comparison of the control and the three untreated diabetic groups followed by Tukey's Honestly Significant Difference test for pair-wise multiple comparisons. A value of $p<0.05$ was considered statistically significant.

[a] Significantly different from the control group.

[b] Significantly different from the 3-week diabetic group.

[c] Significantly different from the 6-week diabetic group.

[d] Significantly different from the 9-week untreated diabetic group.

Parameter	Control (n = 4)	9-week untreated diabetic (n = 4)	9-week captopril-treated diabetic (n = 4)	(One-Way ANOVA)	
				F	*P*-value (all levels)
End-diastolic volume (EDV) (μl)	493.8 ± 12.1 $^{+,\S}$	285.8 ± 10.1 *,§	346.3 ± 19.5 $^{*,+}$	54.478	<0.001
End-systolic volume (ESV) (μl)	176.3 ± 10.3 §	166.3 ± 5.2	132.5 ± 9.7 *	6.975	0.015
Stroke volume (SV) (μl)	317.5 ± 4.8 $^{+,\S}$	119.5 ± 7.5 *,§	213.8 ± 10.1 $^{*,+}$	162.217	<0.001
Ejection fraction (EF) %	64.4 ± 1.3 $^{+}$	41.7 ± 1.6 *,§	61.8 ± 0.8 $^{+}$	92.086	<0.001

Table 9.2: **Absolute (non-normalized) MRI-derived diastolic and systolic volumes and ejection fractions (EF) of the left ventricles of the control and the two 9-week diabetic groups.**

All values expressed as mean ± standard error of the mean (SEM). One-way analysis of variance (One-Way ANOVA) was used in comparison of the control and the two 9-week diabetic groups followed by Tukey's Honestly Significant Difference test for pair-wise multiple comparisons. A value of $p<0.05$ was considered statistically significant.

*Significantly different from the control group.

$^{+}$ Significantly different from the 9-week untreated diabetic group.

§ Significantly different from the 9-week captopril-treated diabetic group.

Parameter	Control (n = 4)	3-week diabetic (n = 4)	6-week diabetic (n = 4)	9-week untreated diabetic (n = 4)	One-Way ANOVA	
					F	*P*-value (all levels)
End-diastolic volume (EDV) (µl)	472.3 ± 10.3 [c, d]	444.3 ± 11.1 [c, d]	361.3 ± 5.5 [a, b, d]	272.5 ± 11.1 [a, b, c]	84.743	<0.001
End-systolic volume (ESV) (µl)	173.8 ± 12	172.5 ± 4.8	175 ± 6.5	162.5 ± 3.2	0.599	0.628
Stroke volume (SV) (µl)	298.5 ± 2.5 [b, c, d]	271.8 ± 6.4 [a, c, d]	186.3 ± 3.1 [a, b, d]	110 ± 8.4 [a, b, c]	230.043	<0.001
Ejection fraction (EF) %	63.3 ± 1.8 [c, d]	61.2 ± 0.2 [c, d]	51.6 ± 1.2 [a, b, d]	40.2 ± 1.6 [a, b, c]	61.845	<0.001

Table 9.3: **Absolute (non-normalized) MRI-derived diastolic and systolic volumes and ejection fractions (EF) of the right ventricles of the control and the three untreated diabetic groups.**

All values expressed as mean ± standard error of the mean (SEM). One-way analysis of variance (One-Way ANOVA) was used in comparison of the control and the three untreated diabetic groups followed by Tukey's Honestly Significant Difference test for pair-wise multiple comparisons. A value of $p<0.05$ was considered statistically significant.

[a] Significantly different from the control group.

[b] Significantly different from the 3-week diabetic group.

[c] Significantly different from the 6-week diabetic group.

[d] Significantly different from the 9-week untreated diabetic group.

Parameter	Control (n = 4)	9-week untreated diabetic (n = 4)	9-week captopril-treated diabetic (n = 4)	(One-Way ANOVA)	
				F	*P*-value (all levels)
End-diastolic volume (EDV) (μl)	472.3 ± 10.3 $^{+,\S}$	272.5 ± 11.1 *,§	322.5 ± 15.1 $^{*,+}$	70.967	<0.001
End-systolic volume (ESV) (μl)	173.8 ± 12 §	162.5 ± 3.2 §	123.8 ± 5.5 $^{*,+}$	11.195	0.004
Stroke volume (SV) (μl)	298.5 ± 2.5 $^{+,\S}$	110 ± 8.4 *,§	198.8 ± 10.5 $^{*,+}$	142.560	<0.001
Ejection fraction (EF) %	63.3 ± 1.8 $^{+}$	40.2 ± 1.6 *,§	61.6 ± 0.8 $^{+}$	77.120	<0.001

Table 9.4: **Absolute (non-normalized) MRI-derived diastolic and systolic volumes and ejection fractions (EF) of the right ventricles of the control and the two 9-week diabetic groups.**

All values expressed as mean ± standard error of the mean (SEM). One-way analysis of variance (One-Way ANOVA) was used in comparison of the control and the two 9-week diabetic groups followed by Tukey's Honestly Significant Difference test for pair-wise multiple comparisons. A value of $p<0.05$ was considered statistically significant.

*Significantly different from the control group.

$^{+}$ Significantly different from the 9-week untreated diabetic group.

§ Significantly different from the 9-week captopril-treated diabetic group.

Parameter	Control (n = 4)	3-week diabetic (n = 4)	6-week diabetic (n = 4)	9-week untreated diabetic (n = 4)	One Way ANOVA	
					F	*P*-value (all levels)
End-diastolic volume (EDV)/ Body weight (μl/g)	1.41 ± 0.01 [c, d]	1.38 ± 0.003 [c, d]	1.26 ± 0.02 [a, b, d]	1.22 ± 0.01 [a, b, c]	61.840	<0.001
End-systolic volume (ESV)/ Body weight (μl/g)	0.5 ± 0.02 [c, d]	0.53 ± 0.01 [c, d]	0.64 ± 0.01 [a, b, d]	0.71 ± 0.02 [a, b, c]	46.637	<0.001
Stroke volume (SV)/ Body weight (μl/g)	0.91 ± 0.02 [c, d]	0.85 ± 0.01 [c, d]	0.63 ± 0.01 [a, b, d]	0.51 ± 0.02 [a, b, c]	110.884	<0.001

Table 9.5: **The MRI-derived diastolic and systolic volumes of the left ventricles of the control and the three untreated diabetic groups normalized with respect to their corresponding body weights.** The body weight-normalized diastolic and systolic volumes of the left ventricles of the experimental rats were calculated using their corresponding body weights determined while they were under anaesthesia.

All values expressed as mean ± standard error of the mean (SEM). One-way analysis of variance (One-Way ANOVA) was used in comparison of the control and the three untreated diabetic groups followed by Tukey's Honestly Significant Difference test for pair-wise multiple comparisons. A value of $p<0.05$ was considered statistically significant.

[a] Significantly different from the control group.

[b] Significantly different from the 3-week diabetic group.

[c] Significantly different from the 6-week diabetic group.

[d] Significantly different from the 9-week untreated diabetic group.

Parameter	Control (n = 4)	9-week untreated diabetic (n = 4)	9-week captopril-treated diabetic (n = 4)	One-Way ANOVA	
				F	*P*- value (All levels)
End-diastolic volume (EDV)/ Body weight (μl/g)	1.41 ± 0.01 $^{+}$	1.22 ± 0.01 *,§	1.4 ± 0.06 $^{+}$	10.299	0.005
End-systolic volume (ESV)/ Body weight (μl/g)	0.5 ± 0.02 $^{+}$	0.71 ± 0.02 *,§	0.54 ± 0.02 $^{+}$	34.443	<0.001
Stroke volume (SV)/ Body weight (μl/g)	0.91 ± 0.02 $^{+}$	0.51 ± 0.02 *,§	0.87 ± 0.04 $^{+}$	57.328	<0.001

Table 9.6: **The MRI-derived diastolic and systolic volumes of the left ventricles of the control and the two 9-week diabetic groups normalized with respect to their corresponding body weights.** The body weight-normalized diastolic and systolic volumes of the left ventricles of the experimental rats were calculated using their corresponding body weights determined while they were under anaesthesia.

All values expressed as mean ± standard error of the mean (SEM). One-way analysis of variance (One-Way ANOVA) was used in comparison of the control and the two 9-week diabetic groups followed by Tukey's Honestly Significant Difference test for pair-wise multiple comparisons. A value of $p<0.05$ was considered statistically significant.

*Significantly different from the control group.

$^{+}$ Significantly different from the 9-week untreated diabetic group.

§ Significantly different from the 9-week captopril-treated diabetic group.

Parameter	Control (n = 4)	3-week diabetic (n = 4)	6-week diabetic (n = 4)	9-week untreated diabetic (n = 4)	One Way ANOVA	
					F	*P*-value (all levels)
End-diastolic volume (EDV)/ Body weight (μl/g)	1.35 ± 0.01 [d]	1.33 ± 0.01 [d]	1.28 ± 0.02 [d]	1.16 ± 0.02 [a, b, c]	25.164	<0.001
End-systolic volume (ESV)/ Body weight (μl/g)	0.49± 0.02 [c, d]	0.51 ± 0.01 [c, d]	0.62 ± 0.01 [a, b, d]	0.69 ± 0.01 [a, b, c]	50.291	<0.001
Stroke volume (SV)/ Body weight (μl/g)	0.85 ± 0.03 [c, d]	0.81 ± 0.003 [c, d]	0.66 ± 0.02 [a, b, d]	0.47 ± 0.03 [a, b, c]	56.998	<0.001

Table 9.7: **The MRI-derived diastolic and systolic volumes of the right ventricles of the control and the three untreated diabetic groups normalized with respect to their corresponding body weights.** The body weight-normalized diastolic and systolic volumes of the right ventricles of the experimental rats were calculated using their corresponding body weights determined while they were under anaesthesia.

All values expressed as mean ± standard error of the mean (SEM). One-way analysis of variance (One-Way ANOVA) was used in comparison of the control and the three untreated diabetic groups followed by Tukey's Honestly Significant Difference test for pair-wise multiple comparisons. A value of $p<0.05$ was considered statistically significant.

[a] Significantly different from the control group.

[b] Significantly different from the 3-week diabetic group.

[c] Significantly different from the 6-week diabetic group.

[d] Significantly different from the 9-week untreated diabetic group.

Parameter	Control (n = 4)	9-week untreated diabetic (n = 4)	9-week captopril-treated diabetic (n = 4)	One-Way ANOVA	
				F	*P*- value (All levels)
End-diastolic volume (EDV)/ Body weight (μl/g)	1.35 ± 0.01 $^{+}$	1.16 ± 0.02 *,§	1.3 ± 0.02 $^{+}$	27.281	<0.001
End-systolic volume (ESV)/ Body weight (μl/g)	0.49± 0.02 $^{+}$	0.69 ± 0.01 *,§	0.50 ± 0.01 $^{+}$	49.590	<0.001
Stroke volume (SV)/ Body weight (μl/g)	0.85 ± 0.03 $^{+}$	0.47 ± 0.03 *,§	0.80 ± 0.01 $^{+}$	74.114	<0.001

Table 9.8: **The MRI-derived diastolic and systolic volumes of the right ventricles of the control and the two 9-week diabetic groups normalized with respect to their corresponding body weights.** The body weight-normalized diastolic and systolic volumes of the right ventricles of the experimental rats were calculated using their corresponding body weights determined while they were under anaesthesia.

All values expressed as mean ± standard error of the mean (SEM). One-way analysis of variance (One-Way ANOVA) was used in comparison of the control and the two 9-week diabetic groups followed by Tukey's Honestly Significant Difference test for pair-wise multiple comparisons. A value of $p<0.05$ was considered statistically significant.

*Significantly different from the control group.

$^{+}$Significantly different from the 9-week untreated diabetic group.

§Significantly different from the 9-week captopril-treated diabetic group.

Parameter	Change occurred over 3 weeks of diabetes without captopril treatment	Change occurred over 6 weeks of diabetes without captopril treatment	Change occurred over 9 weeks of diabetes without captopril treatment	Change occurred over 9 weeks of diabetes with captopril treatment
Absolute LV EDV (µl)	-6.6% [c, d]	-27.6% [a, b, d]	-42.1% [a, b, c, §]	-29.9% [a, d]
Normalized LV EDV (µl/g)	-2.1% [c, d]	-10.6% [a, b, d]	-13.5% [a, b, c, §]	-0.7% [d]
Absolute LV ESV (µl)	+0.7%	+2.1%	-5.7%	-24.8% [a]
Normalized LV ESV (µl/g)	+6.0% [c, d]	+28.0% [a, b, d]	+42.0% [a, b, c, §]	+8.0% [d]
Absolute LV SV (µl)	-10.7% [a, c, d]	-44.1% [a, b, d]	-62.4% [a, b, c, §]	-32.7% [a, d]
Normalized LV SV (µl/g)	-6.6% [c, d]	-30.8% [a, b, d]	-44.0% [a, b, c, §]	-4.4% [d]
LV ejection fraction (%)	-4.5% [c, d]	-22.8% [a, b, d]	-35.2% [a, b, c, §]	-4% [d]

Table 9.9: **The effect of the duration of diabetes on left ventricular (LV) diastolic and systolic volumes and ejection fractions and its modification by captopril treatment.** LV EDV: left ventricular end-diastolic volume, LV ESV: left ventricular end-systolic volume, and LV SV: left ventricular stroke volume respectively.

The (-) and the (+) signs indicate a decrease and an increase in absolute and normalized left ventricular diastolic and systolic volumes and ejection fraction with diabetes respectively.

The symbols **a, b, c, d, and §** repeat the results obtained from Tukey's Honestly Significant Difference test while performing pair wise-multiple comparisons in Tables 9.1, 9.2, 9.5 and 9.6.

Parameter	Change occurred over 3 weeks of diabetes without captopril treatment	Change occurred over 6 weeks of diabetes without captopril treatment	Change occurred over 9 weeks of diabetes without captopril treatment	Change occurred over 9 weeks of diabetes with captopril treatment
Absolute RV EDV (µl)	-5.9% [c, d]	-23.5% [a, b, d]	-42.3% [a, b, c, §]	-31.7% [a, d]
Normalized RV EDV (µl/g)	-1.5% [d]	-5.2% [d]	-14.1% [a, b, c, §]	-3.7% [d]
Absolute RV ESV (µl)	+0.7%	+0.7%	-6.5% [§]	-28.8% [a, d]
Normalized RV ESV (µl/g)	+4.1% [c, d]	+26.5% [a, b, d]	+40.8% [a, b, c, §]	+2.0% [d]
Absolute RV SV (µl)	-8.9% [a, c, d]	-37.6% [a, b, d]	-63.1% [a, b, c, §]	-33.4% [a, d]
Normalized RV SV (µl/g)	-4.7% [c, d]	-22.4% [a, b, d]	-44.7% [a, b, c, §]	-5.9% [d]
RV ejection fraction %	-3.3% [c, d]	-18.5% [a, b, d]	-36.5% [a, b, c, §]	-2.7% [d]

Table 9.10: **The effect of the duration of diabetes on right ventricular (RV) diastolic and systolic volumes and ejection fraction and its modification by captopril treatment.** RV EDV: right ventricular end-diastolic volume, RV ESV: right ventricular end-systolic volume, and RV SV: right ventricular stroke volume respectively.

The (-) and the (+) signs indicate a decrease and an increase in absolute and normalized right ventricular diastolic and systolic volumes and ejection fraction with diabetes respectively. Tables 9.3, 9.4, 9.7 and 9.8.

The symbols **a, b, c, d, and §** repeat the results obtained from Tukey's Honestly Significant Difference test while performing pair wise-multiple comparisons in Tables 9.3, 9.4, 9.7 and 9.8.

Parameter	Between 0 and 3 weeks of diabetes	Between 3 and 6 weeks of diabetes	Between 6 and 9 weeks of diabetes
Absolute LV EDV (µl)	-6.6%	-22.5% [b]	-20.1% [c]
Normalized LV EDV (µl/g)	-2.1%	-8.7% [b]	-3.2% [c]
Absolute LV ESV (µl)	+0.7%	+1.4%	-7.6%
Normalized LV ESV (µl/g)	+6.0%	+20.8% [b]	+10.9% [c]
Absolute LV SV (µl)	-10.7% [a]	-37.4% [b]	-32.7% [c]
Normalized LV SV (µl/g)	-6.6%	-25.9% [b]	-19.0% [c]
LV ejection fraction %	-4.5%	-19.2% [b]	-16.1% [c]

Table 9.11: **Fractional deterioration in left ventricular (LV) diastolic and systolic volumes and ejection fraction through the experimentally induced diabetic state without captopril treatment.** LV EDV: left ventricular end-diastolic volume, LV ESV: left ventricular end-systolic volume, and LV SV: left ventricular stroke volume respectively.

The (-) and the (+) signs indicate a decrease and an increase in absolute and normalized left ventricular diastolic and systolic volumes and ejection fraction with diabetes respectively.

The symbols **a, b, and c** repeat the results obtained from Tukey's Honestly Significant Difference test while performing pair wise-multiple comparisons in Tables 9.1 and 9.5. They only indicate that the deterioration was significant.

Parameter	Between 0 and 3 weeks of diabetes	Between 3 and 6 weeks of diabetes	Between 6 and 9 weeks of diabetes
Absolute RV EDV (µl)	-5.9%	-18.7% [b]	-24.6% [c]
Normalized RV EDV (µl/g)	-1.5%	-3.8%	-9.4% [c]
Absolute RV ESV (µl)	-0.7%	+1.4%	-7.1%
Normalized RV ESV (µl/g)	+4.1%	+21.6% [b]	+11.3% [c]
Absolute RV SV (µl)	-8.9% [a]	-31.5% [b]	-41.0% [c]
Normalized RV SV (µl/g)	-4.7%	-18.5% [b]	-28.8% [c]
RV ejection fraction %	-3.3%	-15.7% [b]	-22.1% [c]

Table 9.12: **Fractional deterioration in right ventricular (RV) diastolic and systolic volumes and ejection fraction through the experimentally induced diabetic state without captopril treatment**. RV EDV: right ventricular end-diastolic volume, RV ESV: right ventricular end-systolic volume, and RV SV: right ventricular stroke volume respectively.

The (-) and the (+) signs indicate a decrease and an increase in absolute and normalized right ventricular diastolic and systolic volumes and ejection fraction with diabetes respectively.

The symbols **a, b, and c** repeat the results obtained from Tukey's Honestly Significant Difference test while performing pair wise-multiple comparisons in Tables 9.3 and 9.7. They only indicate that the deterioration was significant.

Parameter	Control (n = 4)	3-week diabetic (n = 4)	6-week diabetic (n = 4)	9-week untreated diabetic (n = 4)	One-Way ANOVA	
					F	*P*- value (all levels)
25 % SV and DFV (µl)	79.4 ± 1.2 [b, c, d]	70.9 ± 1.9 [a, c, d]	42.9 ± 0.9 [a, b, d]	28.6 ± 1.5 [a, b, c]	278.586	<0.001
Time for 25 % SV (ms) after the R wave trigger	22.0 ± 0.8 [c, d]	21.8 ± 1.6 [c, d]	42.3 ± 2.7 [a, b]	45.3 ± 0.9 [a, b]	55.904	<0.001
Time for 25 % DFV (ms) after the R wave trigger	110.3 ± 0.5 [c, d]	110.3 ± 0.6 [c, d]	124.8 ± 1.1 [a, b]	123.8 ± 1.0 [a, b]	89.829	<0.001
Time for 25 % SV (ms)	14.0 ± 0.8 [c, d]	13.8 ± 1.6 [c, d]	34.3 ± 2.7 [a, b]	37.3 ± 0.9 [a, b]	55.904	<0.001
Time for 25 % DFV (ms)	11.3 ± 0.5	11.3 ± 0.6	12.8 ± 1.1	11.8 ± 1.0	0.686	0.578
Rate of ejection during early systole (µl/ms)	5.7 ± 0.3 [c, d]	5.3 ± 0.5 [c, d]	1.3 ± 0.1 [a, b]	0.8 ± 0.03 [a, b]	70.314	<0.001
Rate of filling during early diastole (µl/ms)	7.1 ± 0.4 [c, d]	6.4 ± 0.5 [c, d]	3.4 ± 0.3 [a, b]	2.5 ± 0.2 [a, b]	36.768	<0.001

Table 9.13: **Indices for the kinetics of left ventricular contraction and relaxation of the control and the three untreated diabetic groups.**

All values expressed as mean ± standard error of the mean (SEM). One-way analysis of variance (One-Way ANOVA) was used in comparison of the control and the three untreated diabetic groups followed by Tukey's Honestly Significant Difference test for pair-wise multiple comparisons. A value of $p<0.05$ was considered statistically significant.

[a] Significantly different from the control group.

[b] Significantly different from the 3-week diabetic group.

[c] Significantly different from the 6-week diabetic group.

[d] Significantly different from the 9-week untreated diabetic group.

Parameter	Control (n = 4)	9-week untreated diabetic (n = 4)	9-week captopril-treated diabetic (n = 4)	One-Way ANOVA	
				F	*P*- value (all levels)
25 % SV and DFV (µl)	79.4 ± 1.2 $^{+,\S}$	28.6 ± 1.5 *,§	53.44 ± 2.5 $^{*,+}$	335.859	<0.001
Time for 25 % SV (ms) after the R wave trigger	22.0 ± 0.8 $^{+}$	45.3 ± 0.9 *,§	22.9 ± 0.9 $^{+}$	265.515	<0.001
Time for 25 % DFV (ms) after the R wave trigger	110.3 ± 0.5 $^{+}$	123.8 ± 1.0 *,§	111.9 ± 0.7 $^{+}$	92.557	<0.001
Time for 25 % SV (ms)	14.0 ± 0.8 $^{+}$	37.3 ± 0.9 *,§	14.9 ± 0.9 $^{+}$	265.515	<0.001
Time for 25 % DFV (ms)	11.3 ± 0.5	11.8 ± 1.0	12.9 ± 0.7	3.510	0.075
Rate of ejection during early systole (µl/ms)	5.7 ± 0.3 $^{+,\S}$	0.8 ± 0.03 *,§	3.7 ± 0.3 $^{*,+}$	137.280	<0.001
Rate of filling during early diastole (µl/ms)	7.1 ± 0.4 $^{+,\S}$	2.5 ± 0.2 *,§	4.2 ± 0.1 $^{*,+}$	72.144	<0.001

Table 9.14: **Indices for the kinetics of left ventricular contraction and relaxation for the control and the two 9-week diabetic groups.**

All values expressed as mean ± standard error of the mean (SEM). One-way analysis of variance (One-Way ANOVA) was used in comparison of the control and the two 9-week diabetic groups followed by Tukey's Honestly Significant Difference test for pair-wise multiple comparisons. A value of $p<0.05$ was considered statistically significant.

*Significantly different from the control group. $^{+}$ Significantly different from the 9-week untreated diabetic group. § Significantly different from the 9-week captopril-treated diabetic group.

Parameter	Control (n = 4)	3-week diabetic (n = 4)	6-week diabetic (n = 4)	9-week untreated diabetic (n = 4)	One-Way ANOVA	
					F	*P*- value (all levels)
25 % SV and DFV (µl)	74.6 ± 0.6 [b, c, d]	67.9 ± 1.6 [a, c, d]	44.6 ± 0.8 [a, b, d]	26.2 ± 2.1 [a, b, c]	250.450	<0.001
Time for 25 % SV (ms) after the R wave trigger	22.0 ± 0.4 [c, d]	22.0 ± 1.0 [c, d]	42.8 ± 2.5 [a, b]	48.3 ± 0.8 [a, b]	93.108	<0.001
Time for 25 % DFV (ms) after the R wave trigger	109.5 ± 0.6 [c, d]	109.3 ± 0.5 [c, d]	123.5 ± 0.9 [a, b]	123.5 ± 1.0 [a, b]	115.054	<0.001
Time for 25 % SV (ms)	14.0 ± 0.4 [c, d]	14.0 ± 1.0 [c, d]	34.8 ± 2.5 [a, b]	40.3 ± 0.8 [a, b]	93.108	<0.001
Time for 25 % DFV (ms)	10.5 ± 0.6	10.3 ± 0.5	11.5 ± 0.9	11.5 ± 1.0	0.748	0.544
Rate of ejection during early systole (µl/ms)	5.3 ± 0.2 [c, d]	4.9 ± 0.3 [c, d]	1.3 ± 0.1 [a, b]	0.6 ± 0.05 [a, b]	206.045	<0.001
Rate of filling during early diastole (µl/ms)	7.2 ± 0.4 [c, d]	6.7 ± 0.5 [c, d]	3.9 ± 0.2 [a, b]	2.4 ± 0.3 [a, b]	36.746	<0.001

Table 9.15: **Indices for the kinetics of right ventricular contraction and relaxation of the control and the three untreated diabetic groups.**

All values expressed as mean ± standard error of the mean (SEM). One-way analysis of variance (One-Way ANOVA) was used in comparison of the control and the three untreated diabetic groups followed by Tukey's Honestly Significant Difference test for pair-wise multiple comparisons. A value of $p<0.05$ was considered statistically significant.

[a] Significantly different from the control group.

[b] Significantly different from the 3-week diabetic group.

[c] Significantly different from the 6-week diabetic group.

[d] Significantly different from the 9-week untreated diabetic group.

Parameter	Control (n = 4)	9-week untreated diabetic (n = 4)	9-week captopril-treated diabetic (n = 4)	One-Way ANOVA	
				F	*P*- value (all levels)
25 % SV and DFV (µl)	74.6 ± 0.6 $^{+,\S}$	26.2 ± 2.1 *,§	49.7 ± 2.6 $^{*,+}$	189.201	<0.001
Time for 25 % SV (ms) after the R wave trigger	22.0 ± 0.4 $^{+}$	48.3 ± 0.8 *,§	23.8 ± 1.0 $^{+}$	565.171	<0.001
Time for 25 % DFV (ms) after the R wave trigger	109.5 ± 0.6 $^{+}$	123.5 ± 1.0 *,§	110.9 ± 0.6 $^{+}$	111.667	<0.001
Time for 25 % SV (ms)	14.0 ± 0.4 $^{+}$	40.3 ± 0.8 *,§	15.8 ± 1.0 $^{+}$	565.171	<0.001
Time for 25 % DFV (ms)	10.5 ± 0.6	11.5 ± 1.0	11.9 ± 0.6	2.053	0.184
Rate of ejection during early systole (µl/ms)	5.3 ± 0.2 $^{+,\S}$	0.6 ± 0.05 *,§	3.2 ± 0.2 $^{*,+}$	152.757	<0.001
Rate of filling during early diastole (µl/ms)	7.2 ± 0.4 $^{+,\S}$	2.4 ± 0.3 *,§	4.2 ± 0.4 $^{*,+}$	54.726	<0.001

Table 9.16: **Indices for the kinetics of right ventricular contraction and relaxation for the control and the two 9-week diabetic groups.**

All values expressed as mean ± standard error of the mean (SEM). One-way analysis of variance (One-Way ANOVA) was used in comparison of the control and the two 9-week diabetic groups followed by Tukey's Honestly Significant Difference test for pair-wise multiple comparisons. A value of $p<0.05$ was considered statistically significant.

*Significantly different from the control group. $^{+}$ Significantly different from the 9-week untreated diabetic group. § Significantly different from the 9-week captopril-treated diabetic group.

CHAPTER 10
DISCUSSION

10.1 Diabetic cardiac disease

Diabetes is associated with substantially increased susceptibility to coronary artery disease (Crall and Roberts, 1978; Jarret, 1979; Kannel, 1985). Diabetes may also lead to a diabetic cardiomyopathy (Hamby et al., 1974; Kannel, 1974; Ahmed et al., 1975; Sanderson et al., 1978; Shapiro et al., 1980, 1981a, b, 1982). It thus increases the incidence of congestive cardiac failure to an extent that could not be fully accounted for by the higher incidence of coronary atherosclerosis, hypertension, or cardiac autonomic neuropathy in such patients (Kannel et al., 1974). The pathophysiology of a possible diabetic cardiomyopathy and its associated haemodynamic abnormalities have accordingly attracted increasing interest. Animal studies using conventional physiological techniques have suggested that diabetic cardiomyopathy may exist as a distinct pathological entity. Thus, intact diabetic dogs showed abnormalities in left ventricular diastolic compliance (Regan et al., 1974). Isolated perfused hearts of diabetic rats similarly demonstrated decreased peak systolic pressures (Miller, 1979), Isolated papillary ventricular muscles obtained from diabetic rat hearts show a delayed onset and reduced rate of relaxation (Fein et al., 1980), increased time to peak tension and reduced sensitivity to increasing concentrations of calcium and adrenaline in the bathing medium (Warley et al., 1995). However, no non-invasive quantitative characterizations or analyses of the structural and functional myocardial changes have been made in intact diabetic animals, even though these potentially provide useful experimental models for diabetic cardiomyopathy.

10.2 Cardiac MRI

However, there have been rapid recent developments in the application of system hardware and pulse sequences for non-invasive cardiac magnetic resonance imaging (MRI). These have made MRI highly applicable for chronic physiological studies of animal models of common human cardiac pathology. MRI has already proven useful for accurate and high-resolution

CHAPTER 10
DISCUSSION

10.1 Diabetic cardiac disease

Diabetes is associated with substantially increased susceptibility to coronary artery disease (Crall and Roberts, 1978; Jarret, 1979; Kannel, 1985). Diabetes may also lead to a diabetic cardiomyopathy (Hamby et al., 1974; Kannel, 1974; Ahmed et al., 1975; Sanderson et al., 1978; Shapiro et al., 1980, 1981a, b, 1982). It thus increases the incidence of congestive cardiac failure to an extent that could not be fully accounted for by the higher incidence of coronary atherosclerosis, hypertension, or cardiac autonomic neuropathy in such patients (Kannel et al., 1974). The pathophysiology of a possible diabetic cardiomyopathy and its associated haemodynamic abnormalities have accordingly attracted increasing interest. Animal studies using conventional physiological techniques have suggested that diabetic cardiomyopathy may exist as a distinct pathological entity. Thus, intact diabetic dogs showed abnormalities in left ventricular diastolic compliance (Regan et al., 1974). Isolated perfused hearts of diabetic rats similarly demonstrated decreased peak systolic pressures (Miller, 1979), Isolated papillary ventricular muscles obtained from diabetic rat hearts show a delayed onset and reduced rate of relaxation (Fein et al., 1980), increased time to peak tension and reduced sensitivity to increasing concentrations of calcium and adrenaline in the bathing medium (Warley et al., 1995). However, no non-invasive quantitative characterizations or analyses of the structural and functional myocardial changes have been made in intact diabetic animals, even though these potentially provide useful experimental models for diabetic cardiomyopathy.

10.2 Cardiac MRI

However, there have been rapid recent developments in the application of system hardware and pulse sequences for non-invasive cardiac magnetic resonance imaging (MRI). These have made MRI highly applicable for chronic physiological studies of animal models of common human cardiac pathology. MRI has already proven useful for accurate and high-resolution

measurements of the major anatomical and functional clinical parameters of human cardiac performance (Stratemeier et al., 1986; Markiewicz et al., 1987; Sechtem et al., 1987; Semelka et al., 1990). There additionally has been recent interest in cine-MRI because of its excellent contrast between blood within the cardiac chambers and the myocardium that in turn would clearly demarcate the heart cavities. (Higgins, 1986; Sechtem et al., 1987; Semelka et al., 1990). The resulting cardiac images would be highly amenable to quantitative assessment of anatomical and functional characteristics. However, there are no published physiological MRI studies of the diabetic heart whether in human or in experimental animals. Yet such studies could both assess the important contribution made by impaired left ventricular function in the increased human morbidity and mortality from diabetic cardiomyopathy (Kannel, 1974) and follow chronic changes in both left and right ventricles in experimental systems. Physiological studies using such an approach could also lead to the application of similar MRI methods in clinical practice with their advantages in soft tissue contrast and avoidance of ionizing radiation.

The present MRI experiments detected and characterized the cardiac structural and functional abnormalities in both ventricles following experimental induction of diabetes in the laboratory rat for the first time. They also quantitatively analyzed the kinetic changes in left and right ventricular contraction and relaxation through the cardiac cycle and so established the presence of changes in the cardiac cycle produced by diabetic cardiomyopathy and characterized them in details. Finally, the experiments investigated the beneficial effects of captopril, an angiotensin-converting enzyme inhibitor in relieving such changes.

10.3 The streptozotocin-diabetic rat

Experimental animal systems offer particular advantages for following the chronic pathological changes when these are used as models for human disease, particularly when used in conjunction with non-invasive imaging techniques as opposed to standard invasive physiological measurements. In the present study, the point of induction of the disease in the streptozotocin-diabetic rat was clearly defined. The relevant pathology developed over weeks permitting chronic study over a manageable time scale. In any case, detailed pathological studies may not be possible in humans in the presence of clinical treatment and in any case human studies may not permit histological comparisons. The high resolution and sensitivity to anatomical and functional change now available to MRI permits early detection of pathology even in the relatively small laboratory rat and such changes can then be followed over time. Furthermore, use of MRI would reduce the number of animals required in physiological studies;

serial repeated studies of a given animal would decrease biological variance. Finally, the non-invasive imaging techniques themselves that emerge from such work would potentially be applicable for subsequent human studies.

10.4 Summary of the experimental approach

Since MRI measures all the major cardiac parameters accurately and non-invasively, the study involved relatively few animals. In addition, the experimental design incorporated diabetic, control and captopril-treated groups. The 20 male Wistar rats (6-week old) reared under standard conditions in animal facilities were randomly divided into five groups (each n = 4). Diabetes was induced at the age of 7 weeks in two groups and at 10 and 13 weeks respectively in two more experimental groups. The fifth group (n = 4) was kept as a control. All the animals, including the four in the control group were then consistently scanned at the age of 16 weeks. The diabetic state thus existed for 3, 6 and 9 weeks respectively before scanning in the groups made diabetic at the ages of 13, 10 and 7 weeks respectively. The untreated control rats were imaged at the same age of 16 weeks as the rats in the four diabetic groups and accordingly provided age and sex matched controls for all the four diabetic groups. Finally, the rats of one of the groups made diabetic at the age of 7 weeks (n = 4) were treated with captopril at a concentration of 2 g/l in the drinking water from immediately after the induction of diabetes.

The experimental studies acquired high-resolution MR images that provided a complete anatomical reconstruction of the intact rat heart at all imaged points through the cardiac cycle. Twelve transverse contiguous slices of the same slice thickness that fully covered each heart, all positioned perpendicular to the principal cardiac axis with each slice obtained at 12 time-points during the cardiac cycle followed both systolic and diastolic events. The animals were sacrificed after imaging and MRI and post-mortem results were then compared. The subsequent image processing provided epicardial, endocardial and myocardial volumes of both ventricles through the cardiac cycle included their end-diastolic and end-systolic volumes.

The study thus clarified the following questions. First, it characterized the changes in the major structural and functional parameters of the left and right ventricles of the diabetic and normal rats and validated some of these against post-mortem evidence. Secondly, the physiological and quantitative analysis derived the kinetics of left and right ventricular contraction and relaxation from the MRI data. Thirdly, the experimental group of the diabetic rats treated with the angiotensin-converting enzyme inhibitor captopril provided an evaluation of the therapeutic

benefits of this class of drugs in relieving left and right ventricular abnormalities associated with diabetes.

10.5 Cardiac parameters investigated

The image analysis procedures provided detailed information on changes in ventricular myocardial volume, end-diastolic volume (EDV), end-systolic volume (ESV), stroke volume (SV), and ejection fraction (EF), and the therapeutic effects of captopril on such experimental diabetic cardiomyopathy for the first time. They covered both the right and the left ventricles; few studies of any kind have been made on right ventricular structure and function whether in human or in experimental models of such systemic disease. The resulting MRI measurements of left and right ventricular parameters were expressed both as absolute values, and normalized to the corresponding body weights to facilitate comparison with earlier studies (Maeda et al., 1995; Hicks et al., 1998).

Major ventricular diastolic and systolic function volumes, ejection fractions, kinetics of contraction and relaxation and myocardial volumes of both ventricles significantly altered at 6 weeks in diabetic rats not treated with captopril, in agreement with previous reports (Rodrigues et al., 1997). Furthermore, further deterioration took place between 6 and 9 weeks of diabetes.

10.6 Ventricular hypertrophy in experimental diabetic cardiomyopathy

Both the measured left and right ventricular myocardial volumes were closely similar at end-systole and end-diastole in all five experimental groups. This expected conservation of both left and right ventricular myocardial volumes confirms consistency of determinations of the myocardial borders in each transverse MRI section and their reconstruction into myocardial volumes. In addition, the MRI measurements closely correlated with the myocardial masses measured post-mortem to give consistent values of myocardial densities that closely agreed with earlier studies at least in normal rats (Wise et al., 1998).

The myocardial volume determinations demonstrated a significant relative left and right ventricular hypertrophy relative to the corresponding body weights after both 6 weeks and 9 weeks of diabetes. This agrees with earlier pathological reports of myocardial hypertrophy and

interstitial fibrosis in diabetic hearts (Rubler et al., 1972; Fischer et al., 1979). They also agree with human echocardiographic findings of an increased left ventricular posterior wall and interventricular septal thicknesses in diabetics (Airaksinen et al., 1984a, 1987). There are, however, no corresponding echocardiographic reports concerning the right ventricle in diabetes.

The left ventricular hypertrophy developed markedly between 3 and 6 weeks of diabetes; this was followed by a smaller percentage increase between 6 and 9 weeks. In contrast, the greatest right ventricular hypertrophy occurred between 6 and 9 weeks of diabetes rather than between 3 and 6 weeks. These observed disparities might reflect the lower right-sided afterload. In contrast, the 9-week captopril-treated diabetic rats showed no such ventricular hypertrophy, suggesting a therapeutic effect of captopril upon the development of experimental diabetic cardiomyopathy.

10.7 Ventricular diastolic dysfunction in experimental diabetes

10.7.1 Diastolic volumes

Left and right ventricular end-diastolic volumes fell substantially over 6- and 9 weeks of diabetes compared with control rats. Furthermore, the greatest alterations took place between 3 and 6 weeks for the left ventricle and between 6 and 9 weeks for the right ventricle. Captopril reduced such changes in the 9-week diabetic group. These findings resolve some discrepancies in the echocardiographic literature that variously report reductions (Airaksinen et al., 1984a, 1987), or normal or modest increases in left ventricular size in diabetics (Shapiro et al., 1981a; Friedman et al., 1982; Fisher et al., 1989). Finally, there are no available existing reports whatsoever concerning right ventricular volumes for comparison.

10.7.2 Rates of diastolic filling

The ascending limbs of left and right ventricular endocardial volume curves derived from MRI and their corresponding initial rates of change, dV/dt, provided indications of diastolic function in the rapid filling phase of the cardiac cycle, which starts with opening of the atrio-ventricular valves. This rapid phase was followed by the slow filling phase in both ventricles. Both left and right ventricles of the 6- and 9-week diabetic rats showed reduced rates of early diastolic filling compared with the normal controls suggesting significant impairment in diastolic function. These results agree with echocardiographic findings of left ventricular diastolic dysfunction indicated by a prolonged isometric relaxation phase in diabetic patients (Sanderson et al., 1978; Shapiro et al., 1980, 1981a; b; Shapiro 1982; Airaksinen et al., 1984a).

A number of changes in cellular calcium handling have been implicated in the left ventricular diastolic dysfunction in diabetic patients. Several studies have reported reductions in sarcoplasmic reticular calcium re-uptake (Ganguly et al., 1983; Dhalla et al., 1998). Other investigators have, however, attributed diastolic dysfunction in diabetes to the collagen accumulation in the myocardial interstitium (Regan et al., 1981).

10.8 Ventricular systolic dysfunction in experimental diabetes

Diabetes impaired systolic function in both ventricles. Thus, there were marked changes in left and right end-systolic volumes, stroke volumes, and ejection fractions in the 6- and 9-week diabetic groups. In addition, the time course of the descending limbs of endocardial volume curves revealed markedly altered systolic dV/dt curves in the 6- and 9-week diabetic groups. The latter findings make it unlikely that the systolic changes solely result from altered diastolic volumes. The present results partially resolve apparent differences in earlier echocardiographic findings, which variously reported either depressed (Shapiro et al., 1981a, b, Uusitupa et al., 1985), normal systolic function (Airaksinen et al., 1984b; Fisher et al., 1989), or enhanced left ventricular systolic function in insulin-dependent patients developing microvascular complications (Thuesen et al., 1988).

Similar discrepancies occur between reports using radionuclide ventriculography. While Zola et al. (1986) reported significant reductions in left ventricular ejection fractions both at rest and with maximal exercise among diabetics with cardiac autonomic neuropathy, other investigators reported normal resting left ventricular ejection fractions with abnormal response only after exercise in diabetics (Vered et al., 1984; Fisher et al., 1985, 1986; Arvan et al., 1988).

It is unlikely that the alterations in systolic function reported here simply reflect altered diastolic volumes. Thus, the descending limbs of both left and right ventricular endocardial volumes and their systolic dV/dt's suggested marked kinetic changes in ventricular contraction. They suggested relatively rapid left end right ventricular systolic ejection in the normal, the 3-week, and the 9-week captopril-treated diabetic rats followed by slower volume decreases and dV/dt values continuing into late systole. In contrast, the 6- and 9-week diabetic rats not treated with captopril showed only small and gradual volume changes during early systole suggesting that both left and right ventricular systolic function was impaired. These observations resolve differing reports of similarly abnormal (Ahmed et al., 1975; Seneviratne, 1977; Shapiro et al.,

1980, 1981a, b; Cellina et al., 1983; Jermendy et al., 1984; Uusitupa et al., 1985), or normal (Airaksinen et al., 1984b) systolic time intervals in diabetic patients.

10.9 Correspondence between changes in left and right ventricles in normal and diabetic hearts

The transverse cardiac MRI sections showed that both right and left ventricles reached end-diastole and end-systole at approximately the same time in the cardiac cycle in the control as well as in all diabetic groups. The left and right ventricular endocardial volume curves and their corresponding dV/dt plots similarly demonstrated very similar systolic and diastolic volume changes over time through the cardiac cycle of both ventricles in all rats studied. A similar correspondence between the right and left ventricles applied to the ventricular end-diastolic volumes, end-systolic volumes, stroke volumes, and ejection fractions. These observations suggest that the mechanisms that match the performance of the right and left ventricles persisted despite diabetes.

10.10 Conclusions

The present work has thus successfully introduced magnetic resonance imaging to detect, quantify and follow up pathophysiological changes in both the left and right ventricles in experimental STZ-diabetes over time. Cine-MRI offered a non-invasive imaging technique that provided excellent soft tissue contrast and high quality anatomical images. Such an approach made it possible to characterize quantitatively the major parameters of myocardial volume, end-diastolic volume, end-systolic volume, stroke volume, and ejection fraction that characterize left and right ventricular function. These findings may be used to derive the cardiac output of both ventricles in vivo and determine how these altered through the disease process. Secondly the plots of endocardial volumes made it possible to determine the time courses of left and the right ventricular contraction and relaxation in detail. Thirdly, the findings could be used to reconcile apparently conflicting earlier findings that used other methods of measurements. Fourthly, the MRI procedures developed in rats would have potential application for the development of cardiac MRI in monitoring and detecting and studying human diabetic cardiac disease. Fifthly, the present approach was used to evaluate the effects of the angiotensin-converting enzyme inhibitor captopril in preventing the cardiac abnormalities associated with experimental cardiomyopathy. The combination of the present imaging with possible therapeutic agents may

be useful for future exploration of other interventions. Thus, there emerge significant justification for future development and application of cine cardiac magnetic resonance imaging in diabetic patients.

Cine cardiac magnetic resonance imaging was successfully applied to detect and characterize left and right ventricular anatomical and functional changes associated with diabetic cardiomyopathy in the STZ-diabetic rat, a widely used animal model for human diabetes. The MRI myocardial volume results gave consistent values through the cardiac cycle that agree with post-mortem findings. Other MRI results obtained from this experimental model concerning the effect of diabetes on the left ventricular systolic and diastolic functional volumes, ejection fraction, and kinetics of contraction and relaxation agree with the findings of a large number of conventional physiological studies of cardiac function in diabetic patients, thus confirming the validity of the STZ-diabetic rat model in studying diabetic cardiomyopathy. This also supports its use to study the therapeutic effects of captopril in diabetic cardiomyopathy. It is also noteworthy that clinical results appear to disagree with each other. The findings of the present work at least partly resolve these differences or at least suggest methods by which it might be possible to do so.

The timing of the MRI studies, at 0 (control), 3, 6, and 9 weeks respectively made it possible to identify the periods during which changes began and were most marked, in each of the ventricles. Firstly, they indicated significant relative left and right ventricular hypertrophy and functional abnormalities at 6 and weeks of diabetes in the absence of captopril treatment. The greatest change in left ventricular hypertrophy and systolic and diastolic parameters took place between 3 and 6 weeks. In contrast, the right ventricle showed the most marked changes between 6 and 9 weeks of diabetes. Finally, our results demonstrate that captopril both markedly reduced the left and right ventricular hypertrophy and improved left and right ventricular systolic and diastolic functions; such findings imply that the latter functional abnormalities might be the consequence of hypertrophy.

In conclusion, these results demonstrate significant anatomical and functional cardiac changes in experimental diabetes and demonstrate the utility of MRI as a physiological tool for the investigation of cardiac changes in other systemic diseases.

10.11 Possible future studies

This study thus explores a number of important pathophysiological aspects resulting from diabetic cardiomyopathy for the first time. It could additionally form the basis for further work that may both complement the present detailed findings as well as taking the analysis to a more sophisticated level. Thus further studies may follow the development of the cardiac changes at closer time intervals than the 3, 6 and 9 weeks described here, but use serial studies in individual rats. The latter would preserve the advantage of using MRI as an approach that requires relatively few animals. This may also facilitate explorations of the changes associated with the diabetic state over longer durations than those used here. The experimental approach used here may also be developed for use in screening studies although this might entail the development of more automated analyses for the more rapid and also more objective extraction of quantitative data from the images. Finally, the present MRI techniques might be combined with the more traditional physiological measurements that they complement, such as those that follow aortic flow, and aortic and right atrial pressures. This might enable the introduction of more sophisticated measures of cardiac performance, such as the cardiac hydraulic power output (Tan, 1986). Furthermore, the capacity of MRI to measure both ventricular volume changes and their rates at several time-points through systole offers the possibility of further developments of such a clinical approach, as well as a rigorous method for the assessment of cardiac function in diabetic patients.

CHAPTER 11
MRI ANALYSIS OF RIGHT VENTRICULAR FUNCTION IN NORMAL AND SPONTANEOUSLY HYPERTENSIVE RATS (SHR)

11.1 Introduction

Systemic hypertension refers to a persistent and abnormal increase of blood pressure in the systemic arteries. It most frequently reflects an arteriolar constriction (Frohlich, 1983), which in turn increases the total systemic resistance to blood flow.

Inadequately treated hypertension is associated with increased cardiovascular morbidity and mortality, in particular an increased incidence of ischaemic heart disease and heart failure (Kannel et al., 1972; Frohlich, 1991). Left ventricular hypertrophy resulting from sustained pressure over-load is considered to be one of the most important cardiac complications of systemic hypertension. The resulting increase in functional demands on the left ventricular myocytes stimulates them to increase in size (Frohlich, 1983, 1991), reflecting a physiological adaptive mechanism that would perhaps postpone the development of left ventricular failure (Grossman, 1980; Frohlich, 1991).

However such hypertrophy is associated with increased cardiovascular morbidity and mortality independent of the height of arterial pressure (Frohlich, 1991) including unifocal and multifocal premature ventricular electrocardiographic complexes as well as higher-grade ventricular ectopic activity such as coupled premature ventricular complexes (Messerli et al., 1984). Accordingly a major goal in the management of hypertension is the prevention or reversal of myocardial hypertrophy.

Hypertrophy also results in a decreased left ventricular compliance that impairs its diastolic function (Frohlich, 1991). Moreover, the hypertrophy increases the diffusion distance for oxygen and other nutrients delivered form capillaries to tissues. Finally, chronic systemic

hypertension predisposes to atherosclerosis (Dustan et al., 1974). All these changes predispose the hypertrophied myocardium to ischaemic injury.

Neither radiography nor electrocardiography effectively detect minor changes in left ventricular mass and echocardiography has been a frequent investigative tool for the assessment and follow up of left ventricular structure and function in hypertensive patients with left ventricular hypertrophy (Savage et al., 1979). The latter has been assessed through measurements of inter-ventricular septal and posterior wall thickness. Echocardiography has thus proven to be a valuable technique in cardiac anatomical and haemodynamic evaluations in the majority of patients with hypertension (Savage et al., 1979). However, assessment of left ventricular hypertrophy could be inaccurate with 2-dimensional measurements when hypertrophy is asymmetric and the ventricle is deformed. Furthermore, adjacent lung tissue and limited cardiac windows may make it difficult to image certain myocardial regions. Finally, the resulting images may not be of sufficient echogenicity to allow an accurate definition of the endocardial and epicardial borders throughout the left ventricle in a substantial proportion of patients.

Magnetic resonance imaging offers particular advantages as an imaging technique in its non-invasive nature and avoidance of ionizing radiation. Moreover, images can be obtained in any anatomical plane and can then be reconstructed for a complete three-dimensional analysis. There has seen rapid progress and development and application of MRI techniques to the cardiovascular system. This has resulted in a marked improvement of the accuracy in measurements of cardiac parameters such as left and right ventricular stroke volumes, ejection fractions and left and right ventricular myocardial volumes (Stratemeier et al., 1986; Markiewicz et al., 1987; Sechtem et al., 1987; Semelka et al., 1990; Wise et al., 1998). Recently, such techniques have been extended from human to animal physiological studies in the quantitative evaluation of myocardial volume in left ventricles of spontaneously hypertensive rats (SHR) (Wise et al., 1998). These demonstrated and quantitatively characterized a hypertrophy and a parallel reduction in left ventricular ejection fraction.

The SHR rats show some histological features of hypertensive changes in the pulmonary system (Aharinejad et al., 1996). The present study investigates right ventricular structure and function in the spontaneously hypertensive rats (SHR) using MRI. This involves the development of magnetic resonance (MR) imaging and quantitative techniques for characterization of dynamic and functional changes in the right ventricle in the hypertensive and normal rat heart.

11.2 Materials and methods

11.2.1 The experimental rats

Magnetic resonance imaging studies were performed on a total of 16 male rats ranging in weight from 203 g to 334 g. Four male 8-week old spontaneously hypertensive (SHR) were examined and compared with four age and sex-matched normotensive Wistar Kyoto rats (WKY). Similarly, four male 12-week old SHR were examined and compared with four age and sex-matched normotensive control WKY. This made it possible to obtain some indication both of the onset of pathological changes in young adult rats and of their progression as the rats become older.

11.2.2 Magnetic resonance imaging

The principles used in these experiments were essentially the same as those mentioned in Chapter 6. However, in order more directly to assess the right ventricular myocardial volume the studies employed a multi-slice gradient-echo pulse sequence known to give significant myocardial signal that would contrast with low signal intensity from the thoracic cavity. The effective echo-time (TE) used in this study was 4.3 ms, which was essentially the same as that used in the cine imaging protocol. The repeat time for each slice was, however, different from that used in the cine imaging protocol, being approximately 200 ms in this study. Nevertheless, a similar gating protocol triggered image acquisition with every alternate heartbeat rather than every cardiac cycle giving an effective repeat-time (TR) of approximately 400 ms was adopted. An interleaved multi-slice gradient-echo pulse sequence employed a cyclical multi-slice approach to image acquisition. Thus over one cardiac cycle, signal from one image is acquired from each of twelve selected slices with such images rotating through each of the different 12 time-points during the cardiac cycle (Crooks et al., 1984). Thus having acquired one full image for each of the 12 transverse cardiac slices, the multi-slice excitation order was rotated cyclically in order to obtain 12 magnetic resonance images at the 12 chosen time-points of the cardiac cycle for each of the 12 selected slices.

Since two signal average protocols were used with an image matrix of 128X128 pixels, a total number of 2X2X128X12 cardiac cycles were required to obtain images for the 12 selected slices at the 12 studied time-points through the cardiac cycle. Given that the average heart rate of the rats during the image sessions was approximately 300 beats min^{-1}, the average R-R interval representing the duration of the cardiac cycle was, therefore, 200 ms and the total imaging time was approximately 22 minutes. The heart rate of the rats was continuously

11.2 Materials and methods

11.2.1 The experimental rats

Magnetic resonance imaging studies were performed on a total of 16 male rats ranging in weight from 203 g to 334 g. Four male 8-week old spontaneously hypertensive (SHR) were examined and compared with four age and sex-matched normotensive Wistar Kyoto rats (WKY). Similarly, four male 12-week old SHR were examined and compared with four age and sex-matched normotensive control WKY. This made it possible to obtain some indication both of the onset of pathological changes in young adult rats and of their progression as the rats become older.

11.2.2 Magnetic resonance imaging

The principles used in these experiments were essentially the same as those mentioned in Chapter 6. However, in order more directly to assess the right ventricular myocardial volume the studies employed a multi-slice gradient-echo pulse sequence known to give significant myocardial signal that would contrast with low signal intensity from the thoracic cavity. The effective echo-time (TE) used in this study was 4.3 ms, which was essentially the same as that used in the cine imaging protocol. The repeat time for each slice was, however, different from that used in the cine imaging protocol, being approximately 200 ms in this study. Nevertheless, a similar gating protocol triggered image acquisition with every alternate heartbeat rather than every cardiac cycle giving an effective repeat-time (TR) of approximately 400 ms was adopted. An interleaved multi-slice gradient-echo pulse sequence employed a cyclical multi-slice approach to image acquisition. Thus over one cardiac cycle, signal from one image is acquired from each of twelve selected slices with such images rotating through each of the different 12 time-points during the cardiac cycle (Crooks et al., 1984). Thus having acquired one full image for each of the 12 transverse cardiac slices, the multi-slice excitation order was rotated cyclically in order to obtain 12 magnetic resonance images at the 12 chosen time-points of the cardiac cycle for each of the 12 selected slices.

Since two signal average protocols were used with an image matrix of 128X128 pixels, a total number of 2X2X128X12 cardiac cycles were required to obtain images for the 12 selected slices at the 12 studied time-points through the cardiac cycle. Given that the average heart rate of the rats during the image sessions was approximately 300 beats min^{-1}, the average R-R interval representing the duration of the cardiac cycle was, therefore, 200 ms and the total imaging time was approximately 22 minutes. The heart rate of the rats was continuously

monitored throughout the imaging sessions and typically showed little variation during the acquisition of each complete image data set.

11.2.3 Statistical analyses

Results are presented as means ± standard error of the means (SEM). The statistical significance of differences in the structural and functional parameters in the 8- and 12-week WKY and SHR groups due to the effect of hypertension and age and the interaction between hypertension and age was evaluated by the two-way analysis of variance (Two-Way ANOVA). Differences were considered significant at $p<.05$. When the interaction between hypertension and age on a particular parameter was not significant, the analysis was rerun eliminating the interaction term from the model. Correlations between measured or calculated quantities were quantified by Pearson coefficient denoted by (r).

11.3 Results

11.3.1 General characteristics of the experimental rats

Table 11.1 demonstrates that both the WKY and SHR groups showed an increase in the body weight between 8 and 12 week of age. Table 11.1 also indicates significantly higher systolic blood pressures in the SHR rats compared with the normal WKY groups. Whereas the two normal groups had comparable systolic blood pressures, the SHR groups showed an increase in blood pressure with age. Table 11.1 also shows that the SHR groups had slower heart rates than the WKY groups.

11.3.2 Magnetic resonance cardiac images in transverse section

The main purpose of this study was to study the pathological structural and functional changes that might occur in the right ventricle in the SHR. Accordingly, results related to the right ventricular structural and functional parameters of the four experimental groups studied will be dealt with and analyzed in detail.

Figures 11.2-11.5 show typical transverse cardiac MRI sections taken perpendicular to the principal cardiac axis through the beating heart of representative animals from the four study groups over 12 studied time-points through the cardiac cycle. The images provide a qualitative indication of the dynamic changes in both ventricles through the cardiac cycle.

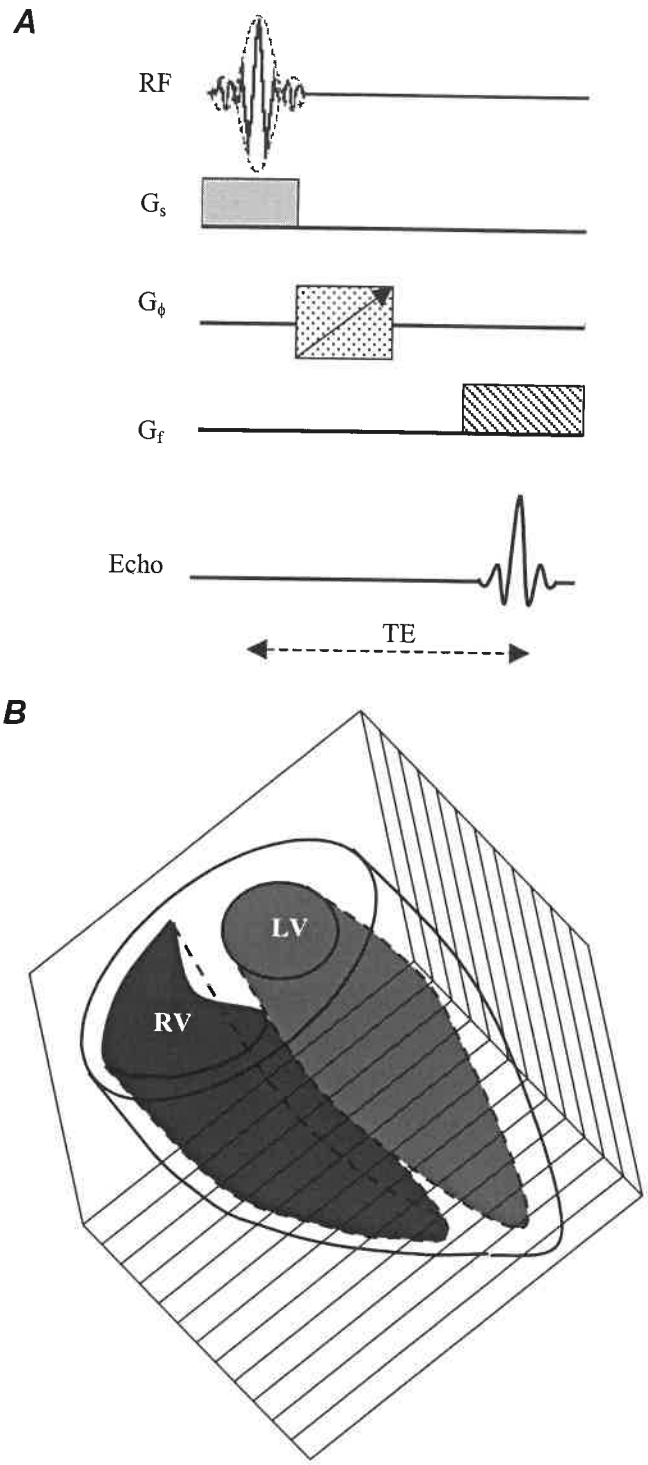

Figure 11.1: **Gradient echo pulse sequence (A), diagrammatic representation of the right and left ventricles of the rat heart.** Typically 12 transverse image slices taken perpendicular to the principal cardiac axis were acquired contiguously covering both ventricles. Each transverse cardiac slice was typically imaged at 12 time-points through the cardiac cycle using an interleaved multi-slice acquisition protocol. Thus, the pulse sequence was applied 12 times during each particular cardiac cycle, exciting first the i^{th} slice then the $(i+2)^{th}$ slice, giving a repeat time (TR) for each slice of the same order as the R-R interval of the animal (200 ms). However, the effective repeat time (TR) for each slice was 400 ms since image acquisition was gated from every alternate heart beat rather than imaging every cardiac cycle. Echo time TE = 4.3 ms. LV and RV indicate left and right ventricles respectively.

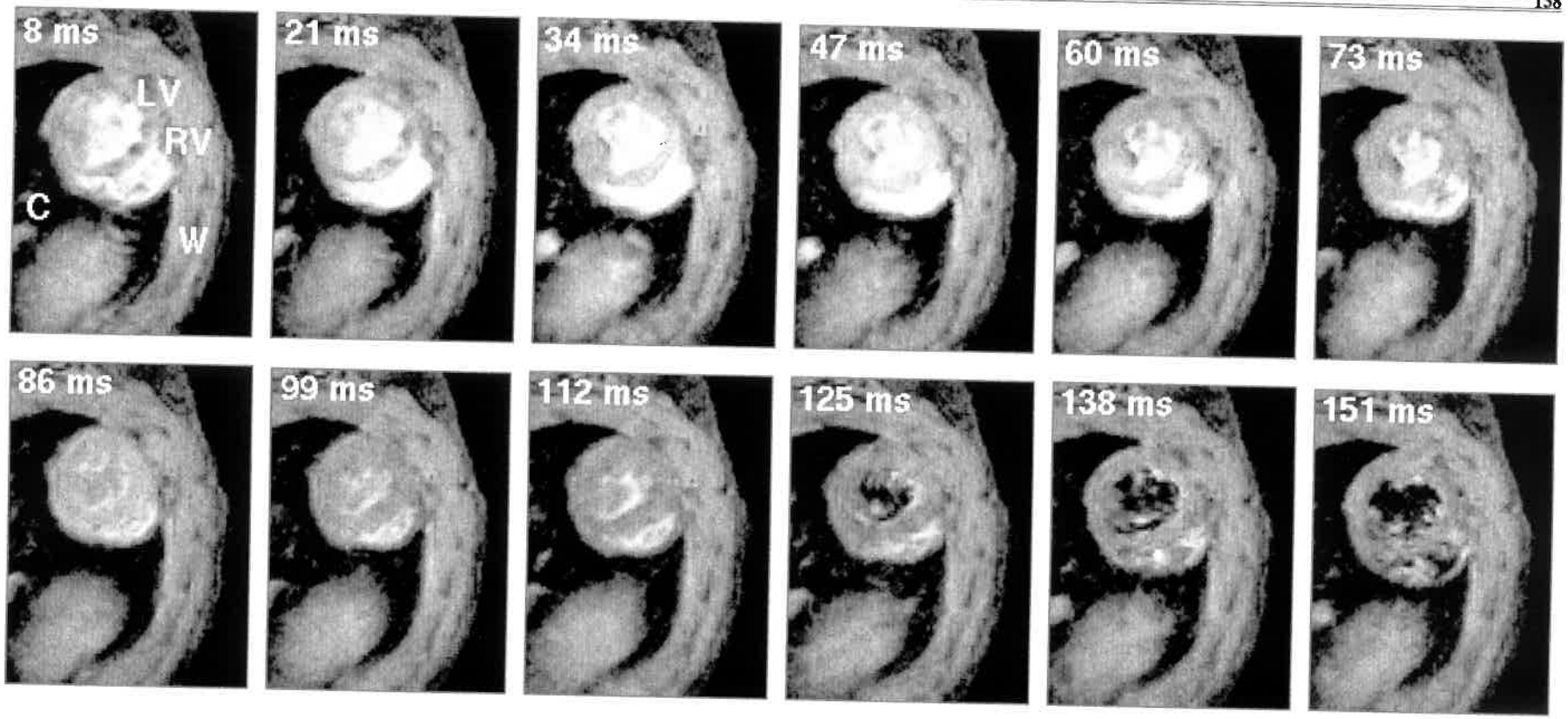

Figure 11.2: **Typical transverse sections obtained from the heart of a typical normal 8-week WKY rat.** A series of typical transverse MR sections obtained from the heart of a typical normal 8 weeks old male WKY rat weighing 210 g. The heart rate was continuously monitored throughout the imaging session giving an intrinsic heart rate of 285 ± 2 beats min^{-1}. The sections were taken perpendicular to the principal cardiac axis at one spatial slice at typically twelve time points during the cardiac cycle. These time points are indicated in the upper left-hand corner of each panel and correspond to the delay after the trigger, taken from the R-wave of the electrocardiogram (ECG), at which the signal was acquired. Each image is the average of two signals obtained at corresponding points in the cardiac cycle following the R wave. LV and RV indicate left and right ventricles respectively and C and W indicate chest cavity and chest wall respectively. Slice thickness was 1.37 mm. Field of view (FOV) was 5 cm and with an image matrix of 128 pixel square, the nominal in-plane resolution was approximately 390.6 μm $pixel^{-1}$. The effective repeat time (TR) was approximately 400 ms.

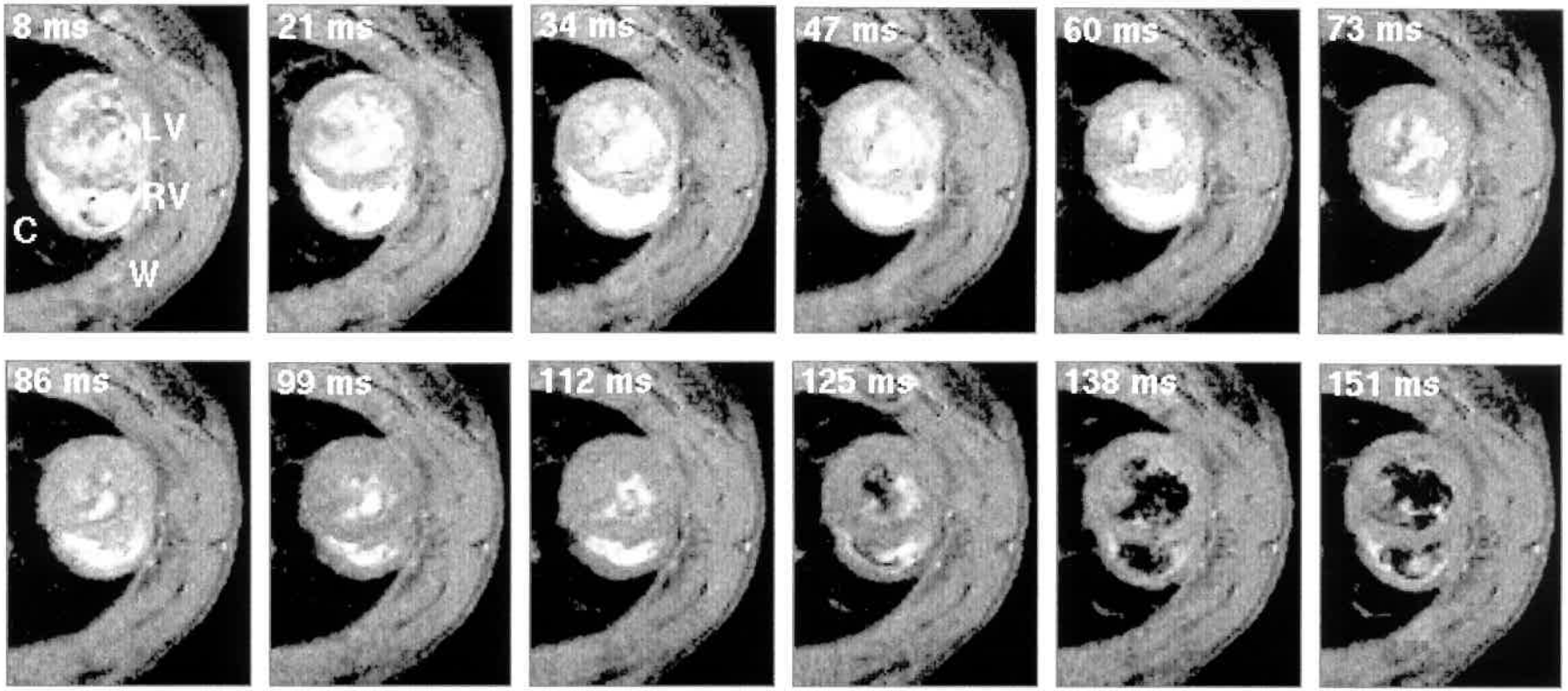

Figure 11.3: **Typical transverse sections obtained from the heart of a typical normal 12-week WKY rat.** A series of typical transverse MR sections obtained from the heart of a typical normal 12 weeks old male WKY rat weighing 273 g. The heart rate was continuously monitored throughout the imaging session giving an intrinsic heart rate of 298 ± 4 beats min^{-1}. The sections were taken perpendicular to the principal cardiac axis at one spatial slice at typically twelve time points during the cardiac cycle. These time points are indicated in the upper left-hand corner of each panel and correspond to the delay after the trigger, taken from the R-wave of the electrocardiogram (ECG), at which the signal was acquired. Each image is the average of two signals obtained at corresponding points in the cardiac cycle following the R wave. LV and RV indicate left and right ventricles respectively and C and W indicate chest cavity and chest wall respectively. Slice thickness was 1.37 mm. Field of view (FOV) was 4.5 cm and with an image matrix of 128 pixel square, the nominal in-plane resolution was approximately 351.6 μm $pixel^{-1}$. The effective repeat time (TR) was approximately 400 ms.

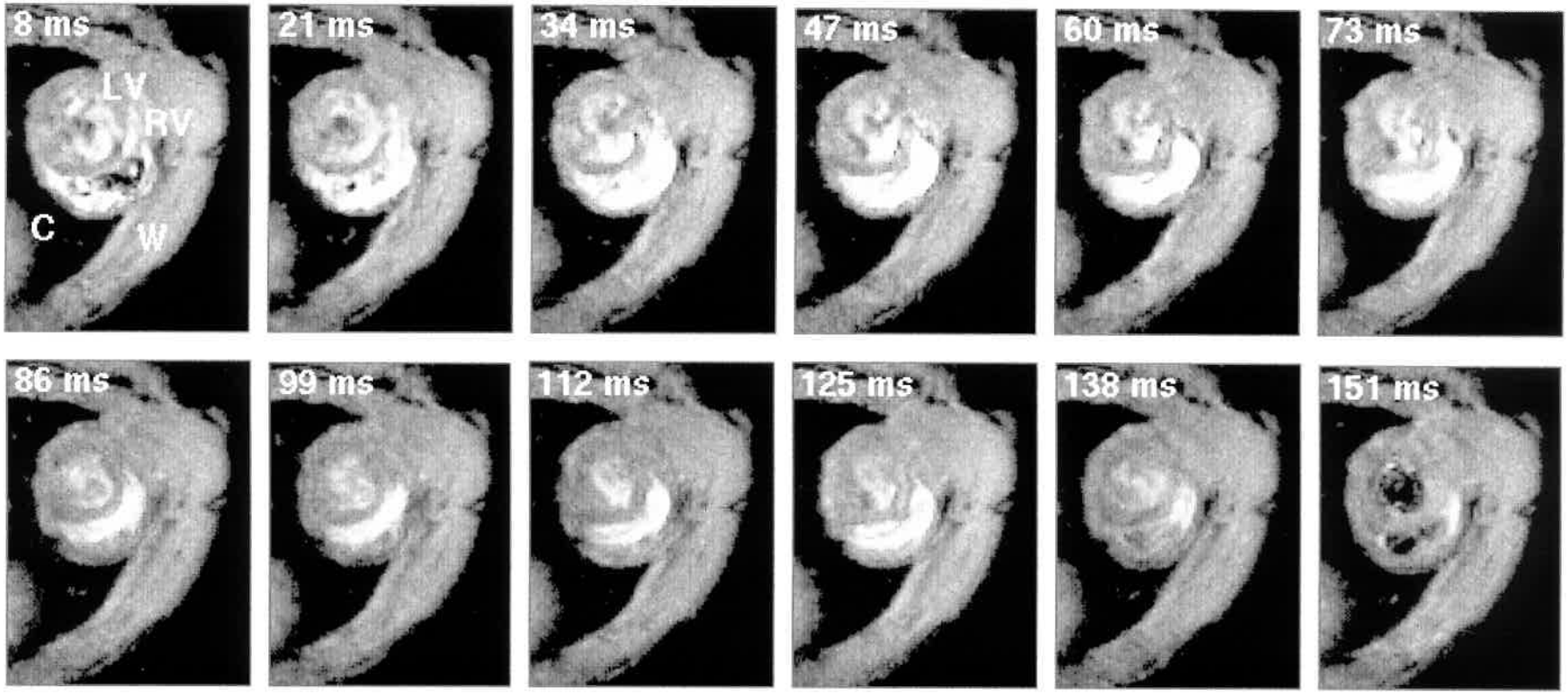

Figure 11.4: **Typical transverse sections obtained from the heart of a typical 8-week SHR rat.** A series of typical transverse MR sections obtained from the heart of a typical 8 weeks old male SHR rat weighing 241 g. The heart rate was continuously monitored throughout the imaging session giving an intrinsic heart rate of 293 ± 3 beats min^{-1}. The sections were taken perpendicular to the principal cardiac axis at one spatial slice at typically twelve time points during the cardiac cycle. These time points are indicated in the upper left-hand corner of each panel and correspond to the delay after the trigger, taken from the R-wave of the electrocardiogram (ECG), at which the signal was acquired. Each image is the average of two signals obtained at corresponding points in the cardiac cycle following the R wave. LV and RV indicate left and right ventricles respectively and C and W indicate chest cavity and chest wall respectively. Slice thickness was 1.37 mm. Field of view (FOV) was 5 cm and with an image matrix of 128 pixel square, the nominal in-plane resolution was approximately 390.6 μm $pixel^{-1}$. The effective repeat time (TR) was approximately 400 ms.

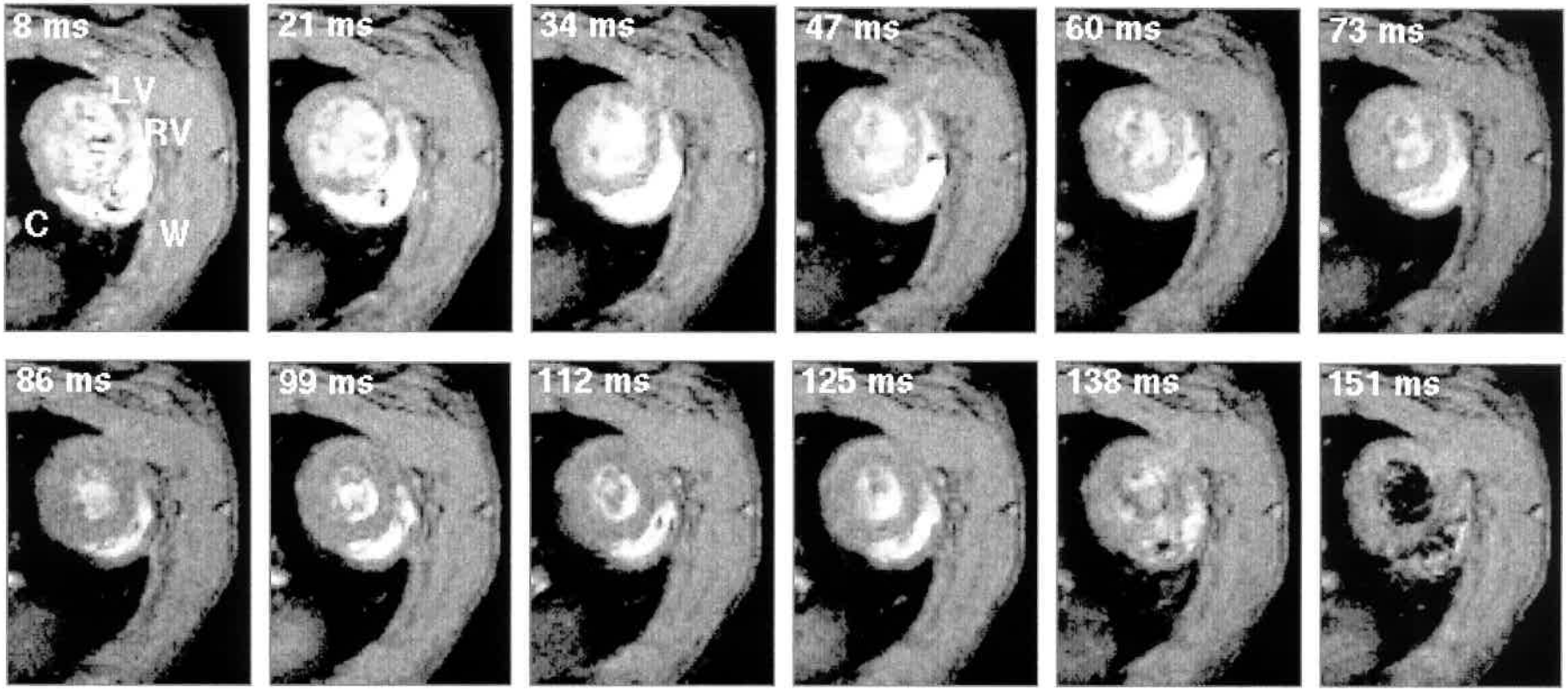

Figure 11.5: **Typical transverse sections obtained from the heart of a typical 12-week SHR rat.** A series of typical transverse MR sections obtained from the heart of a typical 12 weeks old male SHR rat weighing 319 g. The heart rate was continuously monitored throughout the imaging session giving an intrinsic heart rate of 287 ± 7 beats min^{-1}. The sections were taken perpendicular to the principal cardiac axis at one spatial slice at typically twelve time points during the cardiac cycle. These time points are indicated in the upper left-hand corner of each panel and correspond to the delay after the trigger, taken from the R-wave of the electrocardiogram (ECG), at which the signal was acquired. Each image is the average of two signals obtained at corresponding points in the cardiac cycle following the R wave. LV and RV indicate left and right ventricles respectively and C and W indicate chest cavity and chest wall respectively. Slice thickness was 1.37 mm. Field of view (FOV) was 5 cm and with an image matrix of 128 pixel square, the nominal in-plane resolution was approximately 390.6 μm $pixel^{-1}$. The effective repeat time (TR) was approximately 400 ms.

The right ventricles in both normal and the hypertensive groups appeared thinner than the left ventricle and were crescentic in cross section in contrast to the circular symmetry of the epicardial and endocardial borders of the left ventricle at all points through the cardiac cycle.

The myocardium of both ventricles could be clearly distinguished from the surrounding anatomical structures in the thoracic cavity. As already mentioned, this study applied a multi-slice imaging protocol, which ensured that significant signal was obtained from the myocardium. Such an approach ensured a clear definition of the epicardial border, which was important for measurements of myocardial volume from the magnetic resonance images. The images that were acquired 8 ms after the electrocardiographic R wave trigger typically demonstrated fully dilated right and left ventricles in both normal and hypertensive rats. The subsequent frames then demonstrate right ventricular systole with a thickening of the ventricular wall in all the four study groups. The systolic patterns in the right ventricles of the two SHR groups thus appeared to be similar to those of the two normal WKY groups. All the experimental groups reached end-systole at similar times, at approximately 100 ms following the triggering electrocardiographic R-wave. This was followed by diastolic refilling of both ventricles in all four groups. The right ventricles in all four groups also demonstrated similar diastolic patterns with early diastolic filling being more marked than at times late in diastole. However, the right ventricles of the two SHR groups showed a slower diastolic refilling compared with the right ventricles of the two normal WKY groups.

11.3.3 Epicardial, endocardial, and myocardial volume curves

Figures 11.6A-11.6D summarize the results of a quantification of the dynamic changes shown by the right ventricles through complete cardiac cycles of all the four experimental groups. It plots changes in right ventricular endocardial, epicardial, and myocardial volumes as derived from measurements from the transverse cardiac magnetic resonance sections with time. Figures 11.6A-11.6D display the respective curves obtained from the 8-week WKY, the 12-week WKY, the 8-week SHR, and the 12-week SHR groups respectively.

Both epicardial and endocardial borders of right ventricular chambers were traced 4 times for each slice using in-house software. Right ventricular epicardial, endocardial and myocardial volumes were then derived by combining data individually obtained for all twelve imaging sections that were taken perpendicular to the principal cardiac axis, and reconstructed for each of the twelve time-points that were studied during the cardiac cycle. The sections thus provided full coverage of the heart of each experimental rat during both systole and diastole. In all cases, the error bars defining the standard errors of the means of the volumes were smaller than the

sizes of the symbols. In the plots the ascending and descending limbs of the endo- and epicardial volume curves represent diastole and systole respectively.

Figures 11.6A-11.6D demonstrate a prompt onset of right ventricular contraction in the four experimental groups following the electrocardiographic R wave. Furthermore, contraction was more rapid, early in systole and slowed down towards end-systole, which was reached approximately 100 ms after the electrocardiographic R-wave trigger in all the four experimental groups. Diastole similarly began with a more marked right ventricular filling in early as opposed to late diastole in all the rats. However, the SHR showed a slower refilling rate during diastole confirming impressions derived from the transverse cardiac magnetic resonance images.

11.3.4 Myocardial volume

The right ventricular myocardial volumes of all the rats studied were calculated by subtracting their endocardial volumes from their corresponding epicardial volumes at all the 12 examined time-points through the cardiac cycle. Figure 11.7 confirms that such an approach consistently demonstrated constant volumes throughout systole and diastole. Table 11.1 reveals that right ventricular myocardial volumes increased between 8 and 12-weeks in both the WKY groups and SHR groups. In addition, SHR groups showed higher volumes than the WKY groups. Such findings were confirmed even when the right ventricular myocardial volumes were normalized to the corresponding body weights. Figure 11.8 also shows that the 2 SHR groups had higher right ventricular myocardial volumes than the 2 WKY groups for a given body weight.

11.3.5 Functional ventricular volumes

Table 11.1, similarly shows that right ventricular EDV increased between 8 and 12 weeks in both WKY and SHR groups. Furthermore, the SHR groups had larger right ventricular EDV's than the WKY groups.

Table 11.1 similarly shows that right ventricular end-systolic luminal volumes (ESV's) increased in both WKY and SHR rats between 8 and 12 weeks. However, the ESV's were consistently higher in the two SHR groups when compared with their age-matched WKY groups. Taken together, the EDV and ESV findings indicate significantly reduced right ventricular ejection fractions (EF's) in the two SHR groups compared with their age-matched WKY groups.

Figure 11.6 (next page): **Epicardial (squares), endocardial (circles), and myocardial (triangles) right ventricular (RV) volume curves.** Epicardial, endocardial and myocardial right ventricular (RV) volume curves obtained from the transverse MRI images of the normal 8-week WKY group (A), the normal 12-week WKY group (B), the 8-week SHR group (C), and the 12-week SHR group. The average body weight of the two normal groups was 214 ± 9 g and 284 ± 13g for the 8-week WKY (n = 4) and the 12-week WKY (n = 4) groups, respectively, and the average body weight of the two hypertensive groups was 246 ± 9 and 307 ± 13 g for the 8-week SHR (n = 4) and the 12-week SHR (n = 4), respectively. The heart rate was continuously monitored throughout the imaging session and the average intrinsic heart rates were 326 ± 19 and 319 ± 13 beats min^{-1} for the normal 8-week WKY and the normal 12-week WKY group, respectively and those of the two hypertensive groups were 296 ± 3 and 292 ± 12 beats min^{-1} for the 8-week SHR and the 12-week SHR, respectively.

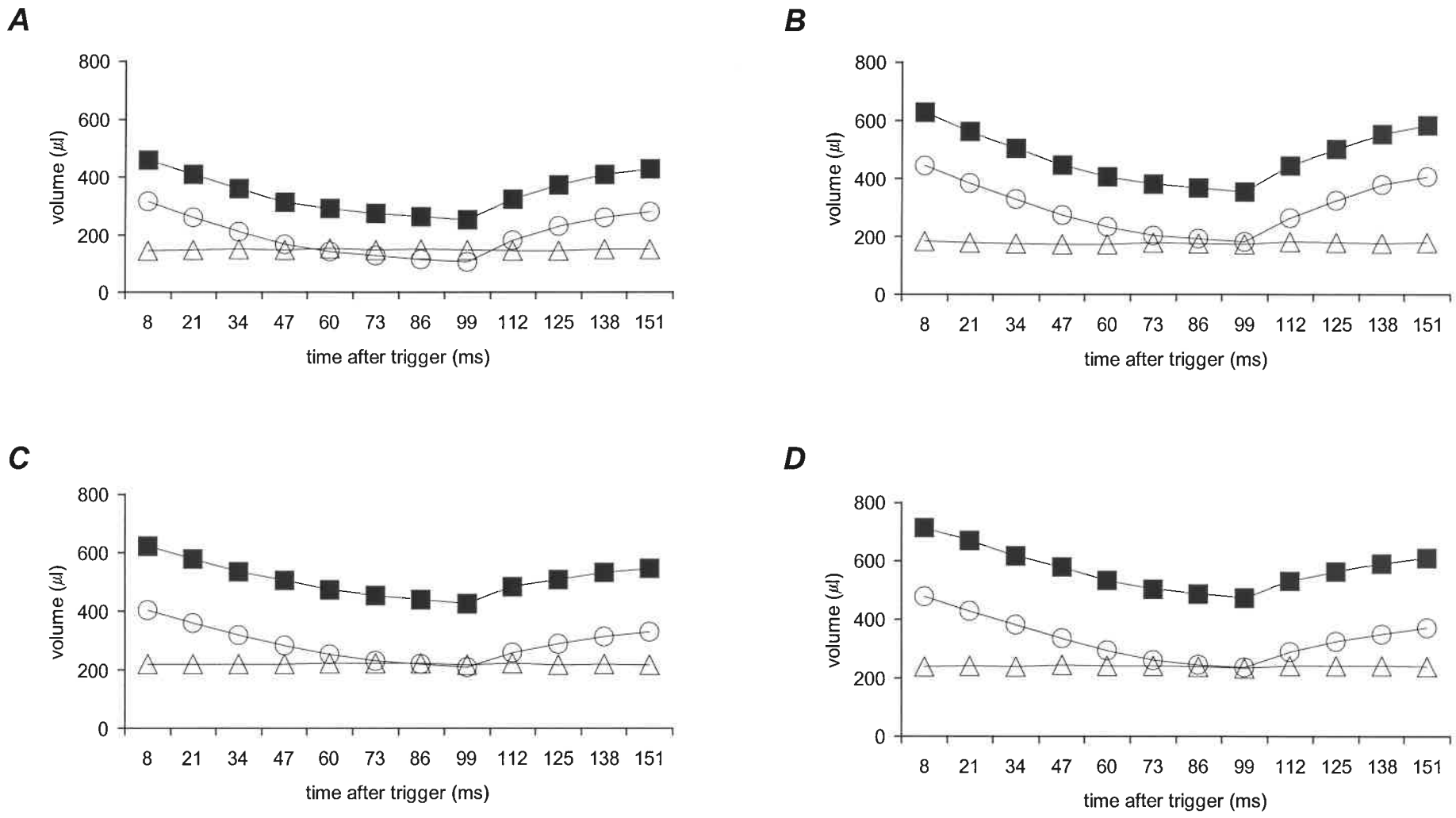
A
B
C
D
800
600
400
200
0
volume (µl)
8 21 34 47 60 73 86 99 112 125 138 151
time after trigger (ms)

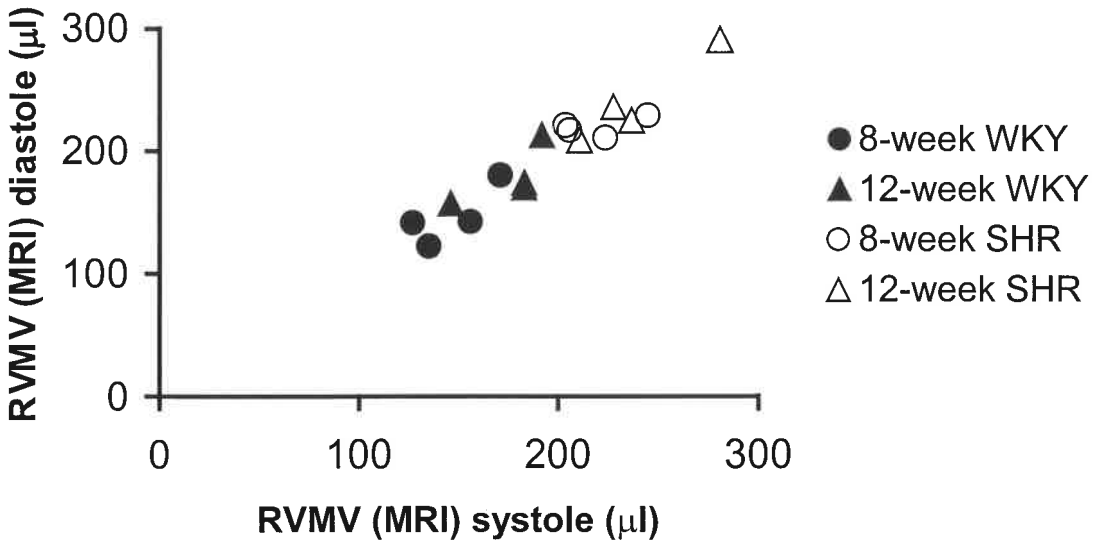

Figure 11.7: **Right ventricular muscle volumes.** A comparative plot of the MRI-determined right ventricular (RV) myocardial volume during systole and diastole (r = 0.95). The right ventricular myocardial volume at the 12 time points during the cardiac cycle for each rat. The right ventricular myocardial volume measured by MRI during systole, for each individual rat, was taken from the average value from all the time-points sampled during systole and similarly the right ventricular myocardial volume measured by MRI during diastole for each individual rat, was taken from the average value from all the time-points sampled during diastole in the cardiac cycle. These are the volumes correlated here. As displayed, there was a close correlation between the systolic and diastolic right ventricular myocardial volumes.

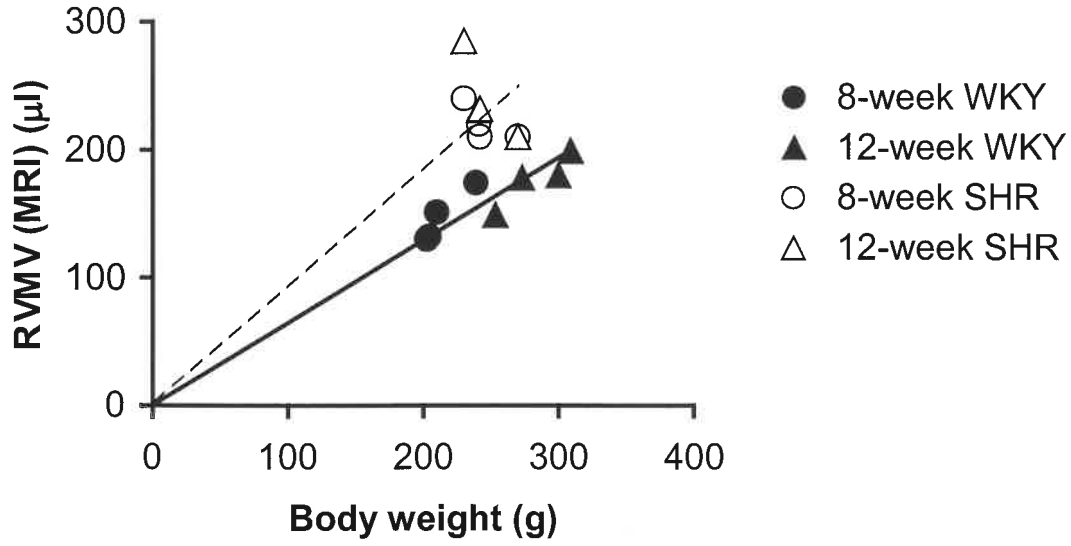

Figure 11.8: **Right ventricular (RV) myocardial volume *versus* body weight.** Correlation of right ventricular (RV) myocardial volume determined by MRI and body weight of the combined age groups of WKY and SHR. An intercept through the origin is assumed. The average RVMV/BW ratios were 0.65 ± 0.03 and 0.84 ± 0.05 µl g^{-1} for combined age groups of WKY and SHR respectively.

11.3.6 Indices for the kinetics of ventricular contraction and relaxation

Table 11.2 summarizes a range of two indices describing the kinetics of right ventricular contraction and relaxation. Thus, Table 11.2 summarizes the systolic and the diastolic time periods required for the right ventricles of the four experimental groups to pump 25% of their SV's and to be filled with 25% of their diastolic filling volumes (DFV's).

Since images typically acquired 8 ms after the R wave trigger showed fully dilated ventricles in all the experimental rats, the ventricles were considered to be at their end-diastole approximately 8 ms following the electrocardiogram R wave trigger. Thus, the time taken by the ventricles to eject 25% of their SV's was calculated by subtracting 8 ms from the time after the R wave trigger taken by the ventricles to eject 25% of their SV's. In a similar way, since the ventricles were found to reach their end-systole at approximately 99 ms, the exact time periods

taken by the ventricles to be filled with 25% of their DFV's were calculated by subtracting 99 ms from the time after the R wave trigger taken by the ventricles to be filled by 25% of their DFV's. Finally, an estimate for the rates of ejection during early systole and filling during early diastole was obtained by dividing the 25% SV by the exact time taken by the each ventricle to eject 25% of its SV or to be filled with 25% of its DFV respectively.

Table 11.2 confirms the presence of right ventricular systolic and diastolic abnormalities in the SHR rats. Thus both the 25% systolic ejection and the 25% diastolic filling times were increased in the SHR compared with WKY rats. These corresponded to reduced rates of initial systolic contraction and diastolic filling.

11.3.7 dV/dt through the cardiac cycle

To obtain further insights into right ventricular dynamics through the cardiac cycle in the four study groups, the right ventricular volume changes with respect to time (dV/dt) through systole and diastole were calculated for all the experimental rats using their time-related endocardial volume curves. The gradients of the 11 lines joining the studied twelve time-points were calculated using the MRI-derived endocardial volume curves and were taken to represent the right ventricular dV/dt throughout the cardiac cycle. Figure 11.9 displays the right ventricular dV/dt of the four experimental groups.

Although the MRI-derived time-related volume curves of the 8-week and 12-week SHR appeared to have similar shapes to those of the normal rats, careful inspection of Figure 11.9 reveals that right ventricles of the two SHR groups had significantly smaller volume changes with respect to time especially during early systole and early diastole when compared with the systolic and diastolic dV/dt of the 2 normal WKY groups.

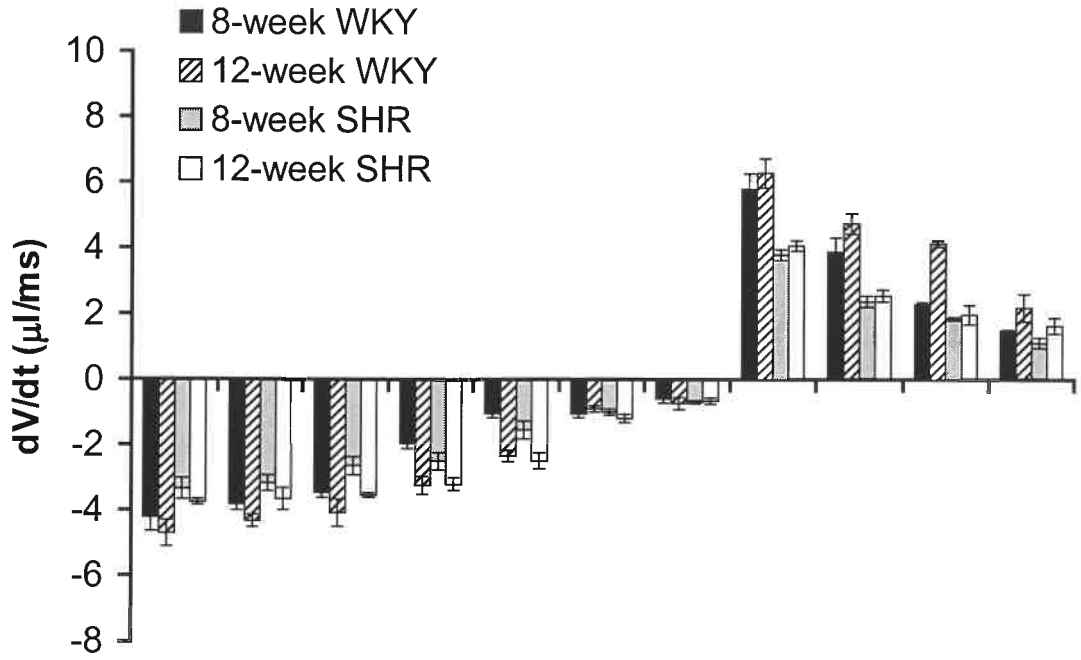

Figure 11.9: **Right ventricular dV/dt.** Block diagram displaying right ventricular (RV) volume changes with respect to time during the 12 studied time points through the cardiac cycle obtained from obtained the normal 8-week WKY group, the normal 12-week WKY group, the 8-week SHR group, and the 12-week SHR group (see legend to Figure 11.6). Data points derived from obtaining the slopes between adjacent points in the right ventricular (RV) volume curves obtained from individual groups themselves summarized in Figure 11.6. Each bar represents the average dV/dt ± SEM between 2 consecutive time points through the cardiac cycle. Negative dV/dt's represent contraction of the cardiac walls during systole and positive dV/dt's represent their relaxation. The bar 1 represents dV/dt between the 1st and 2nd studied time points during the cardiac cycle with the first point timed typically 8 ms after the trigger pulse from the electrocardiographic R wave and 21 ms for the second point. Points 2 to 11 represent dV/dts between volume points successively obtained 21, 34, 47, 60, 73, 86, 99, 112, 125, 138, and 151 ms following the R wave.

11.4 Discussion and conclusions

This report describes the first investigation of changes in right ventricular structure and function in an animal system for systemic hypertension using MRI.

Magnetic resonance imaging provides an effective and non-invasive physiological tool to study ventricular function and myocardial volume in the right ventricle in both normal and spontaneously hypertensive rats. The latter provide the most extensively used laboratory animal models for essential hypertension. In particular, the systemic hypertension developing in the SHR strain appears to be similar in several aspects to the essential hypertension in humans (Trippodo and Frohlich, 1981). Previous studies have used MRI primarily for anatomical cardiac imaging but it has more recently become an established and invaluable physiological tool for the assessment of the dynamic and functional changes that occur in the heart throughout the cardiac cycle (Wise et al., 1998). In the present study, MRI provided consistent measurements of right ventricular myocardial and cavity volumes. This led to a quantitative evaluation of right ventricular myocardial volume and the corresponding changes in contractility and relaxation throughout the cardiac cycle.

The application of MRI to the quantitative evaluations of right ventricular structure and function made it possible to detect subtle morphological and physiological changes of the right ventricle of the hypertensive rats for the first time and should lead to its application as an investigative tool for evaluating similar right ventricular alterations in patients with hypertensive heart disease.

We report for the first time a significant right ventricular hypertrophy in SHR rats as reflected in increases in right ventricular myocardial volumes whether expressed as absolute values, or normalized to the corresponding body weights when these were compared with their sex and age matched WKY groups.

The SHR rats additionally showed right ventricular systolic abnormalities as evidenced by their higher right ventricular ESV's and their lower right ventricular EF's when compared with their age matched WKY rats. Furthermore, right ventricular systolic abnormalities in the SHR rats were also confirmed by the longer time periods required by their right ventricles to pump 25% of their SV's and the abnormally slower rate of early systolic pumping when compared with their age matched WKY rats.

The two SHR groups also showed right ventricular diastolic abnormalities indicated by the longer time periods required by their right ventricles to be filled with 25 % of their DFV's and the much slower rate of early diastolic filling.

Further work may examine the pathogenesis of the right ventricular hypertrophy in SHR rats particularly since the pulmonary circulation pressure would be expected to be significantly lower than the one in the systemic circulation. However, Aharinejad et al. (1996) reported histological evidence that SHR rats develop pulmonary hypertension. If this is so, it may be reasonable to suggest that the right ventricle hypertrophies in response to the elevated pulmonary pressure.

Parameter	WKY		SHR		Two-Way ANOVA		
	8-week (n = 4)	12-week (n = 4)	8-week (n = 4)	12-week (n = 4)	*P*-value for the effect of age	*P*-value for the effect of HS	*P*-value for the interaction (SH * age)
Body weight (BW) (g)	214 ± 9	284 ± 13	246 ± 9	307 ± 13	0.004	0.755	0.044
RV myocardial volume by MRI (RVMV) (μl)	146.8 ± 10.2	176.5 ± 10.3	220 ± 7.1	239.5 ± 16.0	0.044	<0.001	NS
RVMV/BW (μl g^{-1})	0.68 ± 0.02	0.62 ± 0.02	0.90 ± 0.06	0.78 ± 0.05	0.032	<0.001	NS
End-diastolic volume (μl)	315.0 ± 6.5	445.0 ± 24.0	402.3 ± 15.7	476.3 ± 16.0	<0.001	0.006	NS
End-systolic volume (μl)	104.8 ± 12.0	181 ± 17.7	209 ± 8.3	236.3 ± 7.5	0.002	<0.001	NS
Ejection fraction	0.67 ± 0.03	0.60 ± 0.02	0.48 ± 0.03	0.50 ± 0.01	0.384	<0.001	NS
Systolic blood pressure (mmHg)	151 ± 4	150 ± 2	177 ± 10	216 ± 7	0.012	<0.001	0.009
Heart rate (beats min^{-1})	326 ± 19	319 ± 13	296 ± 3	292 ± 12	0.680	0.041	NS

Table 11.1: **General features and major cardiac parameters for the 8- and 12-week WKY and SHR groups.** Data are presented for each age group separately. The right ventricular (RV) myocardial volume measured by MRI, for each individual rat, was taken from the average value from all the time-points sampled in the cardiac cycle. The functional right ventricular parameters were established from the transverse cardiac sections.

All values expressed as mean ± standard error of the mean (SEM). Two-way analysis of variance (ANOVA) was used in comparison of the 8- and 12-week WKY and the SHR groups. A value of $p<0.05$ was considered statistically significant. SH represents spontaneous hypertension and NS represents not significant. When the interaction between SH and age was not significant, the analysis was rerun eliminating the interaction term from the model.

Parameter	WKY		SHR		Two-Way ANOVA		
	8-week (n = 4)	12-week (n = 4)	8-week (n = 4)	12-week (n = 4)	*P*-value for the effect of age	*P*-value for the effect of HS	*P*-value for the interaction (SH * age)
25 % SV and DFV (μl)	52.6 ± 1.8	66.0 ± 1.7	48.3 ± 4.3	60.0 ± 2.6	0.001	0.088	NS
Time for 25 % SV (ms) after the R wave trigger	20.6 ± 1	22.1 ± 0.8	22.6 ± 0.7	24.7 ± 0.3	0.026	0.007	NS
Time for 25 % DFV (ms) after the R wave trigger	108.3 ± 0.7	109.9 ± 0.8	111.9 ± 0.8	114.7 ± 0.8	0.014	<0.001	NS
Time for 25 % SV (ms)	12.6 ± 1	14.1 ± 0.8	14.6 ± 0.7	16.7 ± 0.3	0.026	0.007	NS
Time for 25 % DFV (ms)	9.3 ± 0.7	10.9 ± 0.8	12.9 ±0.8	15.7 ± 0.8	0.014	<0.001	NS
Rate of ejection during early systole (μl/ms)	4.3 ± 0.39	4.8 ± 0.38	3.3 ± 0.32	3.6 ± 0.18	0.252	0.006	NS
Rate of filling during early diastole (μl/ms)	5.8 ± 0.47	6.2 ± 0.52	3.7 ± 0.10	3.8 ± 0.16	0.491	<0.001	NS

Table 11.2: **Indices for the kinetics of right ventricular contraction and relaxation.** Data are presented for each age group separately.

All values expressed as mean ± standard error of the mean (SEM). Two-way analysis of variance (ANOVA) was used in comparison of the 8- and 12-week WKY and the SHR groups. A value of $p<0.05$ was considered statistically significant.

SH represents spontaneous hypertension and NS represents not significant. When the interaction between SH and age was not significant, the analysis was rerun eliminating the interaction term from the model.

CHAPTER 12
RECAPITULATION

12.1 Experimental designs and cardiac MRI

The experiments described in the previous chapters introduced MRI to characterize structural and functional changes in the left and right ventricles associated with diabetic cardiomyopathy for the first time. They followed left and right ventricular contraction and relaxation through the cardiac cycle in normal as well as diabetic hearts and evaluated the therapeutic effects of the angiotensin-converting enzyme inhibitor captopril upon the structural and physiological abnormalities associated with diabetic cardiomyopathy. The final experiments completed earlier studies by characterizing structural and physiological properties in the right ventricle of spontaneously hypertensive rats (SHR).

The studies reflect an increasing interest in the use of animal models to evaluate cardiac pathology in diabetes mellitus and hypertension. Thus, the streptozotocin-induced diabetic (STZ-diabetic) rat is frequently used to study the long-term cardiac complications of diabetes (Warley et al., 1995). Similarly, the spontaneously hypertensive rats (SHR) is now a well-accepted model for the study of the long-term cardiac complications of hypertension (Trippodo and Frohlich, 1981). Animal models make it possible to follow chronic pathology over manageable time scales particularly when combined with the use of non-invasive techniques in the intact animal as opposed to the sole use of more invasive physiological measurements.

Magnetic resonance imaging offers image information to sub-millimetre resolution and has been widely accepted as a clinical investigative technique that can also provide information about biological structure as well as function. Recent developments in magnetic resonance techniques for cardiac imaging have made MRI a feasible and an attractive tool for cardiovascular physiology. (Stratemeier et al., 1986; Markiewicz et al., 1987; Sechtem et al., 1987; Semelka et al., 1990). In particular, MRI offers a high degree of soft tissue contrast attributable to the large differences in the T1 and T2 relaxation times of myocardium, epicardial fat and blood resulting in large differences in signal intensity. This permits successive acquisition of high quality

images without the need for administering contrast media required in conventional or cine x-ray computed tomography. These features made MRI a potentially valuable tool for examining both early and late cardiac physiological changes in diabetic and hypertensive rats. In addition, dynamic or cine magnetic resonance imaging with electrocardiographic gating ensures that data is acquired at similar time-points in the cardiac cycle over many successive cardiac cycles. This provides the basis for characterizing dynamic changes in the human and rat hearts with good time resolution. Thus, the MRI techniques applied to the animal models may prove useful for human MRI studies.

The MRI studies of the diabetic heart studied a total of twenty male Wistar rats randomly subdivided into five equal groups in which experimental diabetes was induced in four by a single streptozotocin (STZ) injection (Warley et al., 1995; Rodrigues et al., 1997). The diabetes was induced at the age of 7 weeks in two groups and at 10 and 13 weeks in the remaining two groups leaving the fifth as a control. The animals of one of the experimental groups with diabetes induced at the age of 7 weeks were maintained on captopril-containing drinking water at a concentration of 2 g/l immediately after the induction of diabetes. As all animals were scanned at the age of 16 weeks, the experimental protocol effectively examined the effects of 9, 6 and 3 weeks of diabetes against a single control group. The magnetic resonance imaging studies provided images of both ventricles at twelve time-points through the cardiac cycle covering systole and most of diastole. The analysis provided a full range of anatomical and functional indices, namely myocardial volume, end-diastolic volume (EDV), end-systolic volume (ESV), stroke volume (SV), and ejection fraction (EF) of both ventricles. They also characterized the kinetics of left and right ventricular contraction and relaxation. Further, the changes in the derived left and right ventricular volumes with time (dV/dt) were plotted at the studied twelve time-points through the cardiac cycle. The myocardial volumes, functional indices and kinetics of the left ventricles were compared with those of the corresponding right ventricles in each experimental group in addition to the comparisons of values for the four diabetic groups with those of the control group. The present studies validated the left and right ventricular myocardial volumes as derived from MRI by comparing these with the corresponding values obtained by conventional gravimetric measurements. Accordingly, all animals were sacrificed immediately after scanning and their hearts were removed and put in 3.7% phosphate buffered formaldehyde. The right and left ventricular muscles were then separated from each other and weighed.

MRI provided self-consistent data sets in agreement with post-mortem results. Thus, the derived myocardial volumes of both ventricles was conserved through all the twelve time-points

through the cardiac cycle in both test and control groups. Furthermore, myocardial densities calculated by dividing the post-mortem weight of either ventricle by such myocardial volumes agreed through all experimental groups and with previous reports. The MRI studies demonstrated significant relative left and right ventricular hypertrophy associated with diastolic and systolic functional abnormalities developed between 3 and 6 weeks of diabetes and deteriorated further between 6 and 9 weeks. The hypertrophy and the associated functional deterioration deteriorated most markedly between 3 and 6 in the left ventricle but between 6 and 9 weeks in the right ventricle. Finally, captopril treatment immediately after the induction of diabetes prevented the development of the relative hypertrophy in both ventricles and markedly relieved the diastolic and systolic abnormalities.

MRI was also used to study and characterize the anatomical and physiological parameters of the left ventricle of the SHR rats (Wise et al., 1998). The SHR rats show some histological features of pulmonary hypertension (Aharinejad et al., 1996). However, there has been no detailed MRI study of the physiological changes in the right ventricle of the SHR rats. The present MRI study characterized the changes in structural and functional properties including the kinetics of contraction and relaxation of the right ventricle through the cardiac cycle. The experiments involved 8 SHR and 8 normotensive control Wistar-Kyoto rats (WKY) subdivided into two age matched 8 and 12 weeks old groups. The right ventricles were imaged at twelve time-points through the cardiac cycle. Right ventricular myocardial volume, EDV, ESV, SV, and EF were the derived from the image data. Right ventricular volume changes with time and the dV/dt at each time-point were also calculated. The MRI results demonstrated a hypertrophy in the right ventricles of SHR rats and these are associated with diastolic and systolic dysfunction.

12.2 Importance of the cardiac complications of diabetes and hypertension

The increased morbidity and mortality among diabetics largely reflects its cardiovascular complications (Crall and Roberts, 1978; Kannel, 1985). The Framingham study reported a substantial increase in the incidence of coronary artery disease in diabetics compared with non-diabetic controls (Kannel and McGee, 1979). Diabetics also show a higher mortality following acute myocardial infarction. This may reflect the higher incidence of congestive cardiac failure and cardiogenic shock following such infarction (Kereiakes, 1985). In addition, poor glycaemic control (Oswald et al., 1984), diabetic ketoacidosis (Husband et al., 1985), high fatty acid levels that might predispose to the development of post-infarction arrhythmias (Oliver et al., 1968),

and the increased incidence of anterior myocardial infarction (Weitzman et al., 1982), which involves more heart muscle and therefore more seriously impairs ventricular function may all contribute to the higher mortality after acute myocardial infarction in diabetics.

Diabetes also appears to be associated with myocardial changes leading to a pathological condition termed diabetic cardiomyopathy (Goodwin and Oakley, 1972; Rubler et al., 1972; Hamby et al., 1974). The Framingham study reported a higher incidence of congestive heart failure in diabetics that could not be completely accounted for by the high incidence of coronary atherosclerosis, hypertension, or cardiac autonomic neuropathy (Kannel et al., 1974).

The cause of diabetic cardiomyopathy has been the subject of considerable discussion. The vascular theory implicates small vessel abnormalities of the coronary microcirculation (Blumenthal, 1960; Ledet, 1968, 1976; Rubler et al., 1972; Hamby et al., 1974; Seneviratne, 1977; Sanderson et al., 1978; Zoneraich et al., 1980). Thus, endothelial cell proliferation, sub-endothelial fibrosis, deposition of periodic acid-Schiff-positive (PAS-positive) material, narrowing of vessel lumens, and thickening vessel walls are common pathological changes seen in the small intramural vessels of diabetics. Capillary basal laminar thickening was also reported in diabetics (Vracko and Benditt, 1970; Williamson and Kilo, 1976; Fischer et al., 1979). Furthermore, diabetic myocardium shows arteriolar and capillary microaneurysms (Factor et al., 1980). Cardiac dysfunction in diabetes has also been attributed to abnormalities of the cardiac fibres themselves, which might arise from uncontrolled hyperglycaemia (Shapiro et al., 1980, 1981a; Uusitupa et al., 1983), changes in myocardial fatty acid metabolism leading to triglyceride accumulation in the myocardium (Paulson and Crass, 1980), changes in calcium handling (Ganguly et al., 1983; Dhalla et al., 1998), or finally a primary hypertrophy of the myocytes themselves (Rubler et al., 1972; Fischer et al.,1979).

Extensive fibrosis due collagen accumulation has also been reported in diabetic hearts; this could explain some of the functional cardiac abnormalities seen in diabetes (Rubler et al., 1972; Regan, 1981).

A growing body of evidence implicates angiotensin II in the pathogenesis of diabetic cardiomyopathy by inducing myocardial interstitial fibrosis caused by proliferation of fibroblasts in the wall of the heart (Schorb et al., 1993), possibly through an intracardiac renin-angiotensin system (Dostal et al., 1992a, b), which is activated in diabetes leading to an enhanced production of angiotensin II (Rösen et al., 1995). It was also reported that streptozotocin diabetic rats have higher levels of angiotensin converting enzyme (ACE) in their

left ventricular tissue and a decrease in left ventricular function, which was prevented by treatment with the angiotensin converting enzyme inhibitor enalapril (Goyal et al., 1998).

Such possible changes in cardiac function in diabetes have been studied in both animal and human systems. However, thus far no single technique has characterized all the anatomical and functional indices of the myocardium in diabetes particularly in the intact heart. Furthermore, studies performed so far focused on the left ventricle and there are no detailed reports concerning the right ventricle in diabetes. Finally, independent investigators report conflicting results. Experimental animal studies included haemodynamic studies of dogs made mildly diabetic for 11 months with alloxan, which revealed abnormally high left ventricular wall stiffness and end-diastolic pressures (Regan et al., 1974). Isolated perfused hearts from diabetic rats demonstrated decreased peak systolic pressures (Miller, 1979). Isolated papillary ventricular muscles from diabetic rats showed a delayed onset and a slower rate of relaxation, depressed shortening velocity (Fein et al., 1980), increased time to peak tension and decreased sensitivity to increased concentrations of calcium and adrenaline (Warley et al., 1995).

Studies in humans involving both invasive and non-invasive techniques have revealed contradictory results. There have been reports of both normal (Airaksinen et al., 1984b), and also abnormal systolic time intervals (Ahmed et al., 1975; Seneviratne, 1977; Shapiro et al., 1980, 1981a, b; Cellina et al., 1983; Jermendy et al., 1984; Uusitupa et al., 1985) among diabetics. Echocardiographic studies have variously described reduced (Airaksinen et al., 1984a, 1987), or normal or modest increases (Shapiro et al., 1981a; Friedman et al., 1982; Fisher et al., 1989) in left ventricular size in diabetics. Reported changes in the dynamics of cardiac cycle have included a prolonged isometric relaxation phase (Sanderson et al., 1978; Shapiro et al., 1980, 1981a; b; Shapiro 1982; Airaksinen et al., 1984a). Other reports have variously described a depressed (Shapiro et al., 1981a, b, Uusitupa et al., 1985), normal (Airaksinen et al., 1984b; Fisher et al., 1989), or even enhanced systolic function in insulin-dependent patients developing microvascular complications (Thuesen et al., 1988).

Radionuclide ventriculography studies have variously reported abnormal (Zola et al., 1986) or normal resting ejection fraction (Vered et al., 1984; Fisher et al., 1985, 1986; Arvan et al., 1988).

Systemic hypertension is a well-known major risk factor for coronary artery disease and heart failure (Kannel et al., 1972; Dustan et al., 1974; Frohlich, 1991). Most of the extensive literature on the cardiac complications of systemic hypertension have considered the anatomical,

electrical and kinetic properties of the left ventricular myocardium (Grossman, 1980; Frohlich, 1991). Thus, left ventricular hypertrophy follows the pressure overload of an elevated systemic vascular resistance (Frohlich, 1983, 1991) and may be viewed as an adaptive physiological process. However, left ventricular hypertrophy increases the risk of ischaemic myocardial injury, myocardial infarction and ventricular arrhythmias (Messerli et al., 1984; Frohlich, 1991). Aharinejad et al. (1996) reported that the SHR rats develop pulmonary hypertension. However, there has been little investigation on the structural and functional properties of the right ventricle in spontaneously hypertensive rats (SHR).

BIBLIOGRAPHY

Aharinejad S, Schraufnagel DE, Böck P, MacKay CA, Larson EK, Miksovsky A, Marks SC Jr. Spontaneously hypertensive rats develop pulmonary hypertension and hypertrophy of pulmonary venous sphincters. *Am J Pathol.* 1996;**148**(1):281-290.

Ahmed SS, Jaferi GA, Narang RM, Regan TJ. Pre-clinical abnormalities of left ventricular function in diabetes mellitus. *Am Heart J.* 1975;**89**(2):153-158.

Airaksinen KEJ, Ikäheimo M, Kaila J, Linnaluoto M, Takkumen J. Impaired left ventricular filling in young female diabetics. An echocardiographic study. *Acta Med Scand.* 1984;**216**(5):509-516.

Airaksinen KEJ, Ikäheimo M, Kaila J, Linnaluoto M, Takkunen J. Systolic time intervals and the QT-QS2 interval in young female diabetics. *Ann Clin Res.*1984;**16**(4):188-191.

Airaksinen KEJ, Ikäheimo MJ, Linnaluoto MK, Huikuri HV, Takkumen JT. Increased left atrial size relative to left ventricular size in young women with insulin dependent diabetes: a pre-clinical sign of the specific heart disease of diabetes? *Diabetes Res.* 1987;**6**(1):37-41.

Arvan S, Signal K, Knapp R, Vagnucci A. Subclinical left ventricular abnormalities in young diabetics. *Chest.* 1988;**93**(5):1031-1034.

Barnes AJ, Locke P, Scudder PR, Dormandy TL, Dormandy JA, Slack J. Is hyperviscosity a treatable component of diabetic microcirculatory disease? *Lancet.* 1977;**2**(8042):789-791.

Barzilay J, Warram JH, Rand LI, Pfeifer MA, Krolewski AS. Risk for cardiovascular autonomic neuropathy is associated with the HLA-DR3/4 phenotype in type 1 diabetes mellitus. *Ann Intern Med.* 1992;**116**(7):544-549.

Bell DS. Diabetic cardiomyopathy. A unique entity or a complication of coronary artery disease? *Diabetes Care.*1995;**18**(5):708-714.

Blumenthal HT, Alex M, Goldenberg S. A study of lesions of intramural coronary artery branches in diabetes mellitus. *Arch Pathol.* 1960;**70**:13-28.

Brown MA, Semelka RC. *MRI: Basic Principles and applications.* New York, Chichester, Brisbane, Toronto, Singapore: Wiley-Liss, Inc., 1995.

Cellina G, Lo Cicero G, Brina A, Zanchetti A. Reversible alteration of myocardial function in gestational diabetes. *Eur Heart J.* 1983;**4**(1):59-63.

Clark RS, English M, McNeill GP, Newton RW. Effect of intravenous infusion of insulin in diabetics with acute myocardial infraction. *Br Med J.* 1985;**291**(6491):303-305.

Cohn JN, Levine TB. Angiotensin-converting enzyme inhibition in congestive heart failure: the concept. *Am J Cardiol.* 1982;**49**(6):1480-1483.

Crall FV Jr, Roberts WC. The extramural and intramural coronary arteries in juvenile diabetes mellitus. Analysis of nine necropsy patients aged 19 to 38 years with onset of diabetes before age 15 years. *Am J Med.* 1978;**64**(2):221-230.

Crooks LE, Barker B, Chang H, Feinberg D, Hoenninger JC, Watts JC, Arakawa M, Kaufman L, Sheldon PE, Botvinick E, Higgins CB. Magnetic resonance imaging strategies for heart studies. *Radiology.* 1984;**153**(2):459-465.

Crowley JJ, Huang CL, Gates AR, Basu A, Shapiro LM, Carpenter TA, Hall LD. A quantitative description of dynamic left ventricular geometry in anaesthetized rats using magnetic resonance imaging. *Exp Physiol.* 1997;**82**(5):887-904.

D'Elia JA, Weinrauch LA, Healy RW, Libertino JA, Bradley RF, Leland OS Jr. Myocardial dysfunction without coronary artery disease in diabetic renal failure. *Am J Cardiol.* 1979;**43**(2):193-199.

Dhalla NS, Panagia V, Makino N, Beamish RE. Sarcolemmal Na^{+}-Ca^{2+} exchange and Ca^{2+}-pump activities in cardiomyopathies due to intracellular Ca^{2+}-overload. *Mol Cell Biochem.* 1998;**82**(1-2):75-79.

Dostal DE, Rothblum KN, Chernin MI, Cooper GR, Baker KM. Intracardiac detection of angiotensinogen and renin: a localized renin-angiotensin system in neonatal rat heart. *Am J Physiol.* 1992;**263**(4 Pt 1):C838-C850.

Dostal DE, Rothblum KN, Conrad KM, Cooper GR, Baker KM. Detection of angiotensin I and II in cultured rat cardiac myocytes and fibroblasts. *Am J Physiol.* 1992;**263**(4 Pt 1):C851-C863.

Dunn FG, Oigman W, Ventura HO, Messerli FH, Kobrin I, Frohlich ED. Enalapril improves systemic and renal hemodynamics and allows regression of left ventricular mass in essential hypertension. *Am J Cardiol.* 1984;**53**(1):105-108.

Dustan HP. George Lyman Duff Memorial Lecture. Atherogenesis complicating chronic hypertension. *Circulation.* 1974;**50**(5):871-879.

Edelman RR, Zlakkin MB, Hesselink JR. *Clinical Magnetic Resonance Imaging.* Philadelphia, London, Toronto, Montreal, Sydney, Tokyo: W. B. Saunders, 1996.

English PT, Moore C. *MRI for Radiographers.* Berlin, Heidelberg, New York, Barcelona, Budapest, Hong Kong, London, Milan, Paris, Tokyo: Springer, 1995.

Ewing DJ, Clarke BF. Autonomic neuropathy: its diagnosis and prognosis. *J Clin Endocrinol Metab.* 1986;**15**(4):855-888.

Factor SM, Bhan R, Minase T, Wolinsky H, Sonnenblick EH. Hypertensive-diabetic cardiomyopathy in the rat: an experimental model of human disease. *Am J Pathol.* 1981;**102**(2):219-228.

Factor SM, Okun EM, Minase T. Capillary microaneurysm in the human diabetic heart. *N Engl J Med,*.1980;**302**(7):384-388.

Farr RF, Allisy-Roberts PJ. *Physics for Medical Imaging.* Philadelphia, London, Toronto, Montreal, Sydney, Tokyo: W. B. Saunders, 1996.

Fein FS, Kornstein LB, Strobeck JE, Capasso JM, Sonnenblick EH. Altered myocardial mechanics in diabetes. *Circ Res.* 1980;**47**(6):922-933.

Fein FS, Strobeck JE, Malhotra A, Scheuer J, Sonnenblick EH. Reversibility of diabetic cardiomyopathy with insulin treatment in rats. *Circ Res.* 1981;**49**(6):1251-1261.

Felner JM, Blumenstein BA, Schlant RC, Carter AD, Alimurung BN, Johnson MJ, Sherman SW, Klicpera MW, Kutner MH, Drucker LW Sources of variability in echocardiographic measurements. *Am J Cardiol.* 1980; **45**(5):995-1004.

Fischer VW, Barner HB, Leskiw ML. Capillary basal laminar thichness in diabetic human myocardium. *Diabetes.* 1979;**28**(8):713-719.

Fisher BM, Cleland JGF, Dargie HJ, Frier BM. Non-invasive evaluation of cardiac function in young patients with type 1 diabetes. *Diabet Med.* 1989;**6**(8):677-681.

Fisher BM, Gillen G, Lindop GBM, Dargie HJ, Frier BM. Cardiac function and coronary arteriography in asymptomatic type 1 (insulin-dependent) diabetic pateints: evidence for a specific heart disease. *Diabetologia.* 1986;**29**(10):706-712.

Fisher BM, Gillen G, Ong Tone L, Dargie HJ, Frier BM. Cardiac function and insulin-dependent diabetes: radionuclide ventriculography in young diabetics. *Diabet Med.* 1985;**2**(4): 251-256.

Friedman NE, Levitsky LL, Edidin DV, Vitullo DA, Lacina SJ, Chiemmongkolti P. Echocardiographic evidence for impaired myocardial performance in children with type 1diabetes mellitus. *Am J Med.* 1982;**73**(6):846-850.

Frohlich ED. The heart in hypertension: a 1991 overview. *Hypertension.* 1991;**18**(5 suppl III):62-68.

Frohlich ED. Mechanisms contributing to high blood pressure. *Ann Intern Med.* 1983;**98**(5 Pt 2):709-714.

Ganguly PK, Pierce GN, Dhalla KS, Dhalla NS. Defective sarcoplasmic reticular calcium transport in diabetic cardiomyopathy. *Am J Physiol.* 1983;**244**(6):E528-E535.

Goodwin JF, Oakley CM. The cardiomyopathies. *Br Heart J.* 1972;**34**(6):545-552.

Goyal RK, Satia MC, Bangaru RA, Gandhi TP. Effect of long-term treatment with enalapril in streptozotocin diabetic and DOCA hypertensive rats. *J Cardiovasc Pharmacol,* 1998;**32**(2):317-322.

Grossman W. Cardiac hypertrophy: Useful adaptation or pathophysiologic process? *Am J Med.* 1980;**69**(4):576-584.

Hamby RI, Zoneraich S, Sherman S. Diabetic cardiomyopthay. *JAMA.*1974;**229**(13):1749-1754.

Hanseen KF, Dahl-Jørgensen K, Lauritzen T, Field-Rasmussen B, Brinchmann Hansen O, Deckert T. Diabetic control and microvascular complications: the near normoglycemic experience. *Diabetologia.* 1986;**29**(10):677-684.

Heickendorff L, Ledet T, Rasmussen LM. Glycosaminoglycans in the human aorta in diabetes mellitus: a study of tunica media from areas with and without atherosclerotic plaque. *Diabetologia.* 1994;**37**(3):286-392.

Herfkens RJ, Higgins CB, Hricak H, Lipton MJ, Crooks LE, Lanzer P, Botvinick E, Brundage B, Sheldon PE, Kaufman L. Nuclear magnetic resonance imaging of the cardiovascular system: normal and pathologic findings. *Radiology.* 1983;**147**(3):749-759.

Hicks KK, Seifen E, Stimers JR, Kennedy RH. Effects of streptozotocin-induced diabetes on heart rate, blood pressure and cardiac autonomic nervous control. *J Auton Nerv Syst.* 1998;**69**(1):21-30.

Higgins CB, Hricak H, Helms CA. *Magnetic Resonance Imaging of the Body.* Philadelphia, New York: Lippincott-Raven, 1997.

Higgins CB. Overview of MR of the heart. *AJR Am J Roentgenol.* 1986;**146**(5):907-918.

Husband DJ, Alberti KGMM, Julian DG. Methods for the controal of diabetes after acute myocardial infraction. *Diabetes care.* 1985;**8**(3):261-267.

Jaffe AS, Spadaro JJ, Schechtman K, Roberts R, Geltman EM, Sobel BE. Increased congestive heart failure after myocardial infraction of modest extent in patients with diabetes mellitus. *Am Heart J.* 1984;**108**(1):31-37.

Jarrett J. Diabetes and heart: coronary heart disease. *Clin Endocrinol Metab.*1977;**6**(2):389-402.

Jauch KW, Hartl W, Guenther B, Wicklmayr M, Rett K, Dietze G. Captopril enhances insulin responsiveness of forearm muscle tissue in non-insulin-dependent diabetes mellitus. *Eur J Clin Invest.* 1987;**17**(5):448-454.

Jermendy G, Koltai ZM, Kammerer L, Cserhalmi L, Istvánffy M, Szelényi J, Pogátsa G. Myocardial systolic alterations of insulin-dependent diabetics in rest. *Act Cardiol.* 1984;**39**(3):185-190.

Kannel WB, Castelli WB, Mc Namara PM, Mc Kee PA, Feinleib M. Role of blood pressure in the development of heart failure. The Framingham study. *N Engl J Med.*. 1972;**287**(16):781-787.

Kannel WB, Hjotland M, Castelli WP. Role of diabetes in congestive heart failure: the Framingham study. *Am J Cardiol.* 1974;**34**(1):29-34.

Kannel WB, McGee DL. Diabetes and cardiovascular disease. The Framingham study. *JAMA.* 1979;**241**(19):2035-2038.

Kannel WB. Lipids, diabetes, and coronary heart disease: insights from the Framingham Study. *Am Heart J.* 1985;**110**(5):1100-1107.

Katz AM. *Physiology of the heart, 2nd ed.* 1185 Avenue of the Americas, New York, New York 10036: Raven Press Ltd., 1992.

Kereiakes DJ. Myocardial infarction in the diabetic patient. *Clin Cardiol.* 1985;**8**(8):446-450.

Lababidi ZA, Goldstein DE. High prevalence of echocardiographic abnormalities in diabetic youth. *Diabetes Care.* 1983;**6**(1):18-22.

Ledet T. Histological and histochemical changes in the coronary arteries of old diabetic patients. *Diabetologia.* 1968;**4**(5):268-272.

Ledet T. Diabetic cardiopathy. Quantitative histological studies of the heart from young juvenile diabetics. *Acta Pathol Microbiol Scand (A).* 1976;**84**(5):421-428.

Lemp GF, Vander Zwaag R, Hughes JP, Maddock V, Kroetz F, Ramanathan KB, Mirvis DM, Sullivan JM. Association between the severity of diabetes mellitus and coronary arterial atherosclerosis. *Am J Cardiol.* 1987;**60**(13):1015-1019.

Maeda CY, Fernandes TG, Lulhier F, Irigoyen MC. Sterptozotocin daiabetes modifies arterial pressure and baroreflex sensitivity in rats. *Brazilian Journal of Medical and Biological research.* 1995;**28**(4):497-501.

Margolis JR, Kannel WS, Feinleib M, Dawber TR, McNamara PM. Clinical features of unrecognized myocardial infarction-silent and symptomatic. Eighteen years follow-up: The Framingham Study. *Am J Cardiol.* 1973;**32**(1):1-7.

Markiewicz W, Sechtem U, Higgins CB. Evaluation of the right ventricle by magnetic resonance imaging. *Am Heart J.* 1987;**113**(1):8-15.

Messerli FH, Ventura HO, Elizardi DJ, Dunn FG, Frohlich ED. Hypertension and sudden death: Increased ventricular ectopic activity in left ventricular hypertrophy. *Am J Med.* 1984;**77**(1):18-22.

Miller TB Jr. Cardiac performance in isolated perfused hearts from alloxan diabetic rats. *Am J Physiol.* 1979;**230**(6):H808-H812.

Neil HA, Thompson AV, John S, McCarthy ST Mann JI. Diabetic autonomic neuropathy: the prevalence of impaired heart rate variability in a geographically defined population. *Diabet Med.* 1989;**6**(1):20-24.

Nesto RW, Phillips RT, Ket KG, Hill T, Perper E, Young E, and Leland OS Jr. Angina and exertional myocardial ischemia in diabetic and nondiabetic patients: Assessment by exercise thallium scintigraphy. *Ann Intern Med.* 1988;**108**(2):170-175.

Nesto RW, Watson FS, Knowalchuk GJ, Zarich SW, Hill T, Lewis SM, Lane SE. Silent myocardial ischemia and infarction in diabetics with peripheral vascular disease: assessment by dipyridamole thallium-201 scintigraphy. *Am Heart J.* 1990;**120**(5):1073-1077.

Newhouse JH, Wiener JI. *Understanding MRI.* Boston, Toronto, London: Little, Brown and Company, 1991.

Oliver MF, Kurien VA, Greenwood TW. Relation between serum-free-fatty-acids and arrhythmias and death after acute myocardial infraction. *Lancet.* 1968;**1**(7545):710-714.

Orlander PR, Goff DC, Morrissey M, Ramsey DJ, Wear ML, Labarthe DR, Nichaman MZ.The relation of diabetes to the severity of acute myocardial infarction and post-myocardial infarction survival in Mexican-Americans and non-Hispanic whites. The Corpus Christi Heart Project. *Diabetes.* 1994;**43**(7):897-902.

Oswald GA, Corcoran S, Yudkin JS. Prevalence and risks of hyperglycemia and undiagnosed diabetes in patients with acute myocardial infraction. *Lancet.* 1984;**1**(8389):1264-1267.

Paulson DJ, Crass MF.Myocardial triacylglycerol fatty acid composition in diabetes mellitus. *Life Sci.* 1980;**27**(23):2237-2243.

Regan TJ, Ettinger PO, Khan MI, Jesrani MU, Lyons MM, Oldewurtel HA, Weber M. Alterated myocardial function and metabolism in chronic diabetes mellitus without ischemia in dogs. *Circ Res.* 1974;**35**:222-237.

Regan TJ, Wu CF, Yeh CK, Oldewurtel HA, Haider B. Myocardial composition and function in diabetes: the effect of chronic insulin use. *Circ Res.* 1981;**49**(6):1268-1277.

Rennert G, Saltz Rennert H, Wanderman K, Weitzman S. Size of acute myocardial infarcts in patients with diabetes mellitus. *Am J Cardiol.* 1985;**55**(13 Pt 1):1629-1630.

Rodrigues B, Cam MC, Kong J, Goyal RK, McNeill JH. Strain differences in susceptibility to streptozotocin-induced diabetes: Effects on hypertriglyceridemia and cardiomyopathy. *Cardiovasc Res.* 1997;**34**(1):199-205.

Rösen R, Rump AF, Rösen P. The ACE-inhibitor captopril improves myocardial perfusion in spontaneously diabetic (BB) rats. *Diabetologia.* 1995;**38**(5):509-517.

Rubler S, Dlugash J, Yuceoglu YZ, Kumral T, Branwood AW, Grisham A. New type of cardiomyopathy associated with diabetic glomerulosclerosis. *Am J Cardiol.* 1972;**30**(6):595-602.

Sanderson JE, Brown DJ, Rievellese A, Kohner E. Diabetic cardiomyopathy? An echocardiographic study of young diabetics. *Br Med J.* 1978;**1**(6110):404-407.

Savage DD, Drayer JI, Henry WL, Mathews EC Jr, Ware JH; Gardin JM, Cohen ER, Epstein SE, Laragh JH. Echocardiographic assessment of cardiac anatomy and function in hypertensive subjects. *Circulation.* 1979;**59**(4):623-632.

Schaffer SW, Tan BH, Wilson GL. Development of a cardiomyopathy in a model of non-insulin-dependent diabetes. *Am J Physiol.* 1985;**248**(2 Pt 2):H179-H185.

Schorb W, Booz GW, Dostal DE, Conrad KM, Chang KC, Baker KM: Angiotensin II is mitogenic in neonatal rat cardiac fibroblasts. *Circ Res.* 1993;**72**(6):1245-1254.

Schunkert H, Sadoshima J, Cornelius T, Kagaya Y, Weinberg EO, Izumo S, Riegger G, Lorell BH. Angiotensin II-induced growth responses in isolated adult rat hearts. Evidence for load-independent induction of cardiac protein synthesis by angiotensin II. *Circ Res.* 1995;**76**(3):489-497.

Schwartz CJ, Valente AJ, Spargue EA, Kelley JL, Cayatte AJ, Kerbacher JJ, Mowery J, Rozek MM. Pathogenesis of atherosclerotic lesion: implication for diabetes mellitus. *Diabetes Care.* 1992;**15**(9):1156-1167.

Sechtem U, Pflugfelder PW, Gould RG, Cassidy MM, Higgins CB. Measurement of right and left ventricular volumes in healthy individuals with cine MR imaging. *Radiology.* 1987;**163**(3): 697-702.

Semelka RC, Tomei E, Wagner S, Mayo J, Kondo C, Suzuki J, Caputo GR, Higgins CB. Normal left ventricular dimensions and function: interstudy reproducibility of measurements with cine MR imaging. *Radiology.* 1990;**174**(3 Pt 1):763-768.

Seneviratne BI. Diabetic cardiomyopathy: the preclinical phase. *Br Med J.* 1977;**1**(6074):1444-1446.

Shapiro LM, Howat AP, Calter MM. left ventricular function in diabetes mellitus. I: Methodology, and prevalence and spectrum of abnormalities. *Br Heart J.* 1981;**45**(2):122-128.

Shapiro LM, Howat AP, Calter MM. Left ventricular function in diabetes mellitus: II: Relation between clinical features and left ventricular function. *Br Heart J.* 1981;**45**(2):129-132.

Shapiro LM, Leatherdale BA, Coyne ME, Fletcher RF, Mackinnon J. Prospective study of heart disease in untreated maturity onset diabetics. *Br Heart J.* 1980;**44**(3):342-348.

Shapiro LM. Echocardiographic features of impaired ventricular function in diabetes mellitus. *Br Heart J.* 1982;**47**(5):439-444.

Smith JW, Buckels LJ, Carlson K, Marcus FI. Clinical characteristics and results of non-invasive tests in 60 diabetic patients after acute myocardial infarction. *Am J Med.* 1983;**75**(2): 217-224.

Solaro RJ, Briggs FN. Estimating the functional capabilities of sarcoplasmic reticulum in cardiac muscle. *Cir Res.* 1974;**34**(4):531-540.

Stehouwer CD, Lambert J, Donker AJ, van Hinsbergh VW. Endothelial dysfunction and pathogenesis of diabetic angiopathy. *Cardiovasc Res.* 1997;**34**(1):55-68.

Stone PH, Muller JE, Hartwell T; York BJ, Rutherford JD, Parker CB, Turi ZG, Strauss HW, Willerson JT, Robertson T, et al. The effect of diabetes mellitus on prognosis and serial left ventricular function after acute myocardial infarction: contribution of both coronary disease and diastolic left ventricular dysfunction to the adverse prognosis. The MILIS Study Group. *J Am Coll Cardiol.* 1989;**4**(1):49-57.

Stratemeier EJ, Thompson R, Brady TJ, Miller SW, Saini S, Wismer GL, Okada RD, Dinsmore RE. Ejection fraction determination by MR imaging: comparison with left ventricular angiography. *Radiology.* 1986;**158**(3):775-777.

Tan LB. Cardiac pumping capability and prognosis in heart failure. *Lancet.* 1986;**2**(8520): 1360-1363.

Thuesen L, Christiansen JS, Mogenson CE, Henningen P. Cardiac hyperfunction in insulin-dependent diabetic patients developing microvascular complications. *Diabetes.* 1988;**37**(7):851-856.

Trippodo NC, Frohlich ED. Similarities of genetic (spontaneous) hypertension. Man and rat. *Circ Res.* 1981;**48**(3):309-319.

Uusitupa M, Siitonen O, Aro A, Korhonen T, Pyörälä K. Effect of correction of hyperglycemia on left ventricular function in non-insulin-dependent (type 2) diabetics. *Act Med Scand.* 1983;**213**(5):363-368.

Uusitupa M, Siitonen O, Pyörälä K, Länsimies E. Left ventricular function in newly diagnosed non-insulin dependent (type 2) diabetes evaluated by systolic time intervals and echocardiography. *Acta Med Scand.* 1985;**217**(4):379-388.

Vered A, Battler A, Segal P, Liberman D, Yerushalmi Y, Berezin M, Neufeld HN. Exercise-induced left ventricular dysfunction in young men with a symptomatic diabetes mellitus (diabetic cardiomyopathy). *Am J Cardiol.* 1984;**54**(6):633-637.

Vracko R, Benditt EP. Capillary basal lamina thickening: its relationship to endothelial cell death and replacement. *J Cell Biol.* 1970;**47**(1):281-285.

Warley A, Powell JM, Skepper JN. Capillary surface area is reduced and tissue thickness from capillaries to myocytes is increased in the left ventricle of streptozotocin-diabetic rats. *Diabetologia* 1995;**38**(4):413-421.

Weir GC, Clara ET, Zmachinski CJ, Weir SB. Islet secretion in a new model for non-insulin-dependent diabetes. *Diabetes.*1981;**30**(7):590-595.

Weitzman S, Wagner GS, Heiss G, Haney TL, Slome C. Myocardial infarction site and mortality in diabetes. *Diabetes Care.* 1982;**5**(1):31-35.

Williamson JR, Kilo C. Basement-membrane thickening and diabetic microangiopathy. *Diabetes.* 1976;**25**(suppl 2):925-927.

Wise RG, Huang CL-H, Gresham GA, Al-Shafei AIM, Carpenter TA, Hall LD. Magnetic resonance imaging analysis of left ventricular function in normal and spontaneously hypertensive rats. *J Physiol (Lond).* 1998;**513**(Pt 3):873-887.

Zola B, Kahn JK, Juni JE, Vinik AI. Abnormal cardiac function in diabetic patients with autonomic neuropathy in the absence of ischemic heart disease. *J Clin Endocrinol Metab.* 1986;**63**(1):208-214.

Zoneraich S, Silverman G, Zonereich O. Primary myocardial disease, diabetes mellitus, and small vessel disease. *Am Heart J.* 1980;**100**(5):754-755.